論文 / 著書情報
Article / Book Information

題目(和文)	
Title(English)	Perpendicular magnetic anisotropy and exchange bias in CoNi/(Co,Ni)O layered structures
著者(和文)	GaoHangxian
Author(English)	Hangxian Gao
出典(和文)	学位:博士(工学), 学位授与機関:東京工業大学, 報告番号:甲第11306号, 授与年月日:2019年9月20日, 学位の種別:課程博士, 審査員:史 蹟,中村 吉男,須佐 匡裕,木村 好里,林 幸,中川 茂樹
Citation(English)	Degree:Doctor (Engineering), Conferring organization: Tokyo Institute of Technology, Report number:甲第11306号, Conferred date:2019/9/20, Degree Type:Course doctor, Examiner:,,,,,
学位種別(和文)	博士論文
Type(English)	Doctoral Thesis

TOKYO INSTITUTE OF TECHNOLOGY

DOCTORAL THESIS

Perpendicular magnetic anisotropy and exchange bias in CoNi/(Co,Ni)O layered structures

---

Author:
Hangxian GAO

Supervisor:
Prof. Ji SHI
Prof. Yoshio NAKAMURA

A thesis submitted in fulfillment of the requirements
for the degree of Doctor of Engineering

in the

Nakamura-shi Laboratory
School of Materials and Chemical Technology

TOKYO INSTITUTE OF TECHNOLOGY

Abstract

Department of Materials Science and Engineering
School of Materials and Chemical Technology

Doctor of Engineering

Perpendicular magnetic anisotropy and exchange bias in CoNi/(Co,Ni)O layered structures

by Hangxian GAO

This work focus on the study of magnetic anisotropy and exchange bias of ferromagnetic CoNi and antiferromagnetic (Co,Ni)O layered structures. Samples with sharp interfaces show strong perpendicular magnetic anisotropy (PMA) and room temperature perpendicular exchange bias (PEB). This PMA preserves above the blocking temperature. Such PMA is considered originate from the interfacial anisotropy at the metal/oxide interface. The room temperature PEB indicates the well-balanced Néel temperature and anisotropy energy of the AFM oxide layer. Moreover, when the polycrystalline film is of an "isotropic" magnetization, magnetic anisotropy can be tuned by exchange coupling at the FM/AFM interface. For epitaxial samples deposited on MgO single crystal substrate, metal/oxide interface sharpening occurs upon annealing. This perpendicular magnetization FM/AFM structure can serve as a promising building block for future spintronic devices.

Contents

List of Figures

List of Tables

Chapter 1

Introduction

1.1 Technological background

1.1.1 In-memory computing

Fast development of the information technology has been dramatically changed the human life for the past few decades. The computing technology has been evolving at an exponential rate since the first transistor was invented in 1940s. The famous derived law to shape this speed is the popular Moore's Law[1], which predicts that the density of transistors in a large scale integrated circuits(LSI) doubles every 18 months. The Moore's law has successfully predicted the development of complementary metal-oxide-semiconductor (CMOS) technology for more than 50 yeares.

Nowadays, we are witnessing a revolution in artificial intelligence(AI). Normally, an AI system needs to be trained based on huge amount of data to reach a high precision in prediction[2]. At the training phase, an enormous amount of data is shuttling back and forth inside a computing system. However, the conventional computing technology based on the von Neumann architecture is not efficient to deal with this task. The reason is shown in Figure 1.1(a), in von Neumann computer architecture, the processor and memory unit are physically separated. During the computation, a tremendous amount of data is shuttled between the processor and memory unit. This process generates a performance bottleneck, since a memory access process consumes roughly 500 times more energy and 100 times more time than a processor operation[3].

To overcome this bottleneck, it is clear that the processor and memory should be collocated. In other words, prossors are seamlessly embedded inside the memory

unit, as shown in Figure 1.1(b). This new kind of computing design, belongs to "Non-von Neumann architecture", is called "in-memory computing"[4]. In this new structure, data operation is directly carried out on the memory unit. There is no need to transfer the data between the memory unit and the processor. Thus, it is more energy and time efficient to perform AI system training on in-memory computers than conventional computers[5].

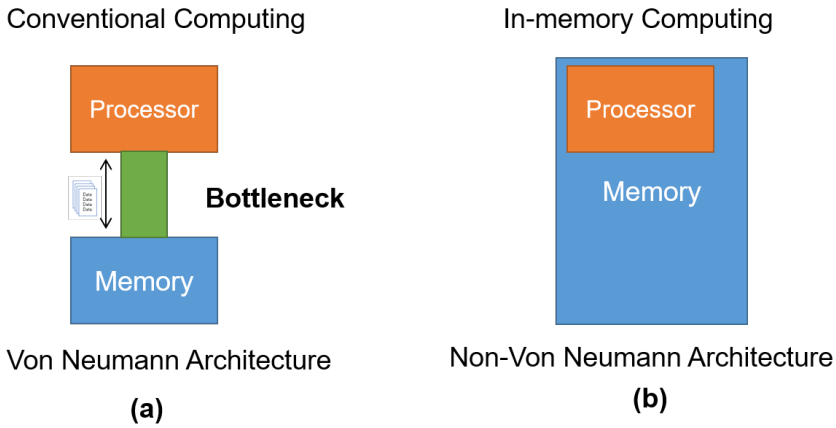

FIGURE 1.1: Concept of computing architectures: (a)Schematical of conventional von neumann computing; (b) Schematical of non-von neumann in-memory computing

1.1.2 Non-volatile memory technology

The in-memory computing technology requires high-density energy-efficient memory tehnologies, which could store and operate gigantic data at a low cost. With the characteristics of ultra-high density and low energy-consumption, Non-volatile memory technology is the ray of hope and the possible answer[6].

Table 1.1 compares the properties of advanced memory technologies. DRAM and SRAM are two commodity volatile memory technologies. On the other hand, flash is a commodity non-volatile memory technology. STT-MRAM, PCM and ReRAM are three emerging non-volatile memory technologies[7].

SRAM, which is short for static random access memory, can retains data as long as power is presented. As a fast-access memory, SRAM is usually applied in computer cache memory and digital signal processing. However, SRAM usually shows high leakage power, which pose challenges to the LSI design[8].

As a volatile memory, DRAM requires consistent data refresh during the operation, which consume large amount of power. It is said that DRAM main memory systems consumes 30% $\sim$ 50% of the power for a computing node. This refresh dynamic power is becoming a key design limiter for new computing architectures. DRAM(Dynamic random access memory) is widely used as main memory in modern computing devices for its relatively fast read/program speed and high storage density[8]. On the other hand, flash memory is non-volatile, which means the data will not deteriorate when the power goes off. It is mainly used in mobile devices such as cell phone, digital camera and tablets. Flash is usually applied as a main storage device rather than a main memory devices due to its high storage density but large access time/energy[8].

PCM, which is short for phase-change memory, uses chalcogenide materials. Chalcogenide materials have reversible phase conversion between a textured state and an amorphous state[8, 9]. These two states can be switched by the joule heat produced by the current flow. As a programmable memory, PCM is promising to replace DRAM. However, the problem for PCM is the low endurance which only has a writability of $10^5 \sim 10^9$. The heat cross-talk between adajacent memory cells is also a challenge for the future scaling of PCM.

ReRAM. also called Resistive Random Access Memory, is another new non volatile memory technology. It utilizes the redox reaction inside a material to generate two states with distinct difference in resistance. ReRAM has a significant low read/write time, an extremely low access energy. Moreover, ReRAM has excellent compatibility in the integration with the current CMOS techology. ReRAM is considered as a strong candidate for the next generation memory. However, the main problem for ReRAM is the relatively low endurance. Also, the random nature of redox reaction yield low stability and repeatability[8, 10].

MRAM technology, which is short for magnetoresistance random access memory, is also a new emerging memory technology[8]. Unlike the above mentioned memory technologies, MRAM use spins of electrons instead of charges of electron to store data. MRAM is potential to become an universal memory as it combines high density, very low read time, extremely long endurance, significant low leakage power and good scalability. However, the MRAM still needs to be further optimized

TABLE 1.1: Overview of memory technologies. (Reproduced from [8, 11])

Types	SRAM	DRAM	Flash	MRAM	PCM	ReRAM
Cell Size	>100F^2	6-10F^2	4-6 F^2	6-50F^2	4-12F^2	4-10 F^2
Read Time	<10ns	50ns	30ns	10ns	50ns	10ns
Write Time	<10ns	50ns	50ms	50ns	500ns	50ns
Access Energy	5pJ/bit	5pJ/bit	10^4pJ/bit	2pJ/bit	100pJ/bit	0.02pJ/bit
Endurance	$> 10^{15}$	$> 10^{15}$	10^5	$> 10^{15}$	$10^5 \sim 10^9$	$10^5 \sim 10^{11}$
Leakage Power	High	Medium	Low	Low	Low	Low
Non-volatility	NO	NO	YES	YES	YES	YES
Scalability	Good	Limited	Limited	Good	Limited	Medium

in terms of access energy and write time.

In every training phase of AI system, the amount of data access is estimated to be an order of 10^7 10^9. Memory with extremely high endurance is required. Among various non-volatile memory technologies, MRAM with the highest endurance shows extremely high potential to be implemented inside the in-memory computing technology.

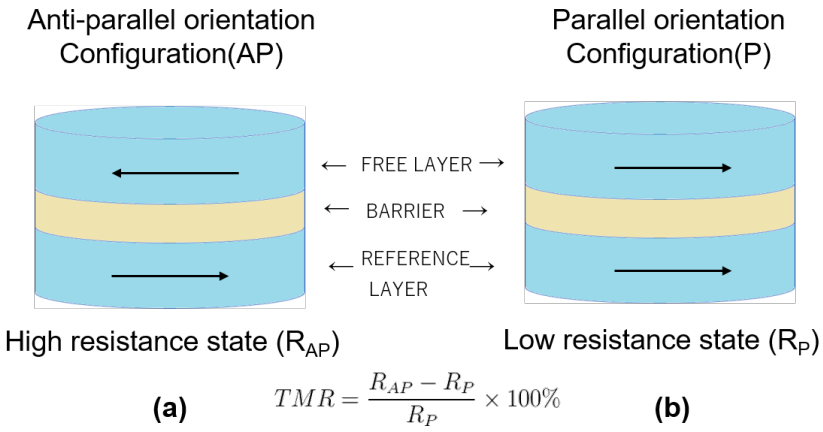

FIGURE 1.2: Schematical of MTJ with two orientations

1.1.3 Magnetoresistance Random Access Memory(MRAM)

As we have mentioned above, MRAM utilizes spins rather than charges of electrons to store and manipulate data. The bit data carrier of an MRAM is a structure of Magnetic Tunnel Junction(MTJ)[12]. Figure 1.2 shows the typical structure of an MTJ. MTJ consists of two ferromagnetic layers(free layer and fixed layer) which are separated by a non-magnetic layer(barrier layer). The magnetization in the free

magnetic layer can be rotated freely while the magnetization in the fixed magnetic layer is pinned and can not be switched during the operation. The resistance of an MTJ is based of the orientations of two separated ferromagnetic layers due to a phenomenon called tunnel magnetoresistance(TMR). There are two possible orientation configurations between the two magnetic layers: parallel or anti-parallel. These two different magnetic orientation configurations show two different electric resistivities, representing two different data forms. If the two ferromagnetic layers show anti-parallel orientation configuration(AP), the possibility of electrons to tunnel across the barrier is small. Thus, the resistance(R_{AP}) of MTJ is high, representing a "1" state. On the other hand, If the two ferromagnetic layers have parallel orientations(R_P), the possibility of electrons to tunnel across the barrier is high. Thus, the resistance(R_P) of MTJ is low, indicating of a "0" state. In the reading process, by measuring the resistivity of the MTJ, signals representing data forms of "0" or "1" can be detected and distinguished. The resistance difference between data state "0" and "1" should be large enough to ensure an unambiguous reading, which means that the TMR should be high for an MTJ structure, as can be described as the equation:

$$TMR = \frac{R_{AP} - R_P}{R_P} \times 100\% \tag{1.1}$$

Well textured MgO barrier is normally used for the MTJ to obtain a high TMR.

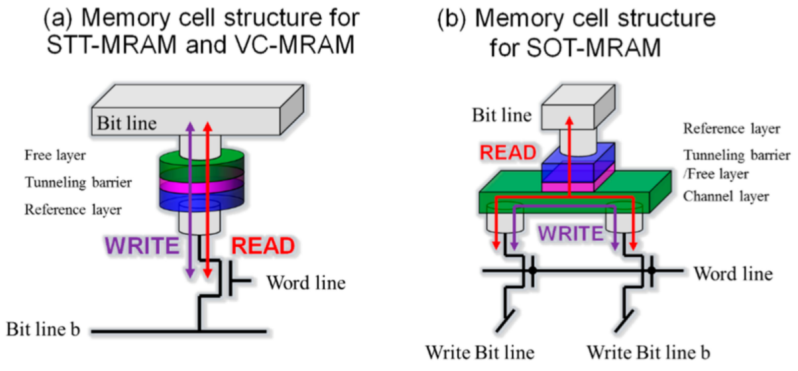

FIGURE 1.3: Schematical of MRAM with various writing schemes: (a)Memory cell structure for STT-MRAM and VC-MRAM; (b)Memory cell structure for SOT-MRAM. (adapted from [13])

For the writing process, depending on writing schemes, there are mainly three

designs of MRAM(See Figure 1.3): spin-transfer torque MRAM(STT-MRAM), spin-orbit torque(SOT-MRAM) and voltage controlled magnetic anisotropy MRAM (VC-MRAM)[13]. Figure 1.3 presents three types of MRAM wih different writing schemes. STT-MRAM and VC-MRAM are two-channel structure, whereas SOT-MRAM shows one-channel structure. These three types of MRAM have same cell structure of MTJ, albeit the different writing scheme. For STT-MRAM, in the writing process, a current is added from the transistor to the MTJ, generating a spin-polarized currentJ_s. This J_s passes through the reference layer and the barrier, finnally exerts a spin-transfer torque on the ferromagnetic layer. The orientation of the ferromagnetic layer is consequently altered by such torque[14]. For VC-MRAM, in the writing process, a voltage is applied on the MTJ from the transistor. If the applied voltage is above a certain threshold value, the magnetic anisotropy of the free layer in the MTJ can be altered from in-plane anisotropy to out-of-plane anisotropy, or vice versa. For SOT-MRAM, there is an additional channel layer attached to the free layer side of the MTJ(See Figure 1.3(b)). Two transistors are linked to the two sides of the channel layer. A charge currentJ_c is applied to pass through the channel layer from transistors. Such charge current produces a spin-polarlized current J_s. This J_s directly exerts a torque on the free layer and flips its orientation.

MTJ has two designs based on the magnetic anisotropy of the materials involved: MTJ with in-plane magnetic anisotropy(i-MTJ) or MTJ with perpendicular magnetic anisotropy(p-MTJ), as shown in Figure 1.4. It is known that better performances can be achieved for MRAM made with p-MTJ rather than i-MTJ.

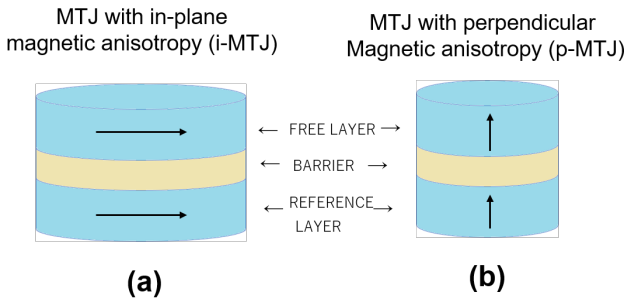

FIGURE 1.4: Schematical of MTJ with different anisotropies:(a)MTJ with in-plane magnetic anisotropy(i-MTJ); (b)MTJ with perpendicular magnetic anisotropy(p-MTJ)

Magnetic thin films with PMA plays a crucial role in modern spintronic devices.

Especially, it is potential for the development of high density MRAM consists of p-MTJ [15]. In the near future, STT-MRAM is competing to replace the incumbent commodity memory technologies such as Dynamic Random Access Memory(DRAM), Static Random Access Memory(SRAM) and Flash memory [16]. However, switching the magnetization needs electric current, the current density is still high at the moment. Thus, the challenging task remains in the development of STT-MRAM is finding methods to reduce the switching current density J_c. The switching current density needed for these two different designs is also different. For i-MTJ, the switching current density J_c can be represented by [17]:

$$J_c = (\frac{2e}{\hbar})\frac{2\alpha}{g(\mathbf{m}\times\mathbf{p})p}(U_k + \pi M_s^2) \tag{1.2}$$

On the other hand, for the p-MTJ, the switching current density can be given by [17]:

$$J_c = (\frac{2e}{\hbar})\frac{2\alpha}{g(\mathbf{m}\times\mathbf{p})p}(U_k) \tag{1.3}$$

where M_s represents the saturation magnetization, U_k means the energy barrier and α is the damping constant. Comparing the Equation 1.2 and Equation 1.3, it is obvious that the switching current density for p-MTJ is much lower than the in-plane MTJ.

Moreover, i-MTJ usually have lower effective magnetic anisotropy than p-MTJ, superparamagnetism effect will occur when the size of i-MTJ is too small. The critical size of p-MTJ can be reduced to a much smaller scale than the i-MTJ without causing the same effect. Thus, much denser storage can be achieved by applying p-MTJ to the MRAM [18].

Thermal stablility is another factor to consider for STT-MRAM. Magnetization orientation of a ferromagnetic layer can be influenced by the temperature. For reliable data storage in STT-MRAM, the thermal barrier between two possible magnetization orientations should be sufficiently large. The thermal barrier can be described by a thermal stability factor, which is given by [14]:

$$\Delta = \frac{E_b}{k_B T} = \frac{K_{eff} M_s V}{2k_B T} \tag{1.4}$$

where E_b is the energy barrier, k_B is a constant, T is the temperature, K_{eff} is the effective magnetic anisotropy, M_s is the saturation magnetization and V is the volumn of the MTJ. For p-MTJ, the thermal stability factor can be enhanced by choosing materials with large PMA.

With the above description, MARM with p-MTJ is a strong candidate for the MRAM applications. Magnetic films with large PMA are favorable for the development of MARM with p-MTJ.

1.2 Theoretical background

1.2.1 Fundamentals of magnetic anisotropy

Ferromagnetic material shows memory effect in M(H) dependence, this property manifests itself as a hysteresis loop. Figure 1.5 shows a typical hysteresis loop(the red loop). If sufficient magnetic field is applied on a ferromagnetic material, the magnetization will reach a complete saturation(Saturation Magnetization M_s). If we reduce the magnetic field back to zero, we can find that the magnetization of the material retains some value(Remnant Magnetization M_r). It takes a significant opposite magnetic field to demagnetize the material. The value of this demagnetization filed is called (Coercivity H_c). For some materials, the magnetic properties is not identical at all possible directions . This kind of materials show magnetic anisotropy. If one direction of the material is prone to be saturated under a small magnetic field, this direction is called the easy-axis magnetization of this material. On the other hand, if another direction of the material requires a large magnetic field to reach saturation magnetization, this direction is the hard-axis of the magnetization[19].

The energy of the magnetic field to saturate the easy-axis magnetization and hard-axis magnetization of a material is different. Magnetic anisotropy is the energy barrier between the easy-axis magnetization and the hard-axis magnetization. For a film, if the easy-axis magnetization lies in the film plane, it is longitudinal magnetic anisotropy(LMA). In contrast, if the easy-axis is perpendicular to the film plane, this film shows perpendicular magnetic anisotropy(PMA). Figure 1.5 shows an ideal hysteresis loop for a film with PMA.

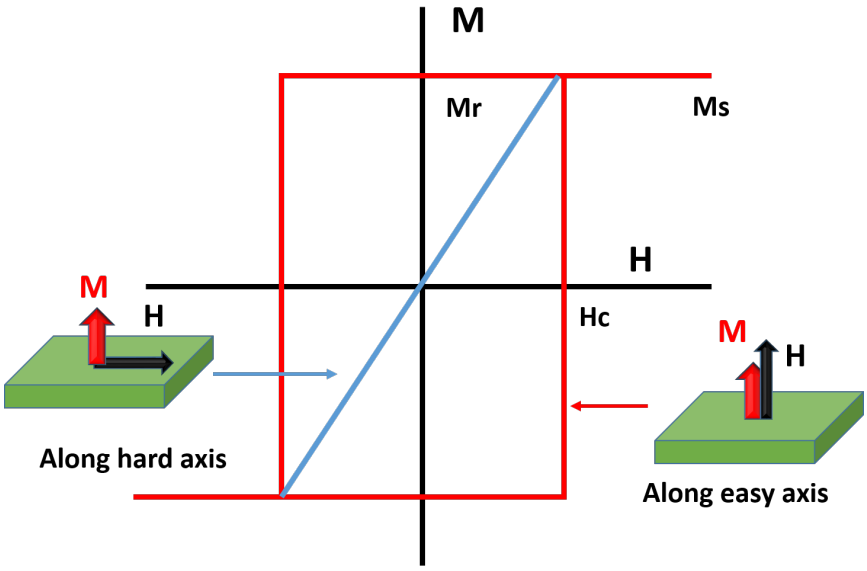

FIGURE 1.5: Schematic drawing of ideal hysteresis loop for film with PMA

To understand the origin of the PMA, we need firstly have a basic understanding of magnetic anisotropy in materials. Magnetic anisotropy can be categorized into three groups based on the sources: (1) magnetic shape anisotropy, (2) magneto-crystalline anisotropy, and (3) magneto-elastic anisotropy. They are detailed described as follows:

Magnetic shape anisotropy

Magnetic shape anisotropy is related with the sample magnetization and sample shape. It mainly originates from the long range magnetic dipolar interaction. Magnetic charges distribute non-uniformly depending on the shape of the materials. This non-uniform distributed magnetic charges produce negative magnetic field(demagnetization field) in response to the external magnetic field [19]. For example, materials with elliptic shape, the demagnetization field is smaller along the long axis than along the short axis, yielding an easy magnetization along the long axis. For thin film systems, the magnetic shape anisotropy(E_{MSA}) can be described as:

$$E_{MSA} = \frac{1}{2}\mu_0 M_S^2 cos^2\theta \tag{1.5}$$

where μ_0 is the vacuum permeability, M_s is the saturation magnetization and θ is the angle between the sample magnetization and sample surface normal. The E_{MSA}

force the sample to exhibit in-plane magneitic anisotropy. To induce PMA in thin film system, the magnetic shape anisotropy is the main anisotropy to overcome.

Magneto-crystalline anisotropy

Magneto-crystalline anisotropy mainly originates from spin-orbit interaction. Crystal lattice structure has influence on this spin-orbit interaction. Magnetization differs along different lattice directions in bulk materials[19].

For cubic systems, the magneto-crystalline anisotropy(E_{MCA}) can normally be written as:

$$E_{MCA} = K_4(\alpha_x^2\alpha_y^2 + \alpha_x^2\alpha_z^2 + \alpha_y^2\alpha_z^2) + K_6(\alpha_x^2\alpha_y^2\alpha_z^2) \tag{1.6}$$

Where $\alpha_x, \alpha_y, \alpha_z$ are the direction cosines with respect to the $\langle 100 \rangle$ crystal axis of cubic lattice with constraint of $\alpha_x^2 + \alpha_y^2 + \alpha_z^2 = 1$ and K_4, K_6 are fourth and sixth orders of MCA constants.

For thin film materials, the magneto-crystalline anisotropy in the interface or surface differs from the bulk materials due to the reduced symmetry or symmetry breaking. Néel firstly predicted this special magneto-crystalline anisotropy and termed it as interface anisotropy [20]. In most cases, the interface anisotropy is an uniaxial out-of-plane anisotropy. Such interface anisotropy can reach a large value, which large enough to overcome the magnetic shape anisotropy and consequently induce a PMA in thin film systems. The interface anisotropy is considered as one of the most importance sources of PMA for the film structures.

Magneto-elastic anisotropy

Magneto-elastic anisotropy mainly originates from the strain inside the materials[19]. Strain may overcome the magneto-crystalline anisotropy and alter the direction of the magnetization. If the energy of the strain inside the material is sufficiently larger than all the other magnetic anisotropies energies, then an uniaxial stress can produce a unique easy magnetization axis. Materials with large lattice misfit usually show magneto-elastic anisotropy.

Categorization of perpendicular magnetic anisotropy

Since its first discovery, ferromagnetic films with perpendicular magnetic anisotropy(PMA) have been proposed in various configurations. These configurations can be categorized into several groups.

Cobalt/heavy metal multilayered structures Layered structures with PMA were firstly reported by Carcia in 1985. Carcia found that the magnetic easy axis turns to perpendicular in Co/Pd multilayer structures and clarified this PMA as a result of interface anisotropy[21]. Since then, PMA was also observed in other Co/heavy metal multilayers, such as Co/Pt, Co/Au and Co/Ru [22–25]. In those structures, PMA are commonly built within critical thickness of Co and influenced by the interface quality. The PMA in these systems is attribute to the interfacial anisotropy. Such interface anisotropy is attributed to the strong SOC of the heavy metal and the d-d orbital hybridization induced charge transfer at the interface. One can note that Co is the key building block of the materials group here. It usually combined with noble or rare metals with large SOC to form a multilayer structure.

Fe(Co)/Metallic oxide layered structures Recently, PMA has also been established at Fe(Co)/MO_x, where M refers to Mg, Al, Ru, Ta etc and x is the oxidation degree[26]. The oxide side can be polycrystalline (MgO, RuO) or be amorphous (AlO_x, TaO_x). The PMA in these systems is attributed to the electric hybridization and Fe(Co) and oxygen at the interface. It is demonstrated that the interfacial PMA is closely related to the oxidation degreee. PMA is found to be reduced both for under-oxidized and overoxidized interfaces. In contrast to the Co/heavy metal multilayered structures, PMA in Fe(Co)/oxide layered struture shows weaker coercivity. The most studied type of this system is the MgO/FeCoB, which shows high interfacial PMA combined with large TMR. This MgO/FeCoB layered structure is considered as a promising building block for STT-MRAM[27].

Metal/ceramic multilayer structures In matallic multilayers, interface diffusion between Co and metal at high temperature usually deteriorates the PMA. In order to overcome the effect of interdiffusion, ceramics like TiN, AlN and CoO are

introduced instead of metals. Strong PMA with high interface quality were obtain in CoPt/AlN, FePt/AlN, CoPt/TiN and CoPt/CoO multilayer films [28–30]. In these systems, magnetic anisotropy can be manipulated through post-deposition thermal annealing process. PMA is considered mainly originates from the interface anisotropy combined with magneto-elastic anisotropy. In addition, in the previous study in our group, we find that strong PMA can be obtained in CoPt/CoO multilayers. [31].

$L1_0$-ordered alloys Recently face-centered-tetragonal(FCT) alloys such as FePt, FePd, CoPt and CoPd, are intensively studied for their potential application in ultra-high density magnetic storage. Those alloys show large coercivity and high magneto-crystalline anisotropy along c-axis after transformation to $L1_0$ ordered phase [32]. The mechanism of this PMA can be explained by the magnetocrystalline anisotropy from hybridization between the Pt 5d band and Co or Fe 3d band electronic states. However, growing $L1_0$ ordered phase requires relatively high substrate temperature or high temperature post-deposition annealing. This brings a processing integration issue for memory devices. In addition, in order to obtain preference texture growth, special treatment such as buffer layer or MgO substrate are needed during the deposition of those alloys.

Rare-earth/transitional metal alloys Rare-earth/Transitional metal alloys such as TbFeCo and GdFeCo has been reported to show PMA [33]. However, the mechanism of this PMA has not been fully understood. Several possible mechanisms have been considered to explain this PMA such as the anisotropy chemical bonding between the rare-earth element and tranistion metal element, exchange anisotropy and anti-parallel dipole.

1.2.2 Fundamentals of exchange bias

In this section, we will discuss a special anisotropy: exchange anisotropy. Exchange anisotropy differs from the above-mentioned anisotropies, which are either due to the magnetic dipolar interaction or spin-orbit interaction.

Exchange bias

In 1956, Meiklejohn and Bean measured the magnetic properties of oxidized Co particles [34]. They found that the hysteresis loop of this particle shifted horizontally and centres at a negative field when the sample was cooled under a magnetic field. Such phenomenon reveals that an additional unidirectional anisotropy is acted on the Co particles. This additional is termed as "exchange anisotropy" at first stage and later renamed as "exchange bias(EB)". It is concluded that this shift is due to the existence of the coupling effect between the ferromagnetic core and the antiferromagnetic shell. Meiklejohn and Bean explained this phenomenon as an interfacial effect. Until now, extensive studies on exchange bias are carried out on structures with FM/AFM interface.

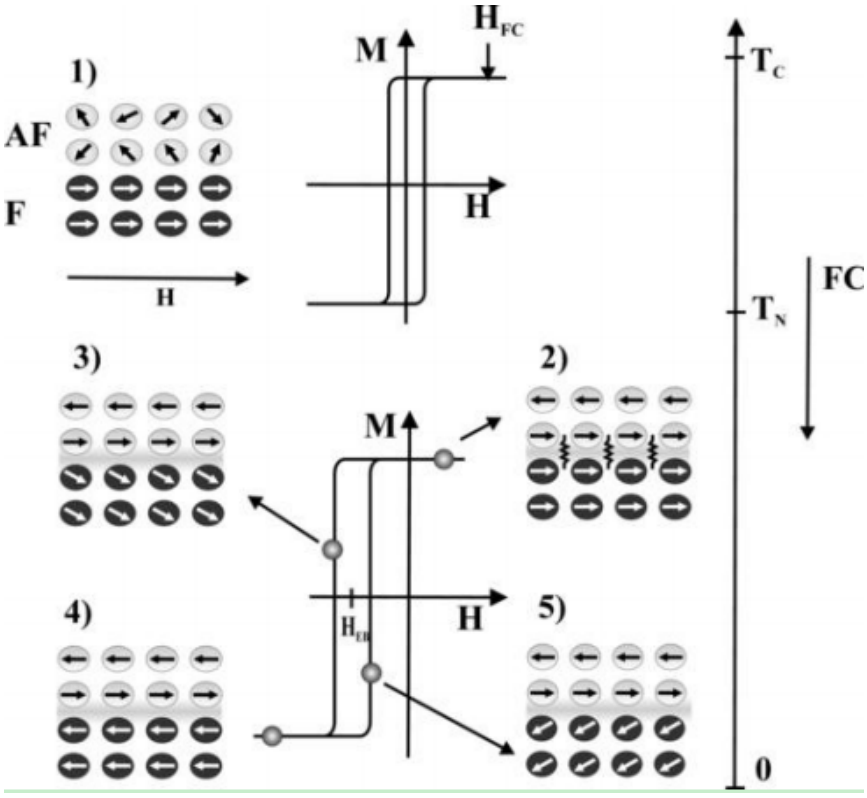

FIGURE 1.6: Phenomenological model of exchange bias for an AF/F bilayer.(adapted from [35])

Figure 1.6 depicted the phenomenological model of this effect [35]. We assume that the ferromagnetic layer and antiferromagnetic layer are magnetically coupled across an atomically smooth layer. The antiferromagnetic layer has an in-plane magnetic anisotropy. When the temperature is above the Néel temperature of the AFM

material and below the Curie temperature of the FM material, the antiferromagnetic layer is in a paramagnetic state and there is no interaction between the FM and AFM material. The hysteresis loop of this structure is centered at the original point. The spin configuration of this state can be seen in Figure 1.6(1). If the structure is field cooled through T_N of the antiferromagnetic layer in a positive applied magnetic field (H_{fc}), the ferromagnetic layer is magnetically coupled to the antiferromagnetic layer through the uncompensated spins at the interface (See in Figure 1.6(2)). It is noted that the applied cooling magnetic cooling field is usually larger than the measurement field. The spin configuration of the antiferromagnetic layer keeps in an energetically stable situation regardless of the applied measurement field. In the interface, the antiferromagnetic spin exerts a spin torque on the ferromagnetic spin, which tend to keep the spins of the ferromagnetic layer in their original direction. This hinders the spin rotation of the ferromagnetic layer to the applied measurement field, yielding a shifted hysteresis loop (See in Figure 1.6(3-5)) [35].

Exchange bias effect has potential application in the field of spintronics. In the previous section, we have mentioned that MTJ is the key component in the MRAM. Ferromagnetic materials serve in two magnetic layers in MTJ: A free sense layer and a fixed reference layer. The orientation of the ferromagnetic free sense layer can be freely switched, whereas the ferromagnetic reference layer is stable against sensing field. Exchange bias is considered as a useful tool to fix the orientation of the reference layer. Thus, the exchange bias is promising for the development of the ultra-high density magnetic recording media.

Perpendicular exchange bias

Until now, exchange bias effects are mostly established in the film plane of FM/AFM multilayers as longitudinal exchange bias(LEB). With the development of materials exhibiting PMA, perpendicular exchange bias(PEB) also receives a lot of attention due to its potential application to stabilize the reference layer inside a pMTJ in MRAM. PEB is firstly established in 2000. By now, many multilayer structures such as CoPt/(CoO, FeMn, IrMn) have been proved to show PEB [36–38].

As shown in Figure 1.7, it is obvious that spin configuration of PEB is similar to LEB [39]. The only main difference is the orientation of all the spins are kept

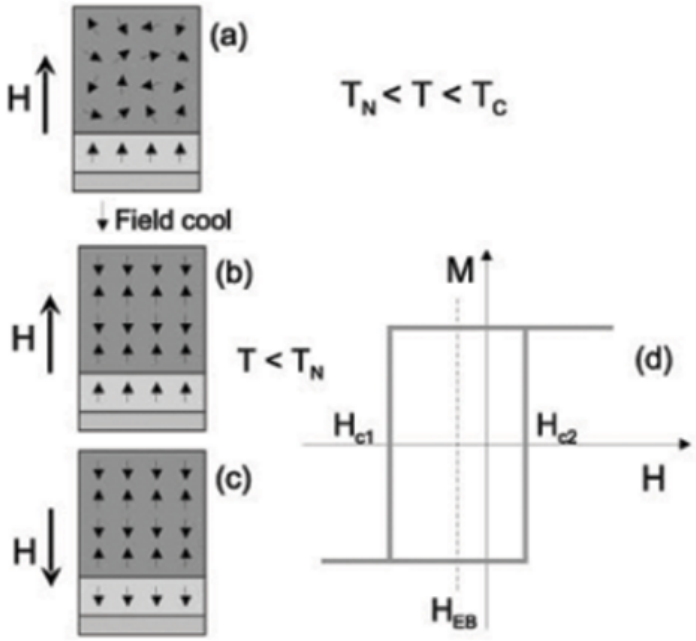

FIGURE 1.7: Schematic illustration of the spin configuration of AF/FM bilayer showing perpendicular exchange bias.(adapted from[35])

perpendicular to the FM/AFM interface. However, due to the difficult to establish PMA in FM materials, PEB is also not easy to be established in a FM/AFM system. High temperature PEB requires the AFM materials to show high Néel temperature, only limited material structures can show room temperature PEB. Moreover, the relationship between PMA and PEB is controversial, which requires more studies.

1.3 Background of this study

As we have discussed in the previous sections, layered structures with PEB requires FM/AFM structure consists of FM layer with PMA and AFM layer with suitable Néel temperature and anisotropy energy. Conventional way of designing an FM/AFM layered structure with PEB is to choose the materials for FM and AFM layer separately, which is to find an FM materials with intrinsic PMA together with an AFM materials with high Néel temperature and anisotropy energy, and thereby combine the FM and AFM materials together.

For the MRAM implementation, FM materilas with large PMA, low damping

parameter and high spin polarization are preferred for the MTJ. A low damping parameter links to the high switching speed of the memory. A high spin polarization is associated with the high TMR for MTJ. It is easy to find that most FM materials exhibiting PMA involve heavy elements, which lead to a large damping parameters and a modest spin polarization.

On ther other hand, from a technological point of view, room temperature PEB is more practical for the application. from a research point of view, room temperature PEB is also convenient to disclose its mechanism of exchange bias. Therefore, it is necessary to establish room temperature PEB in an FM/AFM layered structure. Common AFM materials available to realize room temperature exchange bias are Mn alloys such as PtMn($T_N = 970K$), FeMn($T_N = 490K$), MnAu($T_N = 1500K$) and IrMn($T_N = 690K$), oxides such as NiO($T_N = 520K$), Cr_2O_3($T_N = 310K$) and $BiFeO_3$($T_N = 653K$), and nitrides like MnN ($T_N = 660K$)[40, 41].

1.4 Objectives of this study

Within that spirit, the focus of the study in this thesis is to shed new light on the designing of the FM/AFM layered structures and try to induce PMA directly by FM/AFM interface. By this way, the design of FM/AFM structure could be significantly simplified.

As has been mentioned above, Co/Pt, Co/Pd multilayer films together with their alloy conterparts CoPt and CoPd have been proved to show PMA. In previous study, Co/Ni multilayer has also been proved to show PMA. It is possible to induce PMA in alloy of CoNi by buffer layer materials engineering. CoNi has gained particular interests, because it has potential to show low damping parameter, relatively high polarization and moderate magnetization[42]. These features are quite suitable for the application in MTJ.

Previous study in our group has demonstrated the PMA and PEB in CoPt/CoO[31]. Although room temperature PEB is not realized in CoPt/CoO layered structure due to the low Néel temperature of CoO, it inspires us that its possible to induce PMA directly by an FM/AFM oxide interface. Previous studies have shown that by adding Ni into the CoO, the Néel temperature of the AFM layer can

be elevated to a temperature above room temperature. Thus, room temperature exchange bias is expected by using (Co,Ni)O AFM oxide.

Here, we propose an FM/AFM layered structure with CoNi as the ferromagnetic layer and (Co,Ni)O as the antiferromagnetic layer to establish interface induced interfacial PMA and room temperature PEB.

The objectives of this study are as follows:

1. To establish and disclose the mechanism of the perpendicular magnetic anisotropy in the CoNi/(Co,Ni)O layered structure.

2. To realize and understand the room temperature perpendicular exchange bias in the CoNi/(Co,Ni)O layered structures.

3. To study the relationship between the exchange coupling and magnetic anisotropy in the CoNi/(Co,Ni)O layered structures.

1.5 Organization of this thesis

This master's thesis consists of 5 chapters, including:

Chapter 1: This chapter outlines the technical background knowledge and fundamental theoretical understandings required in the following discussions in this thesis. The chapter contains three major sections. The first section describes the technological background of this study, the second section is committed to the understanding of magnetic anisotropy and exchange bias, the third section briefly introduces the understanding of research background. Objectives and organization of this thesis are also presented.

Chapter 2: This chapter introduces the experiment methods of layered stucture preparation, structural characterization and magnetic property measurement. Preparation condition are optimized based on the results of structural results and magnetic properties.

Chapter 3: This chapter will focus on the realization of the perpendicular magnetic anisotropy in CoNi/(Co,Ni)O multilayers. Influences of ferromagnetic layer thickness and antiferromagnetic layer thickness on the magnetic anisotropy

are investigated and the origin of perpendicular magnetic anisotropy is discussed. The realization of room temperature perpendicular exchange bias effect is also studied.

Chapter 4: This chapter is dedicated to the investigation of the interface effect on the magnetic anisotropy in CoNi/(Co,Ni)O layered structures. MgO single crystal substrate is used for the film preparation. The deposition temperature and post-depostion annealing effect on the microstrcuture and magnetic anisotropies are studied. The main contribution to the perpendicular magentic anisotropy is determined. The interface smoothing phenomenon also discussed.

Chapter 5: This chapter is committed to the study of the relationship between the magnetic anisotropy and exchange coupling effect in the CoNi/(Co,Ni)O layered structures. Microstructure, antiferromagnetic layer thickness effect on the magnetic anisotropy is firstly presented. Then, exchange coupling effect on the magnetic anisotropy is investigated, and the mechanism of the magnetic anisotropy manipulation through exchange coupling is clarified based on a polycrystalline exchange bias model.

Chapter 6: In the general conclusions of this thesis, a summary of the most relevant results and their perspectives are given in this chapter.

Chapter 2

Preparation and characterization of CoNi/(Co,Ni)O layered structures

This chapter introduces the experimental techniques employed to fabricate and characterize the CoNi/(Co,Ni)O multilayered structures. The chapter also presents results regarding the basic structural and magnetic properties of the layered structures. Firstly, for the sample preparation, DC magnetron sputtering is applied for the sample preparation by using a facing target sputtering system. After the deposition, materials characterization techniques are applied to investigate the composition, crystallographic properties and microstructure. Characterization techniques includes x-ray diffraction(XRD), x-ray reflectivity(XRR), transmission electron microscopy(TEM) and Auger Depth Profiling. Lastly, magnetic properties are measured by vibrating sample magnetometer(VSM).

2.1 Sample preparation techniques

2.1.1 DC magnetron sputtering technique

DC magnetron sputtering is a widely used technique for thin film deposition. Various materials can be sputter-deposited using this method, such as pure metals, alloys, metallic oxides, nitrides and carbides. This technique can produce films of high purity, great adhesion, good uniformity and homogeneity.

Generally, sputtering is the ejection of atoms from a solid surface by the bombardment of energic ions. In sputtering, a target consisting of the desired material is bombarded by ions, which are generated in a glow discharge. Normally, argon

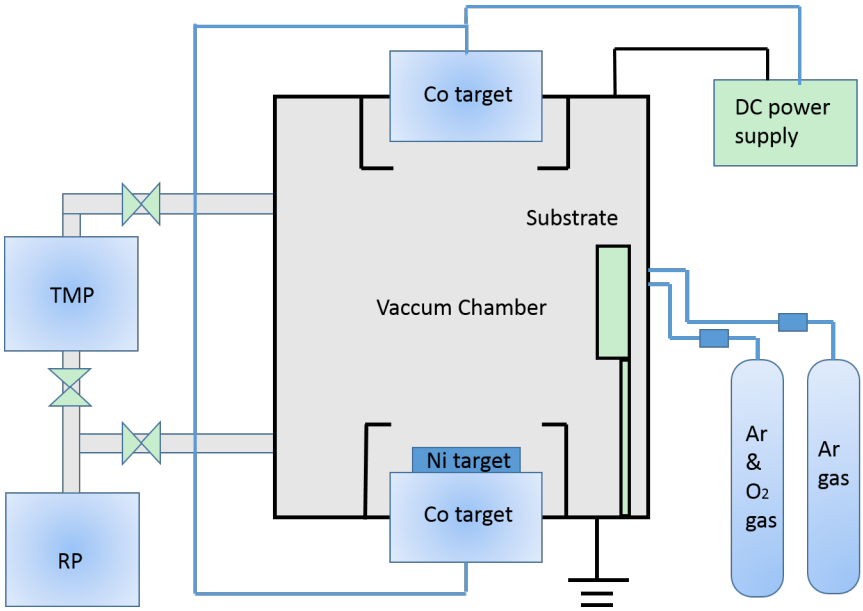

FIGURE 2.1: Schematic diagram of DC magnetron sputtering.

is used as the sputter gas due to its inert properties and relatively high mass. It is beneficial to obtain high sputtering rates. In magnetron sputtering, a magnetic field in front of the target confines the electrons there. They are constrained to be on spiral trajectories around the magnetic field lines, which effectively increases the length of their paths in the plasma. When a gas ion hits the target, momentum transfer from the ion to the atoms of the target. Target atoms are released when the transferred energy is higher than their binding energy. The emitted target atoms lose kinetic energy by elastic scattering at atoms of the sputter gas. Finally, they condense at the surface of the chamber as well as the substrate. If the sputtering gas is consists of elements, which is reactive with the emitted target atoms. Compounds can be obtained at the substrate. Such kind of sputtering is called reactive sputtering.

In this study, DC magnetron sputtering method is employed to deposit the CoNi/(Co,Ni)O layered structure films. A dual facing-target DC magnetron sputtering apparatus is used for the deposition. Figure 2.1 shows the schematic diagram of the DC magnetron sputtering apparatus used in this research. As the diagram presents, the apparatus equips with a pair of facing targets. One of the target is Co with a purity of 99.99%, the other target is Co-Ni target(a 100mm diameter size Co target with a $40mm \times 20mm$ 99.99% purity Ni plate placed on top). The position of the substrate holder is at the middle height of the two targets. Note that during the

deposition, these two targets work simultaneously and can not work separately. The substrate holder is equipped with a heater, which can be used for high temperature deposition. The vacuum system consists of a rotary pump and a turbo-molecule pump. A high vacuum below 5×10^{-5} is kept by this vacuum system. Argon gas or mixed gas (90 $\sim$ 100% argon and 0 $\sim$ 10% oxygen) can be imported into the chamber through two gas lines. The Ar/O_2 ratio can be easily controlled by the flowmeter.

CoNi and (Co,Ni)O films were produced by deposition under different oxygen partial pressures. CoNi layer is deposited at a pure argon atmosphere, (Co,Ni)O layer are deposited at argon and oxygen mix atmosphere($Ar : O_2 = 9 : 1$). To determine the deposition rate, all the films are initially deposited for a relatively long time(40 mins). Then the thickness of the deposited film was measured by x-ray reflectivity technique(to be introduced below). Thus, the deposition rate was determined by dividing the thickness by deposition time. The deposition rate of CoNi layer is calculated as 0.02075nm/s and the deposition rate of (Co,Ni)O layer is 0.02621nm/s. For the deposition of multilayer films, the layer thickness is controlled by changing the deposition time under a constant deposition rate.

2.1.2 Annealing

Vacuum annealing is conducted on the CoNi/(Co,Ni)O films. Vaccum annealing of the samples is performed on a vacuum tube furnace. High vacuum condition ($< 1 \times 10^{-5} Pa$) is achieved to avoid sample oxidation. The annealing process is programmable and control by a monitor. For normal vacuum annealing, no external magnetic field is applied. The filed cooling process to be mentioned below is also performed on a vacuum tube equipped inside a vibrating sample magnetometer.

2.2 Characterization techniques

2.2.1 X-ray diffraction(XRD)

X-ray diffraction is a powerful tool for crystallographic analysis to obtain structural information of the material [43]. The Bragg-brentano x-ray diffraction is the most

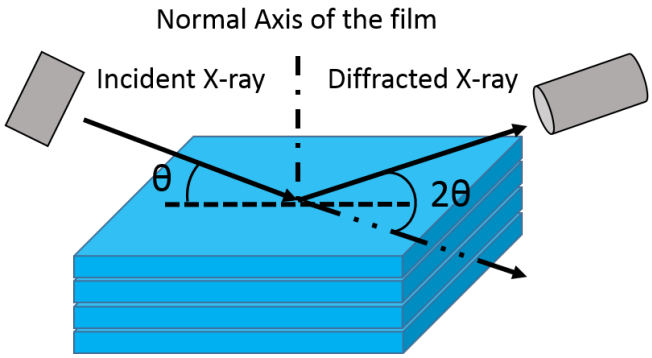

FIGURE 2.2: Geometries of a conventional Bragg-Brentano x-ray diffraction

commonly used technology to detect the film structure from the out-of-plane direction. It's geometry is shown in Figure 2.2. In this technology, a monochromatic x-ray with the wavelength around 1 angstrom is used. This wavelength is comparable with the crystal atomic spacing. When an x-ray beams hit the surface of the film by an incident angle of θ with respect to the film plane, diffracted x-ray with the same wavelength is generated. If the incident beam angle θ satisfies the Bragg's law:

$$n\lambda = 2dsin\theta \tag{2.1}$$

where n is an integer which is called the order of reflection, λ is the wavelength of the x-ray, d is the spacing of a certain crystal plane and θ is the incident angle, a x-ray beam peak with the same angle θ with respect to the film plane could be detected by the detector [44]. With the incident beam direction fixed, if the sample rotates by a certain speed, the detector should rotate at twice speed of the sample to catch the diffracted beam. Therefore, this x-ray detection method is also called $\theta/2\theta$ mode scan. It is worth noting that this method works well only for the atomic planes paralleled to the sample surface.

$\theta/2\theta$ mode scan produces graph of x-ray intensity peaks. Form the peak position, one can determine the lattice plane. Additional to the peak position, the peak shape reveals information about grain size and grain orientation both in direction perpendicular to the film plane.

Figure 2.3 shows XRD profile of a 60 nm thick (Co,Ni)O film prepared on glass substrate. A strong peak near 42° (002) texture of the film.

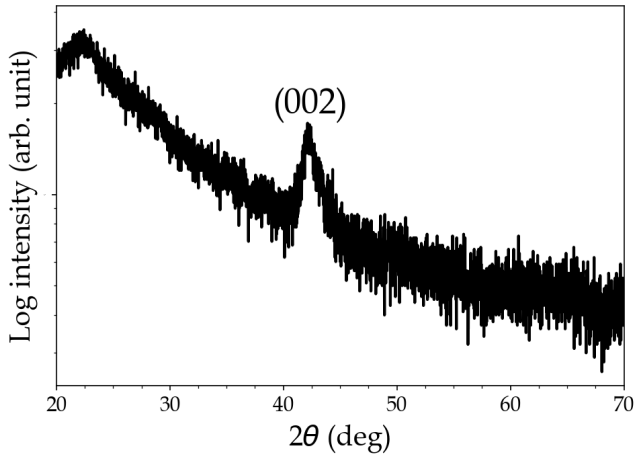

FIGURE 2.3: Xrd profile of a 60nm thick (Co,Ni)O film prepared on glass substrate

2.2.2 X-ray reflectivity(XRR)

X-ray refletivity is a useful technique to study surfaces of films and interfaces of multilayers [45]. Figure 2.4 shows the schematic view of x-ray reflection for multilayer structure. In this technique, a beam of x-ray hits the film by a very low grazing angle (smaller than the critical angle for total reflection), and at the surface and every interface inside the film, a portion of x-rays is reflected and counted by the detected. Interference of these partially reflected x-ray beams creates a reflectometry pattern. By measuring this pattern, information about thickness, density and surface or interficial roughness of thin films can be obtained. For layered structure, the period layer thickness can be calculated by the equation:

$$2D\sqrt{sin^2\theta - sin^2\theta_c} = m\lambda \tag{2.2}$$

where D is the period thickness, m is an arbitrary integer, λ is the x-ray wavelength, θ_c is the critical angle for total reflection and θ is the incident angle. Film commonly shows surface or interface with certain roughness. The deviation of the reflected intensity from the surface and interfaces follows the law of Fresnel reflectivity. Thus, this deviation can be used to determine the surface or interface roughness.

Figure 2.5 presents a typical XRR measurement result of a CoNi/(Co,Ni)O layered structure. Structural information such as density, layer thickness and roughness of the interface/surface can be obtained from the measured XRR curve.

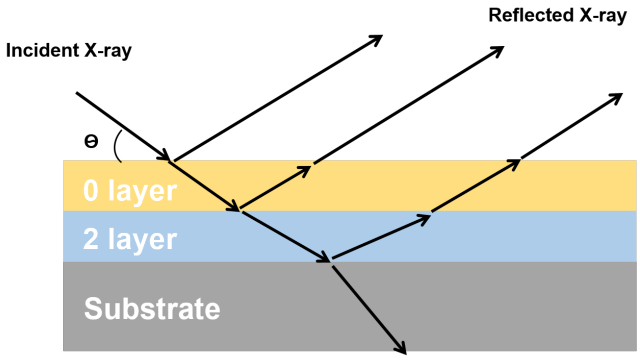

FIGURE 2.4: Schematic view of X-ray reflection for multilayer structure.

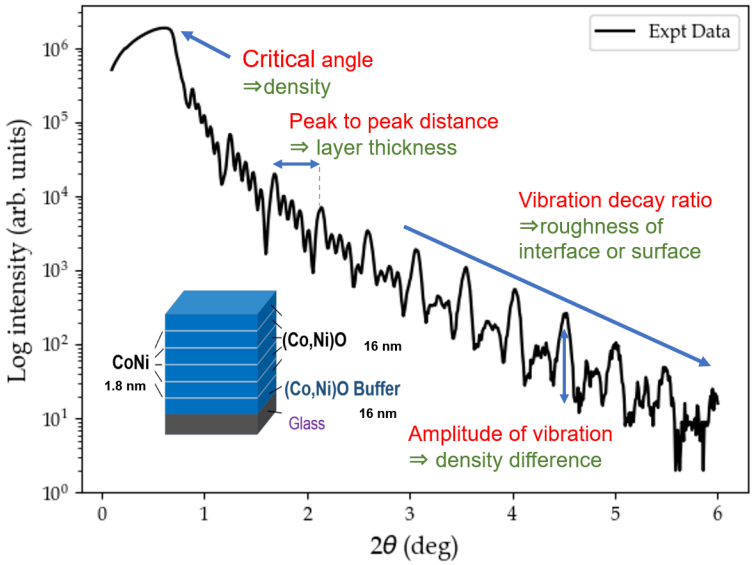

FIGURE 2.5: Example of XRR curve of CoNi/(Co,Ni)O multilayer structure. Structural information can be obtained from the curve

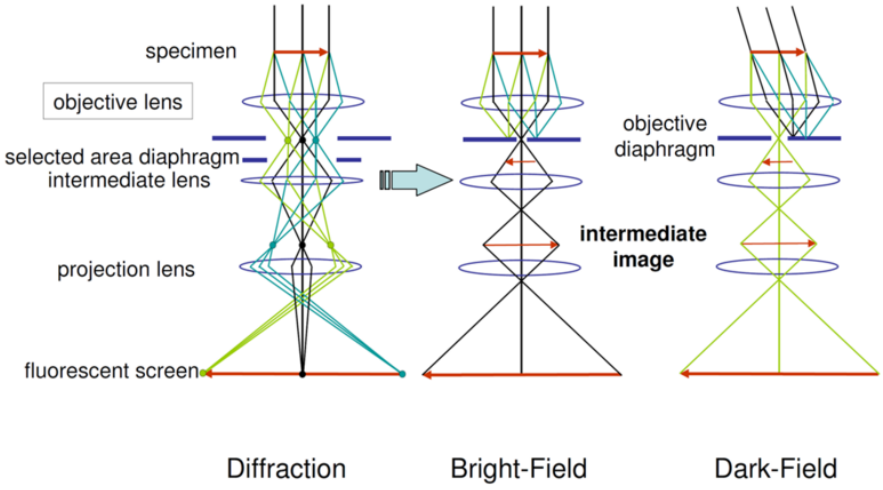

FIGURE 2.6: Ray paths in TEM [47](a) diffraction mode, (b)bright-field imaging, (c)dark-field imaging

2.2.3 Transmission electron microscopy(TEM)

The transmission electron microscopy(TEM) is an analytical tool that allows detailed investigation of crystal structure, orientation and chemical composition [46]. Using TEM, one can look through an ultra-thin sample of material with electron waves at high resolution. Generally, a conventional TEM enables two kinds of work mode: the image mode and the diffraction mode. In the image mode, two kinds of images can be obtained with different mechanisms of image formation: bright-field image and dark-field image.

By changing the optical path, we can switch between the image mode and the diffraction mode of the TEM with the objective diaphragm, as can be seen in Figure 2.6. However, diffraction mode should be operated first before switching between the bright-field image and dark-field image mode. At first step, we will focus on one diffraction spot and move the aperture to the center of that spot. Then, if we allow only the transmitted beam to pass the objective aperture, we can obtain a bright-field image. The bright-field image is normally used to determine the crystal size.

Conversely, if we allow only one diffraction beam to pass through the objective aperture, we can obtain dark-field image. Although dark-field image is not as common as bright-field image, special features from the samples can be obtained because observers can select a particular diffraction beam to perform the imaging.

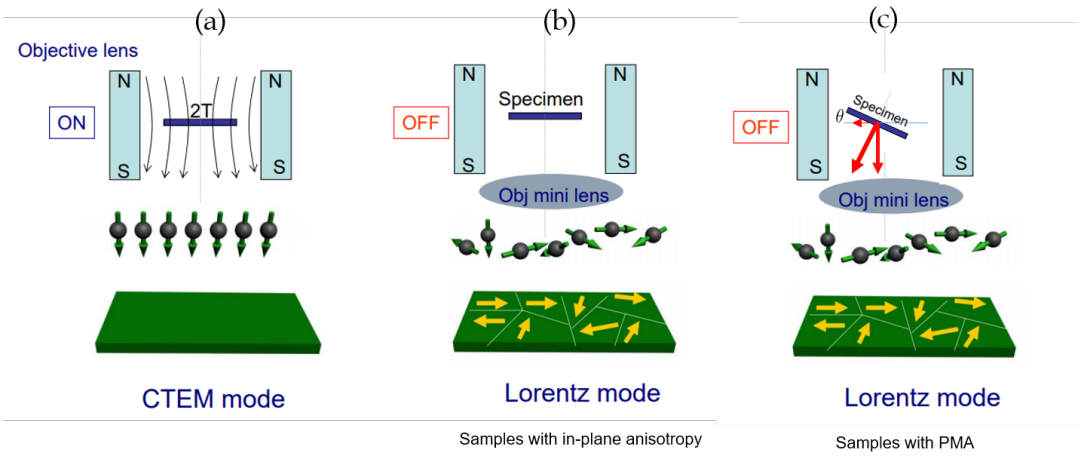

FIGURE 2.7: Schematic image of Lorentz TEM. (a) Conventional TEM mode, (b) Lorentz TEM mode for in-plane magnetic domain observation, (c)Lorentz mode for out-of-plane magnetic domain observation.[48]

In this study, cross-section samples are prepared for the observation of the multilayer structure in the TEM. The cross-section sample is prepared using Ar ion milling(10kV). The conventional Transmission Electron Microscopy(JEM-3010, JEOL) is used in the observation.

Lorentz TEM

We also use another special mode of the TEM to observe the magnetic domain: The Lorentz TEM. Schematic image of this special mode is shown in Figure 2.7. For normal TEM observation, in order to obtain an image with better magnification ratio and better resolution, a strong magnetic field(1-2T) is applied at the objective lens(OL) area to focus the electron beams passing through the sample. Such strong magnetic field consequently saturates the magnetic samples, leaving no magnetic information on the observed image2.7(a). To observe magnetic domains, one need to switch off the OL. The electron beam passes through the magnetic samples refracted by the Lorentz force from the intrinsic magnetic field of the sample. Refracted eletron beams leaves magnetic domain information on the final image(see Figure 2.7). Careful should be taken that, OL should also be kept off during the sample insertion, or sample may be instantly magnetically saturated. However, Lorentz force only acts on the electrons perpendicularly passing through the magnetic field. Only the in-plane magnetic component of the samples can have influence on the electron beams.

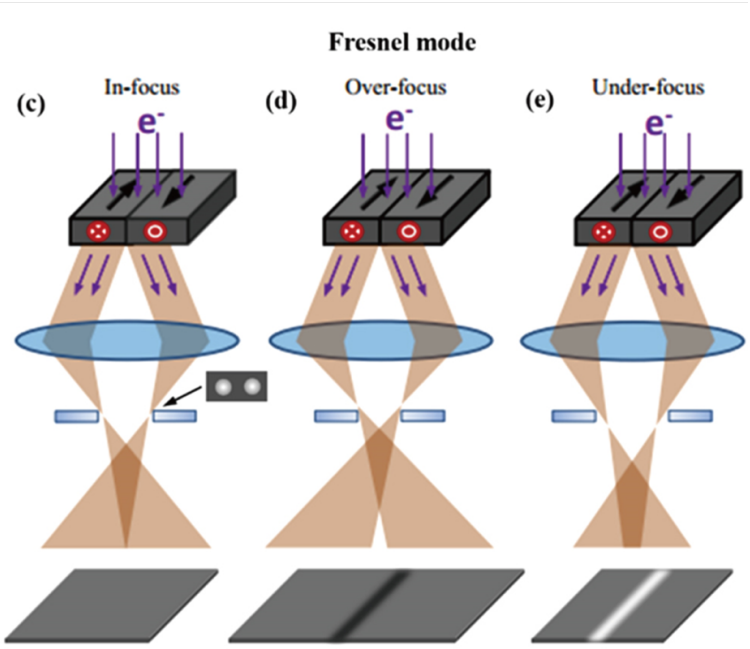

FIGURE 2.8: Focus mode of Lorentz TEM in Fresnel mode [50].

Thus, conventionally, Lorent TEM is used for observing samples with in-plane magnetic anisotropy. To observe samples with out-of-plane magnetic anisotropy, since the electron beam always passes perpendicularly, one can create a horizontal magnetic field component simply by tilting the sample to a certain degree, as shown in Figure 2.7(c)

There are two commonly used modes for magnetic domain observation in TEM: Foucault mode and Fresnel mode. Foucault mode is used to observe the domain structure, whereas Fresnel mode is used for domain wall observation. Compared with Foucault mode, Fresnel modes offer better operability and contrast quality[49]. Thus, we mainly use the Fresnel mode in this work.

Figure 2.8 shows the schematic image of Fresnel mode configuration. In Frensel mode, magnetic domain wall can be observed simply by tuning the focus of the electron beams. As mentioned above, electron beams will be reflected by the intrinsic magnetic field inside the sample. However, at the in-focus mode, the electron beams will finally focus at the final image plane, leaving no magnetic domain information. By tuning the focus, for example, at the over-focus mode, the image of domain wall appears at the final image plane. On the other hand, when the TEM is in a under-focus mode, domain wall appears again at the final image plane with a reversed contrast.

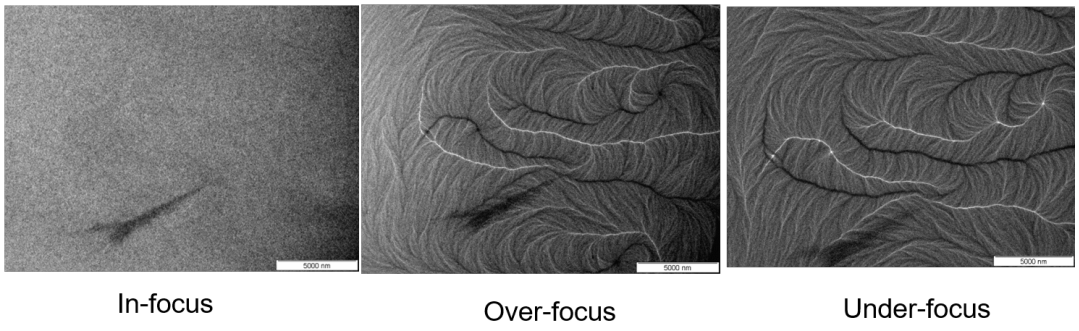

FIGURE 2.9: Typical In-plane Lorentz TEM image of (Co,Ni)O (16nm)/CoNi (30nm)/(Co,Ni)O (12nm) trilayer structure with in-plane magnetic anisotropy on ELS-C10 substrate. (a) In-focus mode, (b) Over-focus mode, (c) Under-focus mode.

Figure 2.9 shows a typical in-plane Fresnel LTEM image of (Co,Ni)O (16nm)/CoNi (30nm)/(Co,Ni)O (12nm) trilayer structure with in-plane magnetic anisotropy prepared on ELS-C10 substrate. Clearly, at in-focus mode, only the topological surface structure is shown. When the TEM is set in an over-focus mode, magnetic domain appears with partly bright and partly dark. When the TEM is turned to an under-focus mode, magnetic domains appear with the reversed contrast with respect to the over-focus mode. It can be seen that the domain walls of this trilayer film exhibit a random pattern.

2.2.4 Auger depth profiling

Sputter depth profiling, which refers to the determination of the elemental composition distribution at in-depth direction is an important method to investigate the diffusion phenomena in the multilayer structure. A rountinely applied method to do sputter depth profiling is using Auger electron spectroscopy(AES), which is referred to as "Auger depth profiling".

Auger electron spectroscopy is a popular surface nondestructive surface element analysis technique with the high sensitivity(an analysis depth of less than 100) and a low detection limit($\sim$ 0.1 atomic depth). When a finely focused electron beam hit the surface of a solid, it irradiates the surface and generate Auger electrons. The compositional information(such as the type and amount of the elements) of the analysis area can be determined by measuring the energy and signal intensity of the auger electrons(See Figure 2.10(a) leftmost). This technique has a wide element coverage

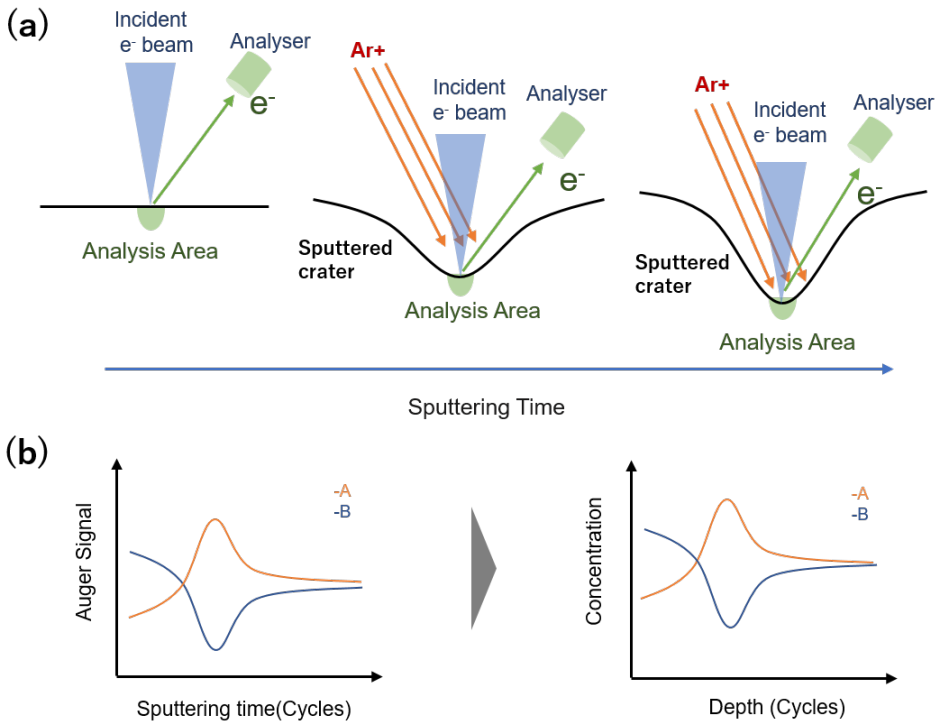

FIGURE 2.10: Schematic diagram of auger depth profiling.(a) illustrative diagram; (b) data conversion

from the lithium to almost the end of the periodic table. Another attractive point of this technique is its ability to distinguish the elements adjacently places at the periodic table.

Auger depth profiling is realized by simultaneously Ar gas ion bombardment sputtering to yield deeply buried interfaces and auger element analysis on the exposed underlying atomic layers. Element analysis are performed at every cycles of sputtering. A schematic image of the auger depth profiling is shown in Figure 2.10(a). Data can be processed to convert the Auger element intensity as a function of sputtering time to the elemential concentration as a function of depth, as shown in Figure 2.10(b)[51].

In this study, the FE-auger(JAMP-9500F) is used for the sputter depth profiling. Co and Ni are two elements located adjacently on periodic table. Auger element analysis is able to distinguish these two elements.

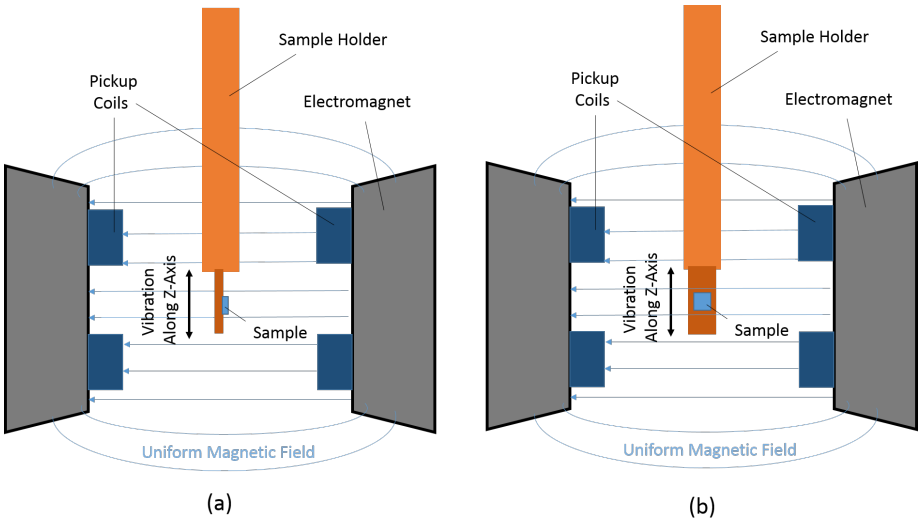

FIGURE 2.11: Schematic diagram of VSM with two different measurement modes: (1)In-plane mode (2)Out-of-plane mode.

2.2.5 Vibrating sample magnetometer(VSM)

Developed about half a century ago, vibrating sample magnetometer(VSM) is a commonly used technique to measure the magnetic properties of materials. The most attractive point of this technique is that it is a no-destructive measurement method.

The principle of the VSM technique is based on Faraday's law electromagnetic induction, which states that the voltage induced V(t) in an electrical circuit is propotional to the rate of change of magnetic flux in the circuit:

$$V(t) = -C \times d\phi/dt \tag{2.3}$$

where C is a constant. As shown in the figure 2.11, in the measurement, sample is placed in the middle of a uniform magnetic field, which is generated by an electromagnet or a superconducting magnet [52]. The sample is set to oscillate at low frequency by a vibrator. Signals are generated in the pick-up coils due to the presence of the oscillating magnetic flux from the sample. According to the Faraday's Law, the amplitude of the detected signals is proportional to the sample magnetization. Thus, the amplitude of the magnetization of the sample can be determined. For samples like films, hysteresis loop in different directions can be measured in by changing the sample orientation, as shown in the Figure 2.11.

The VSM used in this work is a RIKEN BHV-50V vibrating sample magnetometer with a maximum available field of 15kOe. Equipped with a temperature controlling parts, this apparatus can also be used for field cooling. Samples are placed in a holder inside a vacuum tube which can be fixed in the middle of the two electromagnets. Before field cooling, the tube is vacuummed and filled with He gas. The tube can be heated by heater or cooled by liquid nitrogen. During the heating or cooling process, external magnetic field can be applied by the VSM. Magnetic field angle with respect to the sample can be finely tuned by rotating the sample holder. Temperatures are real-time monitored by the platinum thermocouple on the holders. The heating or cooling temperature is controlled by a controlling program. In this work, the field cooling process undergoes as follows: we first heat the sample to 160°C(433K) and kept at this temperature for 10 minutes, and then cool down the sample to room temperature under an external magnetic field of 5KOe.

Note that in this work, since the Néel temperature of the AFM layer is higher than the room temperature, the virtual name of the AFM layer ordering treatment is "field annealing". However, most of the AFM materials have Néel temperature lower or close to the room temperture. Ordering state of these materials can only be observed below the room temperature. Moreover, the external magnetic field is applied only at the descending branch of the annealing process. Thus, in literature, this ordering treatment is unified by the traditional naming:"field cooling". This work will follow this unified naming.

2.3 Sample preparation and characterization

In this section, basic sample characterization results obtained by the above-mentioned techniques are introduced. Optimised parameters are selected for the sample preparation.

Composition determination

Since the films are not deposited from compositional targets with determined elemented ratios. It is necessary to determine the exact ratios of the elements in each

TABLE 2.1: ICP element ratio results

Sample	Sample Number	Co(at%)	Ni(at%)
(Co,Ni)O	No.1	33.4	66.6
	No.2	33.3	66.7
	Average	33.3	66.7
CoNi	No.1	45.6	54.4
	No.2	48.3	51.7
	Average	47.4	52.6

layer. 120nm-thick CoNi and (Co,Ni)O single layer samples are prepared. ICP analysis is conducted to determine the composition of Co and Ni in these two samples(See Tab. 2.1). The Co:Ni ratio in the metal layer is rough 1:1. In contrast, this ratio becomes 1:2 in the oxide layer.

The results indicate that the Ni has a higher content ratio at metal layer than the oxide layer. Though the target area of Ni exposed is much smaller than the Co element, Ni element seems easier to be sputtered from the target than the Co element.

2.3.1 CoNi layer

Co and Ni have the same atomic radius of 1.25 Å [44]. According to the Co-Ni phase diagram(See Figure 2.12), cobalt and nickel can form complete solid solution in the fcc phase when the nickel content is larger than 0.4. Mixing Ni and Co of various contents at a stable fcc phase will not bring any lattice distortion to the alloy. Hence, in this work, the CoNi alloy with roughly equal Co and Ni contents should be a fcc A1 structure. Since we use co-sputtering method to fabricate the CoNi alloy, Co and Ni are expected to position randomly at the lattice site.

It has been reported that PMA can be obtained in Co/Ni multilayer structures with Co:Ni = 1:2, where Co and Ni are deposited using alternate monoatomic layer depostion(AMLD). Such PMA is induced from the Co/Ni interface. The co-sputtered CoNi layer here differs from the past reports due to the half-and-half Co/Ni ratio and disordered structure. Additionally, a lowest damping parameter is expected for CoNi alloy with half-and-half Co and Ni ratio[54].

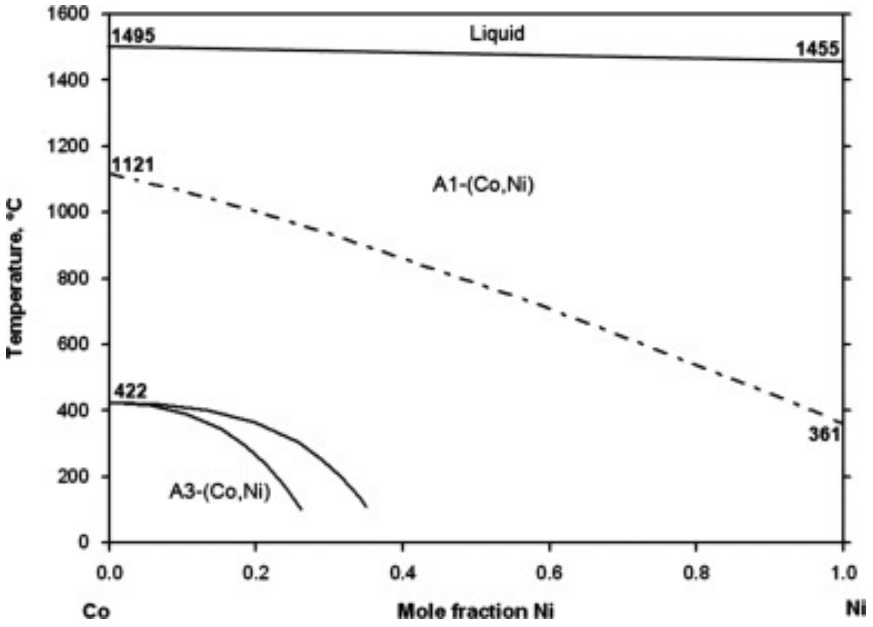

FIGURE 2.12: Co-Ni phase diagram.(adapted from [53])

2.3.2 (Co,Ni)O layer

Structural property

For (Co,Ni)O, it is well known that CoO and NiO can form homogenous solid solution regardless of proportions due to the fact that CoO and NiO share the same NaCl-type structure [55](see Table 2.2). The (Co,Ni)O is expected to have the same structure with CoO and NiO as shown in Figure 2.14 [56].

To confirm the structure of (Co,Ni)O, we observe the structure using TEM. As shown in Figure 2.14, a 12nm (Co,Ni)O single layer deposited on a glass substrate shows polycrystalline texture. The SAED pattern implies that the (Co,Ni)O is of fcc structure.

Magnetic property

We measure the magnetic property of the single (Co,Ni)O layer and find that there is no remanence magnetization, indicating that the (Co,Ni)O layer is fully oxidized.

As shown in Table 2.2, of bulk CoO and NiO, CoO presents lower Néel temperature ($T_N = 295K$) with large magnetocrystalline anisotropy at the easy magnetization plane ($K_1 = 2 \times 10^5 erg/cm^3$ *at* $4.2K$), whereas NiO shows much higher Néel temperature ($T_N = 523K$) but lower magnetocrystalline anisotropy ($K_1 =$

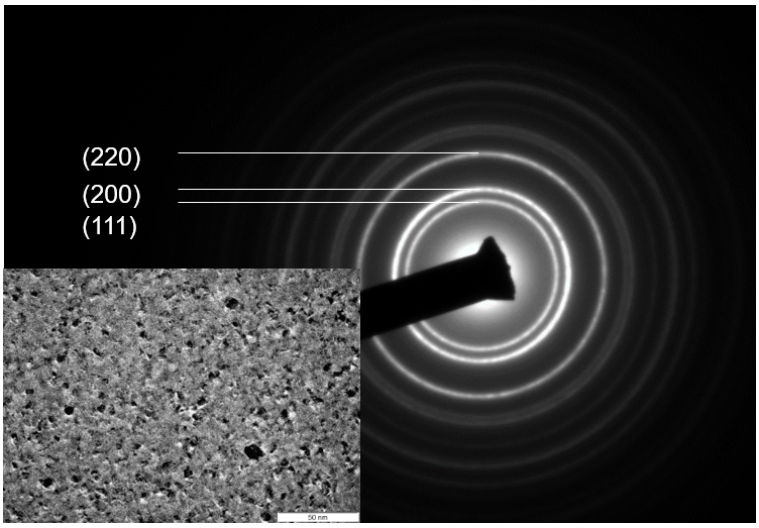

FIGURE 2.13: Transmission electron microscopy (TEM) images of a single 12nm (Co,Ni)O layer

TABLE 2.2: Comparison between CoO and NiO

Oxides	CoO	NiO
Structure	NaCl	NaCl
Lattice Parameter	4.254 Å	4.173 Å
Néel temperature	295K	523 K
Anisotropy Energy K_1	$2 \times 10^5 erg/cm^3$ $(4.2K)$	$3.3 \times 10^2 erg/cm^3$ $(300K)$

$3.3 \times 10^2 erg/cm^3$ at $300K$)[57]. By mixing both oxide, it is expected to obtain an AFM materials with a relatively high magnetocrystalline anisotropy and with a Néel temperature intermediate between those of the two oxides.

According to the previous report, the Néel temperature of $Co_xNi_{1-x}O$ varies linearly with the x. The (Co,Ni)O layer obtained here shows $x = 0.33$, thus it is determined that its $T_N \approx 447K \approx 150°C$. This value is significantly higher than the room temperature. The blocking temperature of the CoNi/(Co,Ni)O is also well above room temperature and will be discussed in the subsection below.

Moreover, it has been demonstrated that the anisotropy energy of the $Co_xNi_{1-x}O$ reaches maximum value when $x \approx 0.4$[58]. The composition of (Co,Ni)O layer in this study is relatively close to this value.

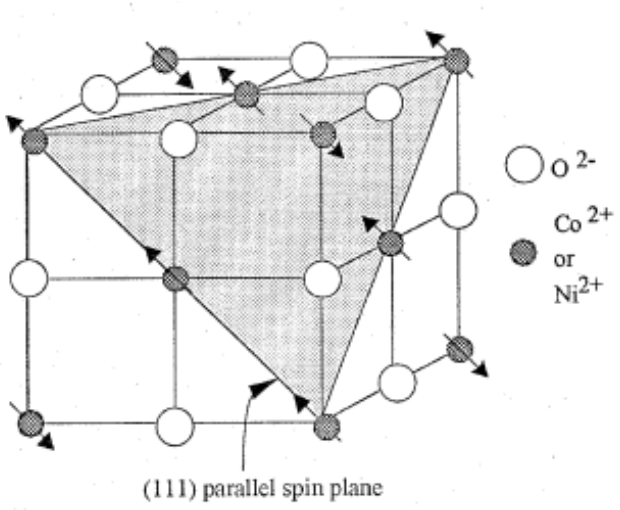

FIGURE 2.14: Possible Structure of (Co,Ni)O, showing the (111) parallel spin plane. (adapted from[56])

2.3.3 CoNi/(Co,Ni)O layered structure

Oxygen partial pressure

To determine the best oxygen partical pressure during deposition, we prepared a series of CoNi/(Co,Ni)O layered structure with same layer configuration but different oxygen partial pressure during the preparation. The results is shown in Figure 2.15. It can been seen that, increasing oxygen partial pressure during the sputtering promotes the PMA. PMA can be obtained as oxygen partial pressure is larger than 5%. However, a relatively large coercivity is still shown for in-plane loop in samples with $p_{O_2} = 7.5\%$ Optimised PMA with slanted in-plane loop is only shown for $p_{O_2} = 10\%$. This is also the maximum oxygen partial pressure available for the sputtering apparatus in this study.

Blocking temperature

Clarifying the blocking temperature of the layered structure helps understanding the discussion in the following chapters. Determination of the blocking temperature of the layered structure is conducted on a VSM. We field cooled the sample and then measure its magnetic properties by gradually heating up the sample on a VSM . The sample we choose has a structure of (Co,Ni)O (16nm)/CoNi (1.8nm)/(Co,Ni)O (16nm), which presents a PMA. The field cooling was performed at the out-of-plane direction. Hysteresis loops at different temperatures are measured while gradually

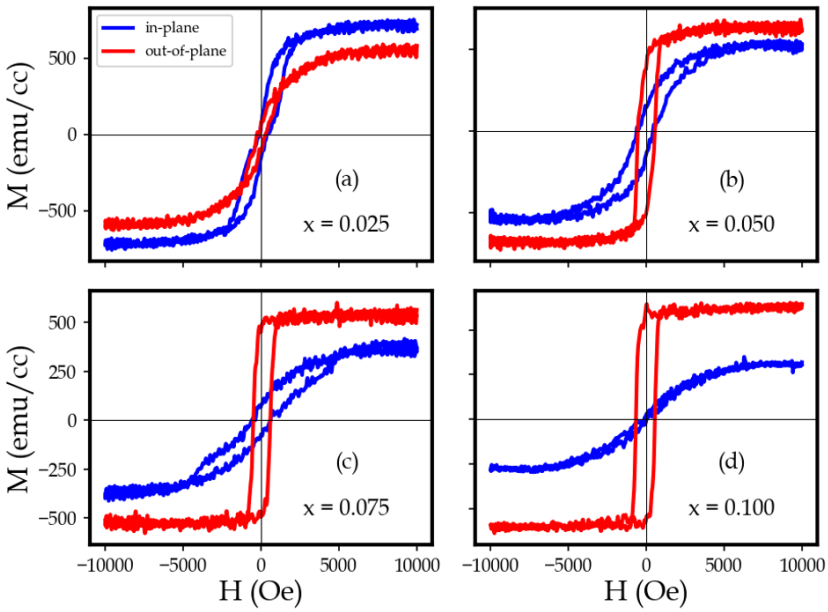

FIGURE 2.15: Effect of oxygen partial pressure on the magnetic anisotropy of the CoNi/(Co,Ni)O layered structure. All the four films have a same structure of glass/(Co,Ni)O(6nm)/[CoNi (1.8nm)/(Co,Ni)O (6nm)] with different oxygen partial pressure $((1-x)\%Ar + x\%O_2$during the preparation. (a): x = 2.5; (b): x = 5; (c): x = 7.5; (d) x = 10

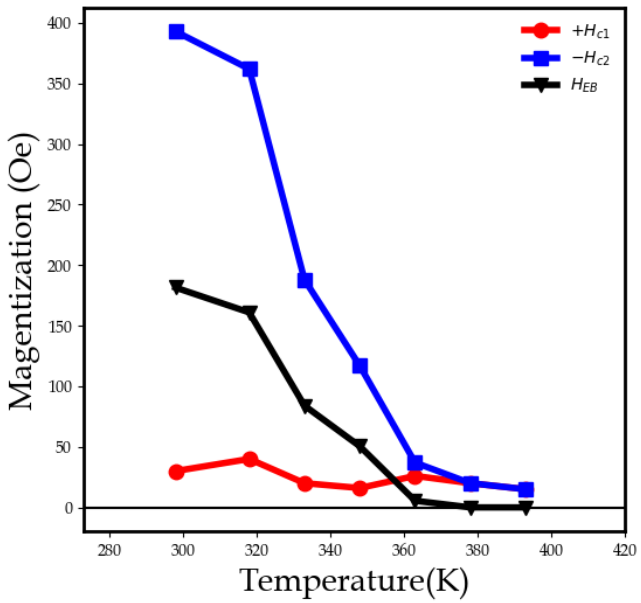

FIGURE 2.16: Measurement of the blocking temperature of (Co,Ni)O (16nm)/CoNi (1.8nm)/(Co,Ni)O (16nm) layered structure.

increasing the measurement temperature. We then extract the coercivity and exchange bias from the hysteresis loops. Figure 2.16 shows the temperature behavior of the magnetic properties of the biased sample. It can be seen that the exchange bias vanishes at the temperature around 380K $\sim$ 400K, which is the blocking temperature of this FM/AFM layered structure. Similar measurement was also performed in the in-plane direction(data not shown), a slight higher in-plane blocking temperature(400K $\sim$ 425K) is obtained.

2.4 Summary

In this chapter, the preparation and characterization methods of the CoNi/(Co,Ni)O layered structure are presented. The compositional information of the CoNi and (Co,Ni)O layer is determined. Basic properties of each layer are investigated. The CoNi layer is expected to show a fcc structure with low damping parameter. The (Co,Ni)O layer is expected to have a fcc structure with relatively high Néel temperature and large anistropy energy. We also optimized the oxygen concentration during the sputtering to ensure a large PMA for the CoNi/(Co,Ni)O layered structure.

Chapter 3

Realization of perpendicular magnetic anisotropy and room temperature perpendicular exchange bias in CoNi/(Co,Ni)O layered structures

3.1 Introduction

Exchange bias effect is a physical phenomenon usually occurs in a ferromagnetic (FM)/antiferromagnetic (AFM) layered heterostructures after field cooling through the Néel temperature(T_N) of AFM layers. Exchange bias phenomenon features as a coercivity enhancement and/or FM hysteresis loop shift in the opposite direction to the field applied during the field cooling direction[59]. The effect was firstly discovered in 1956[60], and recently it shows potential applications in spintronic devices such as magnetic sensors, magnetic recording read heads and magnetoresistance random access memory(MRAM)[61, 62]. To date, majority of the FM/AFM layered heterostructures show in-plane exchange bias since most of the magnetic thin films naturally prefer in-plane magnetization. However, magnetic devices with perpendicular magnetic anisotropy (PMA) have been proven to be better for realization of high-density, high-speed and energy-efficient MRAM applications than the traditional in-plane devices[63]. Thus, perpendicular exchange bias (PEB) receives much

more attention for the research of spintronic devices.

Currently, many film structures have been proposed to establish PMA. Among these structures, surface/interface magnetic anisotropy has been proven to be one of most critical driving mechanisms for perpendicular magnetic anisotropy. Traditionally, PMA is established in magnetic/nonmagnetic metallic multilayers, such as Co/Pt, Co/Pd, Co/Au. In these structures, PMA can be enhanced by improving the interface quality. Broeder found that annealing the Co/Au multilayers lead to a PMA for Co thickness below about 14 Å. This effect is attribute to a strongly enhanced interface anisotropy which is due to the sharpening of the interface. Previously, in our group, we established PMA in a metal/ceramics multilayer, such as CoPt/AlN, FePt/AlN and CoPt/TiN. It is found that much sharper interface can be formed in metal/ceramics multilayer than that of metal/metal multilayer. On the other hand, PMA can also be established in metal/oxide multilayer. Wang reported that CoPt/CoO interface shows good PMA performance. This PMA is attributed mainly to the positive magnetoelastic energy due to the in-plane tensile stress which originates from the local epitaxial growth at the interface. However, these studies usually use materials with heavy metals which is not economically friendly. The oxide layers involved are mostly diamagnetic oxide or antiferromagnetic oxide with low Néel temperature. Room temperature PEB requires the antiferromagnetic layer to exhibit a high Néel temperature. Thus, it is necessary to establish PMA in non-heavy metal/high T_N antiferromagnetic oxide layered structures.

In this work, CoNi/(Co,Ni)O multilayer structure is proposed to obtain PMA and room temperature PEB accordingly. CoNi alloy is a widely used materials for magnetism studies. CoNi alloy normally has a simple FCC structure[64]. (Co,Ni)O is an antiferromagnetic oxide materials also with a simple NaCl-type structure[56]. (Co,Ni)O shows higher Néel temperature and relatively larger magnetocrystalline anisotropy energy than CoO and NiO, respectively. It has been used as an AFM material to induce appropriate exchange bias at room temperature[65, 66]. We show that PMA and room temperature PEB can be observed in CoNi/(Co,Ni)O multilayer structures.

This chapter presents the realization of PMA and room temperature PEB

TABLE 3.1: Sputtering parameters

Name	Values or Description
Base pressure	$< 6.0 \times 10^{-5}$Pa
Sputtering pressure	0.2Pa
Sputtering gas for CoNi layer	Ar: 5.0sccm
Sputtering gas for (Co,Ni)O layer	$90\%Ar + 10\%O_2$: 5.0sccm
Sputtering power for CoNi layer	44W
Sputtering power for (Co,Ni)O layer	30W
Deposition rate of CoNi layer	0.02075nm/s
Deposition rate of (Co,Ni)O layer	0.02621nm/s
Substrate	Corning's EAGLE XG glass
Substrate temperature	Ambient temperature

in CoNi/(Co,Ni)O layered structures, especially in the CoNi/(Co,Ni)O multilayer structures. The investigation of structural and magnetic properties in the CoNi/(Co,Ni)O multilayer films are introduced. The influences of CoNi layer thickness, (Co,Ni)O layer thickness on magnetic anisotropy are studied. The origin of PMA in CoNi/(Co,Ni)O multilayer is discussed. The observation of PEB will also be presented.

3.2 Details on sample preparation

We investigated the role of FM layer thickness and AFM layer thickness play on the magnetic properties of CoNi/(Co,Ni)O multilayers The CoNi/(Co,Ni)O multilayers were deposited by DC magnetron sputtering. Sputtering parameters are shown in Table 3.1. We prepared two series of samples as follows:

- Films with various FM layer thickness while keeping the AFM layer thickness: Glass/(Co,Ni)O(15 nm)/[CoNi(t nm)/(Co,Ni)O(15 nm)]$_5$, t = 1.8, 2.1, 3.1, 3.7, 5.0, 6.2nm.

- Films with various AFM layer thickness while keeping the FM layer thickness: Glass/(Co,Ni)O(t nm)/[CoNi(1.8 nm)/(Co,Ni)O(t nm)]$_5$, t = 2, 4, 6, 8, 10, 16nm.

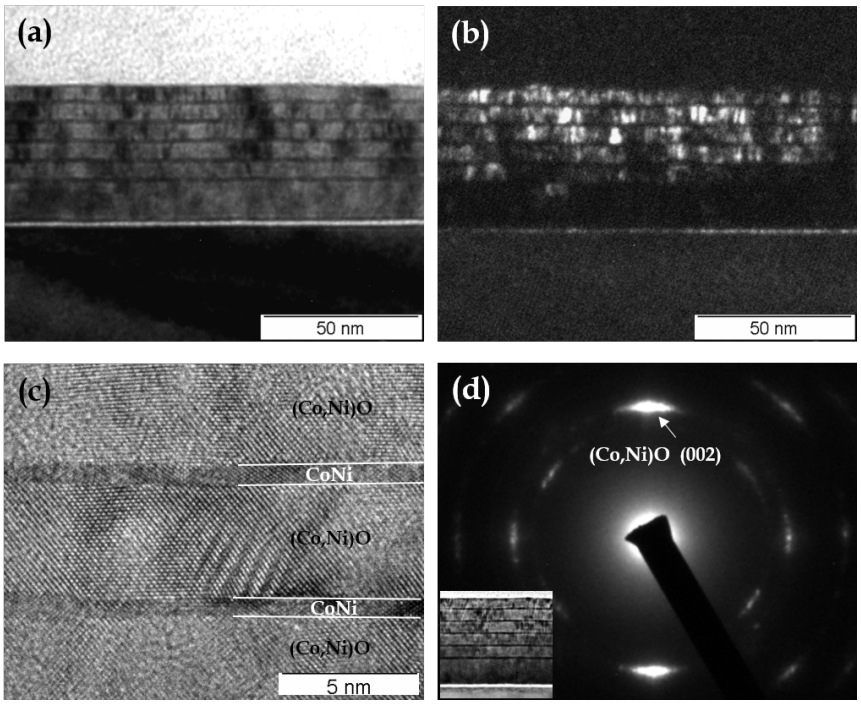

FIGURE 3.1: Cross-sectional TEM observation of $(Co,Ni)O_{16nm}/[CoNi_{1.8nm}/(Co,Ni)O_{6nm}]_5$ multilayer films deposited on thermally oxidized (111) silicon wafer: (a) bright-field (BF) TEM image; (b) dark-field (DF) TEM image; (c)High resolution(HR) TEM image of selected area in (a); (d) selected area electron diffraction (SAED) pattern, inset is the selected area for diffraction.

3.3 Structural characterization

TEM image

A high resolution cross-sectional TEM image of the typical CoNi/(Co,Ni)O multilayer deposited on a thermally oxidized silicon wafer is shown in Figure 3.1. Note that since the PMA is not sensitive to the AFM layer thickness, in order to capture more CoNi layer in a single high resolution picture, the TEM image shown here is intentionally designed with thicker bottom (Co,Ni)O layer and thinner top five (Co,Ni)O layers. We check the magnetic property and confirm that such layer thickness combination still show strong PMA. Basic structural features can be maintained compared to the one with same (Co,Ni)O layer thickness. In bright field images (Figure 3.1(a) and (c)), the CoNi and (Co,Ni)O layers are clearly distinguished. The BF-TEM images clearly show a well formed periodic structure of the multilayer. This period structure is regular through the whole thickness. The multilayer structure with thick bright (Co,Ni)O layers seperated by thin darker CoNi layers with sharp

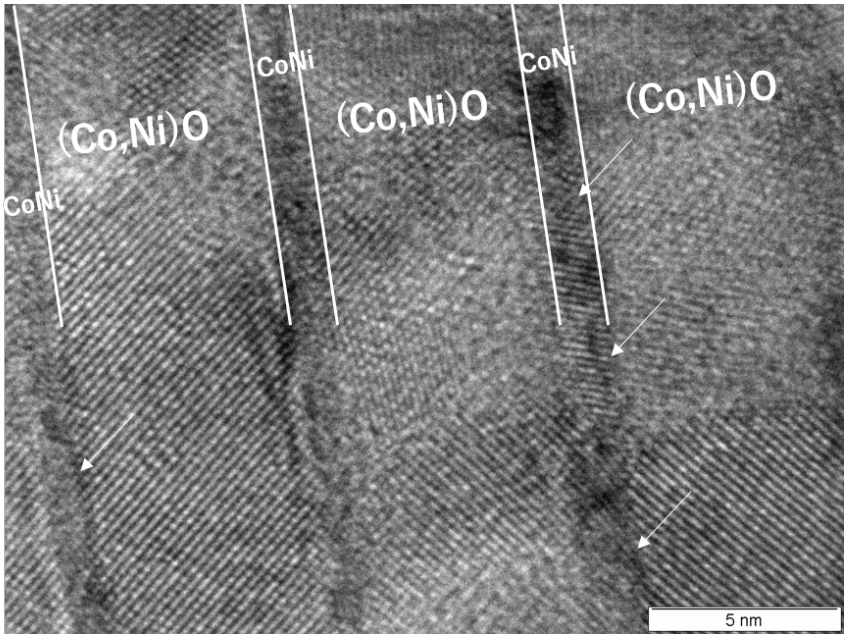

FIGURE 3.2: Cross section high resolution TEM image of the top four layers.

transition at the interface is clearly observed. The HRTEM image (Figure 3.1(c)) indicates that CoNi layers are continuous and the metal/oxide interface is fairly sharp. It is evident that smooth and sharp interface is formed without obvious intermixing or interdiffusion between CoNi and (Co,Ni)O layer.

We further study the crystallinity of the layers in DF mode (Figure 3.1(b)). The presence of bright domains suggest that the (Co,Ni)O layer is mostly polycrystallized. Interestingly, the (Co,Ni)O layers show different crystalline quality. the upper four (Co,Ni)O layers present similar high crystallinity, but the bottom (Co,Ni)O layer show rather poor crystallinity. There is no sign of texture for the CoNi layers in the DF-TEM image (Figure 3.1(b)). This suggests the CoNi layers are of poor crystallinity state. From Figure 3.2, one can see that the distinct texture difference between CoNi layers and (Co,Ni)O layers, CoNi layers do not exhibit specific texture. In some parts, CoNi layers succeed the same lattice orientation of the adjacent (Co,Ni)O layers(pointed out by arrows). However, they do show slight difference in brightness in TEM image.

The selected area electron diffraction (SAED) pattern for the as-deposited CoNi/(Co,Ni)O layer is shown in Figure 3.1 (d). The presence of broad diffraction rings indicate that a polycrystalline structure. However, some spots on the rings are

evidently brighter than the rest of the rings, suggesting that most of the grains are well oriented. The rings can be clearly seen are considered to be the diffraction of (Co,Ni)O, the diffraction pattern of CoNi is too weak to be detected. The d-spacing of the diffraction patterns in Figure 3.1(d) indicates that (Co,Ni)O layer is (002) well textured.

Two questions need to be addressed and discussed. The first question is why the (Co,Ni)O layers grown on CoNi layers show better crystalline texture. We consider that the thin CoNi layers with flat surface serve as crystalline seeds for the initial growth of (Co,Ni)O. (Co,Ni)O layer tends to crystallize easier on CoNi layer than on the glass substrate. The second question is how can we understand the smooth interface between the metal and oxide layers. It can be seen from Figure 3.1(a) the bottom (Co,Ni)O layer is of poor crystallinity, but it grows continuously probably due to the good wetting between the (Co,Ni)O layer and the glass substrate. This layer sacrifices its crystallinity to serve as a flat buffer layer[67]. Co and Ni are the components of the underneath (Co,Ni)O layer. The subsequent CoNi layer show good affinity with the oxide buffer layers. Therefore, although the CoNi layer is very thin, it grows continuously and no significant oxygen diffusion occurs. In some cases, if the residual strains in the film is too large, microtwins could form near the metal/oxide interface to roughen interface[68]. However, near the CoNi/(Co,Ni)O interface, microtwinning is hardly observed. It is considered that the residual strains are small in the film during the growth.

X-ray diffraction profile

X-ray diffraction(XRD) is a powerful tool to investigate the microstructure of thin films. We performed the out-of-plane scan on the thin flim by using the conventional Bragg-Brentano XRD measurements. The measurements are conducted on a JDOX-3500 diffractometer with Cu K_α(λ = 1.5406 Å) irradiation and operated at 40kV, 300mA. Typical results will be given and discussed in this section.

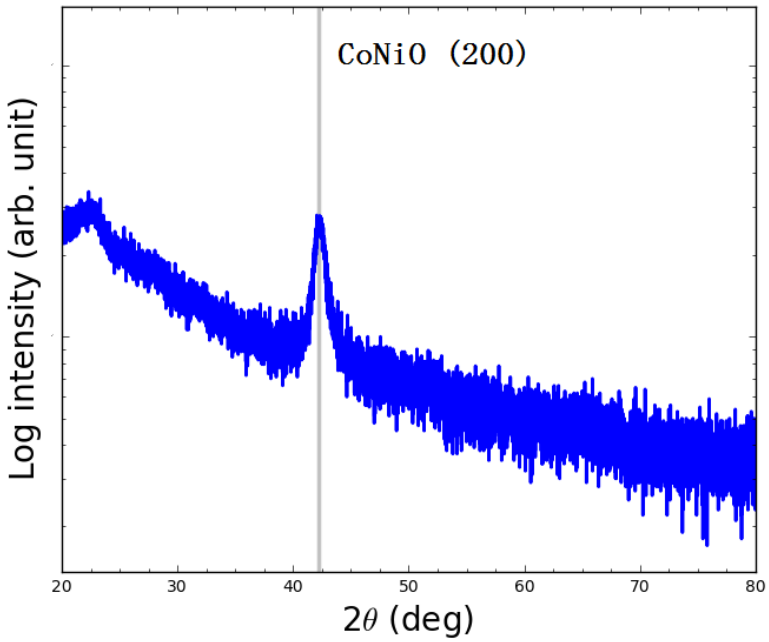

FIGURE 3.3: XRD profile of Sub/(Co,Ni)O(16nm)/[CoNi(1.8nm)/(Co,Ni)O(16nm)]$_5$ at as-deposited state.

Typical XRD profile of CoNi/(Co,Ni)O multilayers

Figure 3.3 shows a typical XRD profile of the CoNi/(Co,Ni)O multilayer sample deposited at glass substrate. Only one significant peak can be observed. The existing film peak is near $2\theta = 42.5°$, which corresponds to the (002) plane of the (Co,Ni)O layers. This indicates that the (Co,Ni)O layer show preferred orientations of FCC[001] parallel to the growth direction, which is consistent with TEM observation. However, no evident diffraction peak for CoNi layer can be found in the XRD profile. One possible reason is the poor crystallinity of the CoNi layer. Another possible reason for the lack of CoNi peak is the layer is too thin to be detected by the normal XRD scan.

To clarify which is the main reason, we conduct XRD scans on samples with various CoNi layer thickness. Figure 3.5 shows the XRD profile of the CoNi/(Co,Ni)O multilayer structure in function of the CoNi layer thickness. It is obvious that no significant difference can be found among the curves. Only one strong peak is observed for all the curves, referring to the (001) plane of (Co,Ni)O. It means that all the multilayer structures show high quality (001) texture of (Co,Ni)O layers and poor crystallinity of CoNi layers.

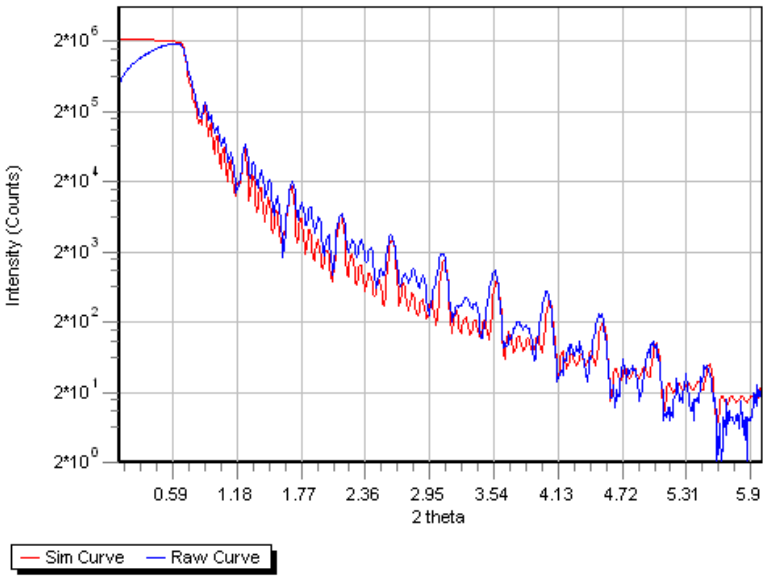

FIGURE 3.4: The typical XRR curve for the as-deposited CoNi/(Co,Ni)O multilayers

X-ray Reflectivity profile

We performed the X-ray reflectivity measurements to investigate the interface roughness of the multilayer structure. The measurement is conducted on a Bruker D8 advance diffractometer with Cu $K_\alpha(\lambda = 1.5406$ Å) irradiation and operated at 40kV and 300mA. Figure 3.4 shows the XRR profile for the CoNi/CoNiO multilayers together with the best fit to the data using Parratt's formalism. Very clear XRR oscillations can be observed. Only well defined interface can produce such evident oscillations. The fitting results show that the average root mean square (RMS) roughness of the interfaces is around 0.46nm. It indicates that the CoNi layer grows continuously with sharp and smooth interfaces, which is consistent with TEM observation.

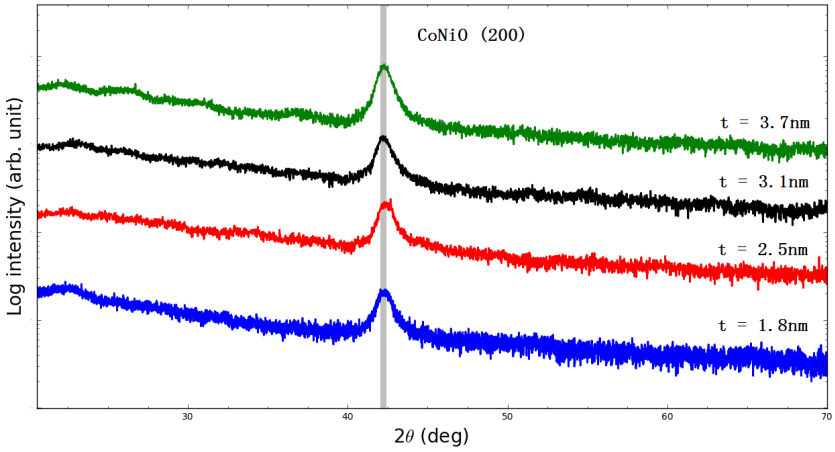

FIGURE 3.5: XRD profile of [(Co,Ni)O(16 nm)/CoNi(t nm)]$_5$/(Co,Ni)O(16 nm).t = 1.8,2.5,3.1,3.7 nm

3.4 Magnetic anisotropy of the CoNi/(Co,Ni)O multilayer structures

Magnetic anisotropy in function of CoNi layer thickness

We next turn to the magnetic properties of the multilayer films. We measure the magnetization of single layer (Co,Ni)O film and find that the (Co,Ni)O film does not show obvious magnetization. It indicates that the Co and Ni are fulled oxidized. The hysteresis loop of CoNi/(Co,Ni)O multilayer structure is measured by varying the thickness of the CoNi layer while fixing the (Co,Ni)O layer thickness. Results are shown in Figure 3.6. It is seen that the easy magnetization axis changes from out-of-plane direction to in-plane direction with the increase of the CoNi layer thickness. Strong PMA is established in the multilayer structure with the CoNi layer thickness of 1.8nm. Larger CoNi layer thickness results in larger in-plane magnetic anisotropy. Between the thickness of 2.5nm and 3.1nm, the films show magnetic "isotropy".

Moreover, the layer thickness affects the coercivity of CoNi/(Co,Ni)O multilayers differently for the in-plane and out-of-plane hysteresis loops.3.7 For the in-plane loop, the coercivity increases as the CoNi layer thickness increases. In contrast, for the out-of-plane loop, the coercivity decreases as the CoNi layer thickness increases.

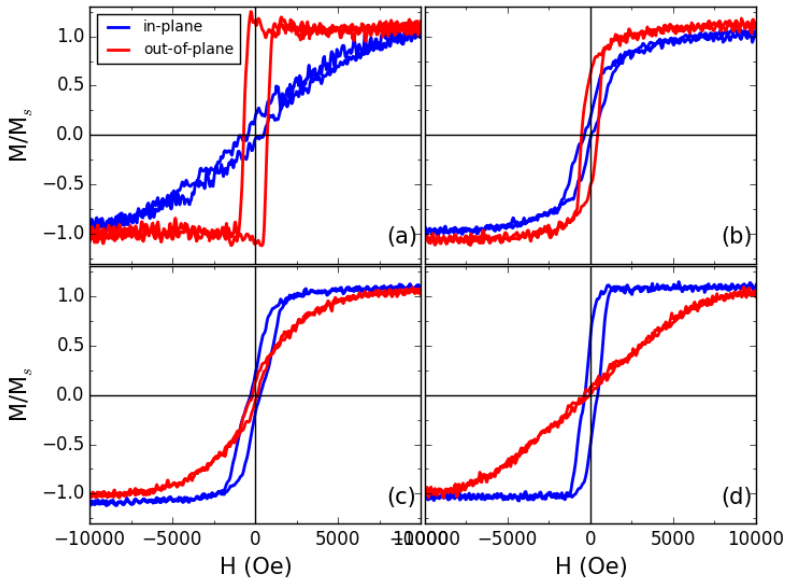

FIGURE 3.6: Magnetic hysteresis loops of [(Co,Ni)O(16 nm)/CoNi(t nm)]$_5$/(Co,Ni)O(16 nm).t = (a)1.8, (b)2.5, (c)3.1, (d)3.7 nm.

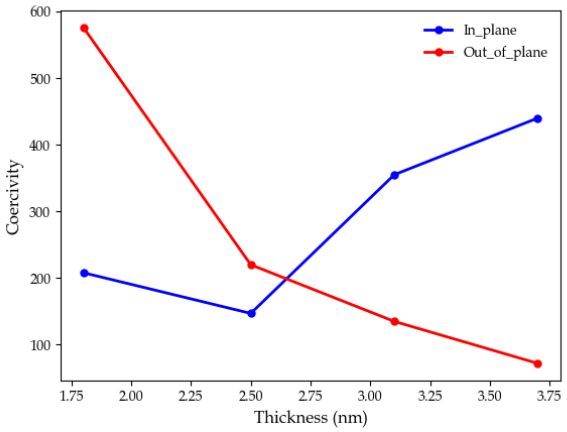

FIGURE 3.7: Coercivity of in-plane and out-of-plane hysteresis loop of [(Co,Ni)O(16 nm)/CoNi(t nm)]$_5$/(Co,Ni)O(16 nm).t = (a)1.8, (b)2.5, (c)3.1, (d)3.7 nm.

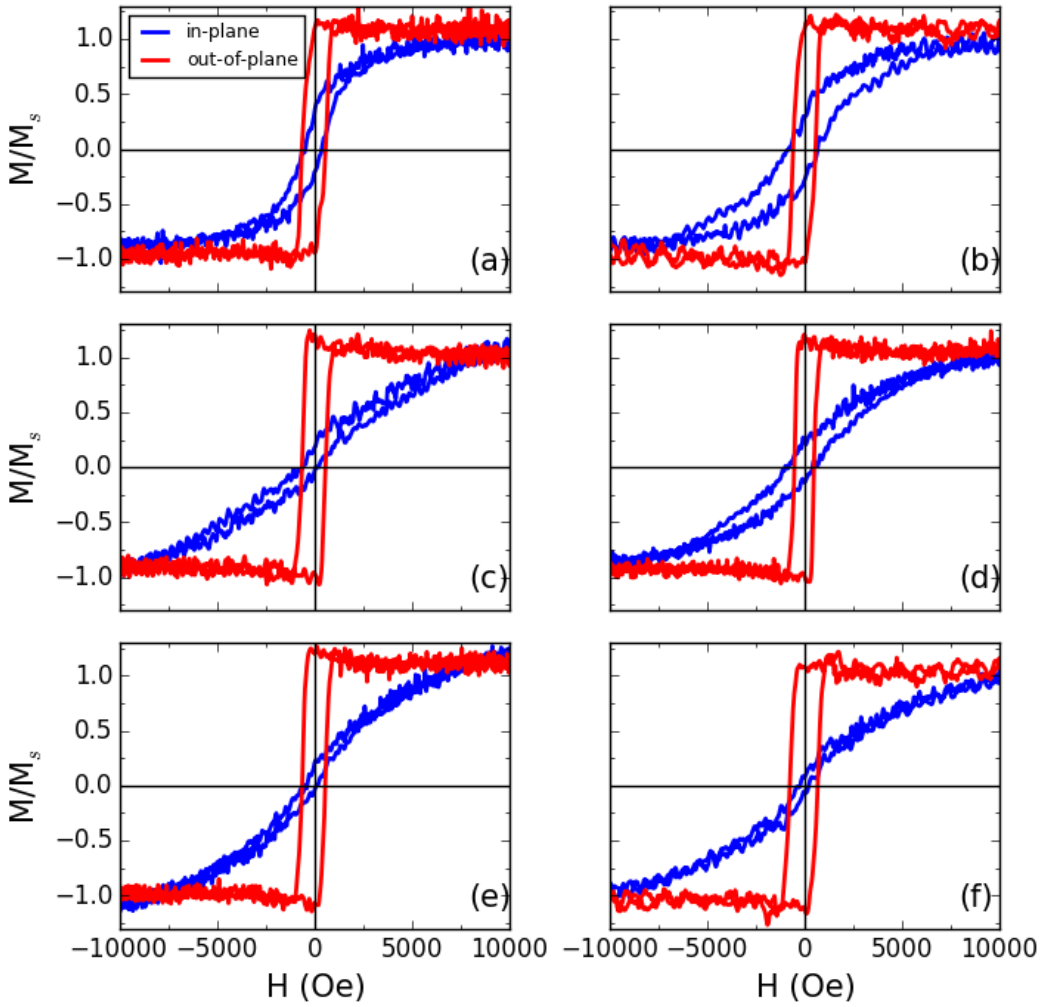

FIGURE 3.8: The hysteresis loops of (Co,Ni)O(t nm)/[CoNi(1.8nm)/(Co,Ni)O(t nm)]$_5$ multilayers with different (Co,Ni)O layer thicknesses: (a) t = 2nm, (b) t = 4nm, (c) t = 6nm, (d) t = 8nm, (e) t = 10nm, (f) t = 16nm

Magnetic anisotropy in function of (Co,Ni)O layer thickness

The (Co,Ni)O layer thickness effect on the magnetic anisotropy in the samples is also investigated. The corresponding results are shown in Figure 3.8. (Co,Ni)O layer thickness varies from 2nm to 16nm. All the hysteresis loops show strong PMA. For multilayer structures with thin (Co,Ni)O layer thickness (t = 2, 4nm), the out-of-plane hysteresis loop shows slightly distorted rectangular shape($M_s \approx M_r$) , whereas the in plane hysteresis loop shows relatively large coercivity(as large as the out-of-plane loop). For multilayer structures with medium (Co,Ni)O layer thickness (t = 6, 8nm), the out-of-plane hysteresis loop shows normal shape of rectangular with

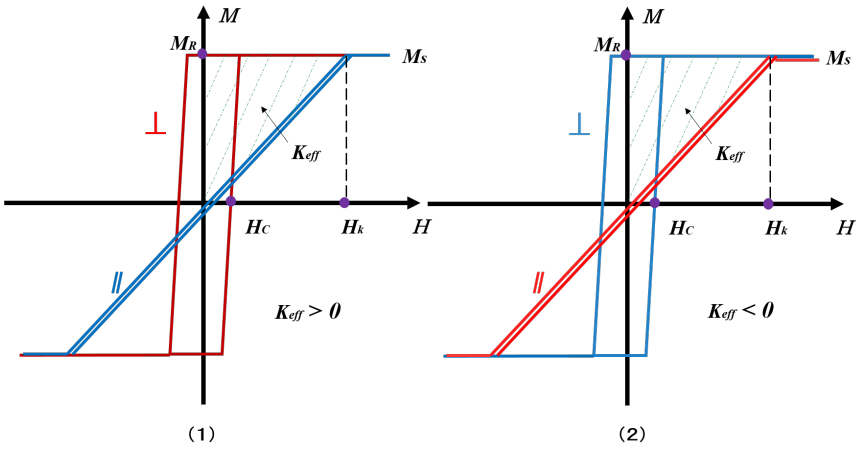

FIGURE 3.9: In-plane ∥ and out-of-plane ⊥ magnetic hysteresis loop of two films with (a) perpendicular magnetic anisotropy, (b) longitudinal magnetic anisotropy

$M_s = M_r$, whereas the in-plane hysteresis loops exhibits a relatively large coercivity. For multilayer structures with large (Co,Ni)O layer thickness (t = 10, 16nm), the out-of-plane hysteresis loops keep in a normal shape of rectangular, and the in-plane hysteresis loop shows small coercivity.

The magnetic anisotropy of the multilayer structure is less sensitive to the (Co,Ni)O layer thickness than the CoNi layer thickness. The (Co,Ni)O layer barely has influence on the PMA unless its thickness is smaller than 2nm. The (Co,Ni)O layer thickness range to show PMA of CoNi/(Co,Ni)O multilayer structure is between 2nm and 20nm.

Origins of the PMA in CoNi/(Co,Ni)O multilayer films

Effective magnetic anisotropy energies K_{eff}. is a quantitative indicator for the quantity of perpendicular exchange bias, which is refer to the area between longitudinal and perpendicular hysteresis loops, as shown in Figure 3.9.

If the sample shows PMA, K_{eff} is defined as positive, otherwise, it is negative. However, if the sample shows large coercivity, we will average the calculation value based the ascending and descending branch.

As shown in Figure 3.10 , the energy density $\frac{E}{V}$ of the CoNi/(Co,Ni)O layered structure can be described as:

$$\frac{E}{V} = K_v sin^2\theta - \frac{1}{2}\mu_0 M_s^2 sin^2\theta + \frac{(K_{s1} + K_{s2})}{t_{FM}} = K_{eff} sin^2\theta \tag{3.1}$$

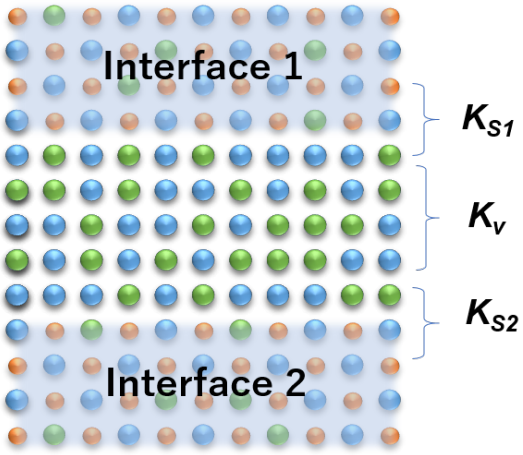

FIGURE 3.10: Energy contributions of the CoNi/(Co,Ni)O layered structures

where the first term $K_v sin^2\theta$ is the bulk anisotropy energy, the second term $\frac{1}{2}\mu_0 M_s^2 sin^2\theta$ is the demagnetization energy(magnetic shape anisotropy energy) and the third term $\frac{(K_{s1}+K_{s2})}{t_{FM}}$ is the interface anisotropy energy. Since K_{s1} and K_{s2} are identical, we can combine them together. Thereby, modifying the Equation 3.1, the K_{eff} of a multilayer can be phenomenologically written as a function in terms of the magnetic layer thickness, the volume anisotropy $(K_v - \frac{1}{2}M_s^2)$ and the interface anisotropy K_s:

$$K_{eff} \times t = (K_v - \mu_0 \frac{1}{2} M_s^2) \cdot t + 2K_s \tag{3.2}$$

where $2K_s$ indicates the interface anisotropy of top and bottom interfaces of a magnetic layer. Here, since the two interfaces are identical, we simplify this term as $2K_s$

Figure 3.11 shows the relationship between the term of $K_{eff} \times t$ and t. The value of $K_{eff} \times t$ decreases linearly with the increase of thickness, in a well agreement with the Equation 3.2. The maximum effective magnetic anisotropy energy is as large as $2.55 \times 10^6 erg/cm^3$ when the CoNi layer thickness is 1.8nm. By fitting the scattered data with a linear line, one can confirm the linear trend of the data and determine the terms of $(K_v - \mu_0 \frac{1}{2} M_s^2)$ and K_s from the vertical-axis and slope of the fitting line. In this case, the volume anisotropy $(K_v - \mu_0 \frac{1}{2} M_s^2)$ is determined as $-0.713 \times 10^6 erg/cm^3$ and the interface anisotropy $K_s^{CoNi/(Co,Ni)O}$ is determined as $0.931 erg/cm^2$. The interface anisotropy term is a significant large positive value and the volume anisotropy is an negative value. Thus, interface anisotropy has a positive contribution to the perpendicular magnetic anisotropy. It indicates

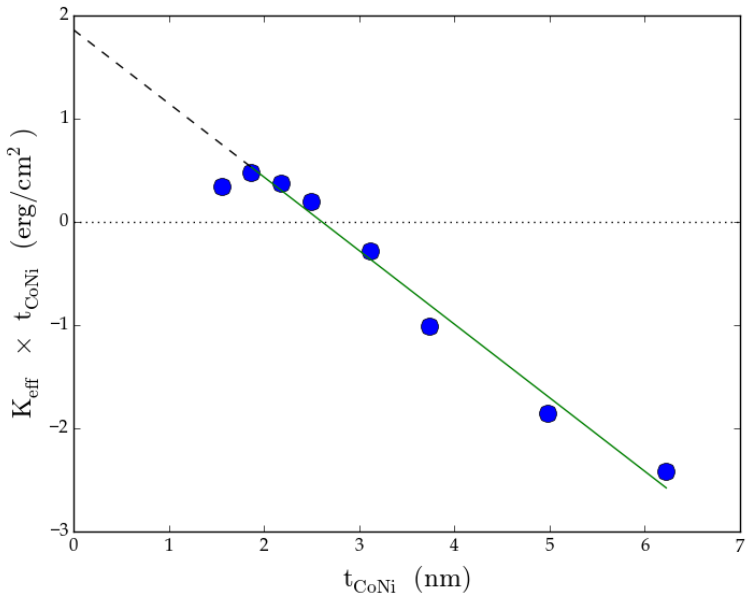

FIGURE 3.11: The effective magnetic anisotropy energy K_{eff} times the individual CoNi layer thickness t_{CoNi} vs t_{CoNi}

that the strong perpendicular magnetic anisotopy(positive K_{eff}) originates from the interface anisotropy. Since the poor crystallinity of the CoNi layers, it is difficult to obtain strain-induced perpendicular anisotropy at the interface. Moreover, the $K_s^{CoNi/(Co,Ni)O}$ is comparable with the interface anisotropy energy density reported at the Co/NiO interface ($K_s^{Co/NiO}$ = 1.075 ergs/cm^2)[69], and much larger than the one at the Ni/CoO interface($K_s^{Ni/CoO}$ = 0.186 ergs/cm^2)[70]. Therefore, we consider that the exchange coupling and the hybridization effect existing at the transition metal/oxide interface both contribute to the PMA[69, 71]. However, at this stage, we can not determine which plays the major role in the PMA. The CoNi layer thickness dependence of PMA can be well explained by the decrease of the contribution from the interface anisotropy due to the increase of CoNi layer thickness.

Annealing effect on the multilayer film

The thermal stability of the multilayer film is also investigated. We annealed the multilayer film samples showing PMA at two temperatures: T$_{ann}$ = 200°C and T$_{ann}$ = 300°C for a relatively long time as 3h. The results are shown in Figure 3.12. Although both of the films show a slight reduction of magnetization, the film annealled at

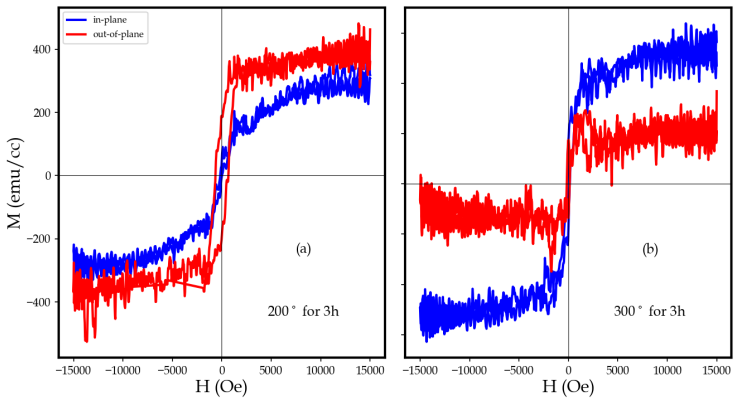

FIGURE 3.12: Annealing effect on the (Co,Ni)O(16 nm)/[CoNi(1.8nm)/(Co,Ni)O(16 nm)]$_5$ multilayers with different temperatures for 3h: (a) T$_{ann}$=200 ∘C, (b) T$_{ann}$=300°C

200°C still exhibits PMA, whereas the film annealed at 300°C becomes totally in-plane anisotropy. It indicates that the PMA sustains after annealing at low annealing temperature, but diminishes at high annealing temperatures.

We also check the thin film sample annealed at 300°C and compare it with the as-deposited samples using auger depth profile. As shown in Figure 3.13, the as-deposited film shows clear wave-like curves for both oxide and metal elements. It indicates the sharp metal/oxide interfaces. Conversely, after annealing, such amplitude of the wave-like curves degrades significantly, especially at bottom layers. Nevertheless, amplitude sustains a relatively large value where is closed to the sample surface. As we have mentioned above, this multilayer shows improved AFM layer texture at top layers than the bottom layers. It is well known that oxygen diffuse at a faster speed at the grain boundary areas than at the volume areas[72]. The well-established texture of the upper AFM layers with larger grain sizes holds lower grain boundary density, reducing the total oxygen diffusion possibility, consequently keeping the CoNi layer from oxidation. It suggests us that the thermal stability of the multilayer structure can be greatly enhanced by improving the texture.

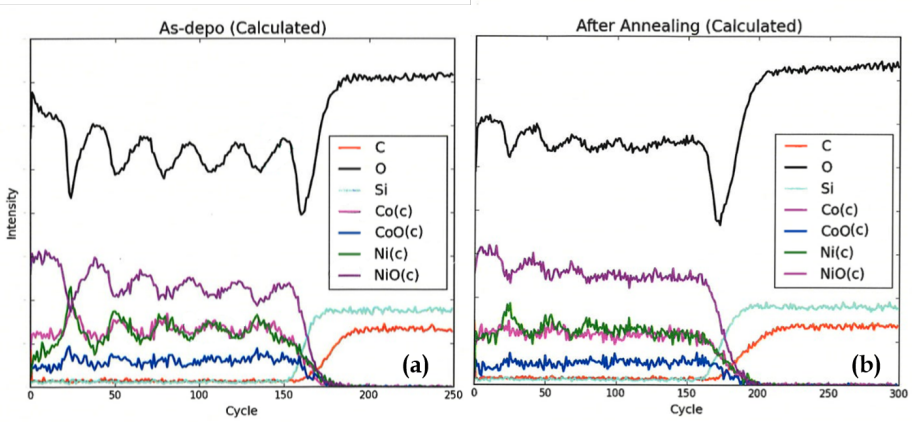

FIGURE 3.13: Auger depth profil of (Co,Ni)O(16 nm)/[CoNi(1.8nm)/(Co,Ni)O(16 nm)]$_5$ multilayers before(as-depo) and after annealing at T_{ann}=300°C for 3h

Domain observation by lorentz transmission electron microscopy

In this subsection, we show the domain observation of the multilayer films using lorentz transmission electron microscopy(LTEM). LTEM is a powerful tool to observe the magnetic domain of thin films at nanometer-scale. Compare with the magnetic force microscopy, LTEM can acquire richer information of the sample, such as the domain structure, domain wall structure and correlation between the domain structure and the morphological materials structure. However, conventionally, LTEM is use for observe in-plane magnetic domain due to the fact that only the electron perpendicularly passes through a horizontal magnetic field could receive the act of lorentz force. To observe the sample with PMA, one should rotate the sample to a certain angle to produce a longitudinal component of the magnetic field.

Multilayer film with several periods of repetition, can provide enough longitudinal component of magnetic field inside a sample upon a rotation. We prepare a sample with structure of (Co,Ni)O_{16nm}/[$CoNi_{1.8nm}$/(Co,Ni)$O_{1.2nm}$]$_5$/$CoNi_{1.8nm}$/(Co,Ni)O_{12nm} on a ELS-10 substrate. Hysteresis loop of the investigated sample is presented in Figure 3.14(a), where a strong PMA is shown. Under a Frensel mode of TEM, we rotate the sample to an angle of 21°. In an in-focus mode, only the surface of the sample can be observed(See Figure 3.14). By tuning the focus to a under-focus or over-focus mode, magnetic domain pattern appears. The under-focus and in-focus image show domain wall structures with reversed contrast to each other.

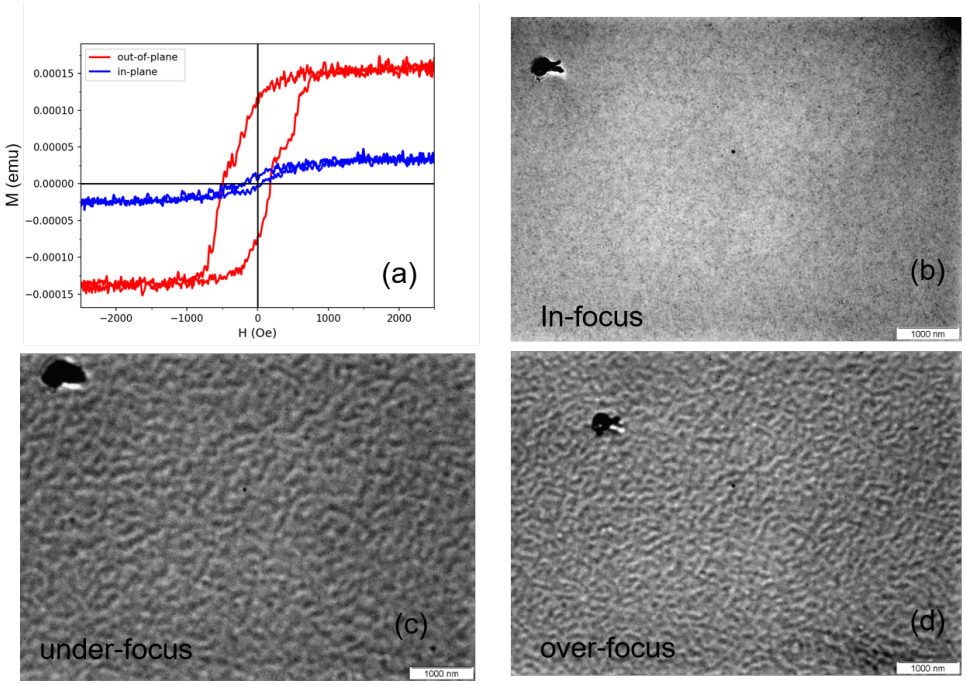

FIGURE 3.14: Lorentz domain observation of (Co,Ni)O_{16nm}/[$CoNi_{1.8nm}$/(Co,Ni)$O_{1.2nm}$]$_5$/$CoNi_{1.8nm}$/(Co,Ni)O_{12nm}:(a) hysteresis loop of the investigated sample; (b)in-focus planar view LTEM image with a 21° tilting; (c)under-focus planar view LTEM image with a 21° tilting; (d)over-focus planar view LTEM image with a 21° tilting;

The remanence domain pattern of the thin film clearly shows thin strip domain wall structures mixed with bubble structures. The sizes of the strip domain wall structures is not homogenous. Owing to the curvature of the sample, it is difficult to determine the domain wall type of the sample. However, stripe domain structures can also be seen in a under-focus or over-focus TEM observation mode without any rotation(data not shown). We consider that, most of the domain walls are Bloch type. Although, there may also exist Néel type of domain walls.

3.5 Exchange bias in the CoNi/(Co,Ni)O multilayer structures

Introduction

Exchange bias (EB), is a horizontal shift of the hysteresis loop due to the interfacial exchange coupling between ferromagnetic (FM) and antiferromagnetic (AFM) layers

after magnetic field cooling below the Néel temperature of the AFM. EB is usually established along the easy magnetization axis of the FM materials of the film.

With the development of perpendicular magnetized FM/AFM structures, perpendicular magnetized FM/AFM structures with PEB is considered to be critical building blocks of spintronics, especially in ultra-high density magnetoresistance random access memory.

Currently, PEB has been observed in CoPt/(CoO, FeMn, IrMn, FeF_2) films with PMA after perpendicular field cooling. In the previous section, we have established PMA in CoNi/(Co,Ni)O multilayer structure and discussed the mechanisms of the PMA. Since CoNi is a FM material and (Co,Ni)O is an AFM material, it can be predicted that this CoNi/(Co,Ni)O layered structure may also show PEB. Moreover, (Co,Ni)O has a Néel temperature higher than the room temperature, PEB may exist at room temperature.

For an initial study of PEB in this structure, in this chapter, we establish and investigate the PEB in this structure, especially the room temperature PEB.

Exchange bias

Exchange bias(H_e) refers to the interfacial interaction between a ferromagnetic(FM) and an antiferromagnetic(AFM) layer, manifesting itself as a horizontal shift of the hysteresis loop away from the zero axis. In the shift state, the spins of the FM layer at the interface are pinned by the uncompensated spins of the AFM layer. The magnitude of this loop shift is related to the strength of this pinning effect in the FM-AFM interface. It is shown that:

$$H_e \propto \sqrt{AK} \tag{3.3}$$

where A and K are refer to the exchange constant and magnetocrystalline anisotropy of the AFM layer, respectively. Typically, for cubic-anisotropy AFM materials, K follows a temperature dependence that:

$$K(T) = K(0)(1 - \frac{T}{T_b})^2 \tag{3.4}$$

where T_b is called the blocking temperature, above which the H_e is zero. Therefore, combining the equation 3.3 and equation 3.4, for temperature below the blocking

temperature $T < T_b$, we can get [57]:

$$H_e \propto \sqrt{AK(0)}(1 - \frac{T}{T_b}) \tag{3.5}$$

Typically, the blocking temperature T_b of an AFM material is related with and slightly smaller than the Néel temperature T_N of the AFM material. In order to obtain large exchange bias at high temperature, AFM materials with large magnetocrystalline anisotropy and high Néel temperature is preferred to couple with the FM materials.

Of bulk CoO and NiO, CoO presents lower Néel temperature ($T_N = 293K$) with large magnetocrystalline anisotropy at the easy magnetization plane ($K_1 = 2 \times 10^5 erg/cm^3$ *at* $4.2K$), while NiO shows much higher Néel temperature ($T_N = 523K$) but lower magnetocrystalline anisotropy ($K_1 = 3.3 \times 10^2 erg/cm^3$ *at* $300K$). By mixing both oxide, we may obtain an AFM materials showing a relatively high magnetocrystalline anisotropy and with a Néel temperature above room temperature.

Exchange bias is usually obtained along the easy magnetization axis of the FM materials. In the previous chapter, we have successfully established PMA in the CoNi/(Co,Ni)O multilayer structures. We expect that room temperature PEB could also be established since CoNi is an FM material with PMA and (Co,Ni)O is an AFM material with high T_N.

Perpendicular exchange bias

The exchange bias effect of the multilayer films is investigated. We field cooled two kinds of samples with different magnetic anisotropy from 160°C to room temperature with 5 kOe external magnetic field applied in different directions. Figure 3.15(a) shows out-of-plane hysteresis loop of CoNi/(Co,Ni)O multilayer film with PMA (same sample shown in Figure 3.15(a)) after perpendicular field cooling. The loop shows an exchange bias field of $H_e = 160Oe$, a coercivity field of $H_c = 675Oe$ and a squareness of $S = M(H_e)/M_{sat} \approx 0.88$. We further measured in-plane hysteresis loop of CoNi/(Co,Ni)O multilayer films with LMA (same sample shown in Figure 3.15(d)) after longitudinal field cooled in Figure 3.15(b). The loops shows an exchange bias field as large as $H_e = 470Oe$, a coercivity field of $H_C = 370Oe$ and a

squareness of $S = M(H_e)/M_{sat} \approx 0.73$. The observed exchange bias in two kinds of anisotropic configurations indicate that the uncompensated spins at the interface could be coupled in both in-plane and out-of-plane directions. Notably, the in-plane exchange bias has a H_e/H_c ratio larger than 1. The exchange bias value we have obtained is relative larger than the one reported in the literature [73]. It indicates that the (Co,Ni)O have a balanced Néel temperature and magnetic anisotropy energy by mixing high T_N, low anisotropy NiO with low T_N, high anisotropy CoO. According to the phenomenological model developed by Carey, (Co,Ni)O AFM materials with NiO concentration near 0.6 shows optimized properties(Néel temperature and magnetic anisotropy) to serve as a pinning layer[58]. The (Co,Ni)O layer we use have a Ni concentration of 0.67, which is quite close to Carey's suggestion. In addition, as an interface effect, the exchange bias is also sensitive to the interface quality. The sharp FM/AFM interface also helps to align interfacial spins, which improves the exchange coupling and results in a large exchange bias field.

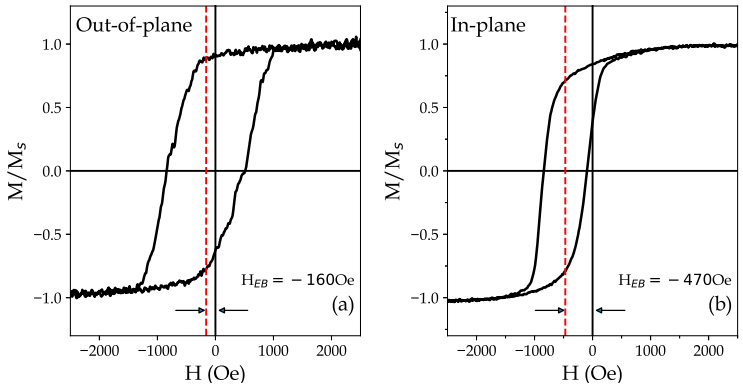

FIGURE 3.15: (a)Out-of-plane room temperature(300K) hysteresis loop of (Co,Ni)O_{16nm}/[$CoNi_{1.8nm}$/(Co,Ni)O_{16nm}]$_5$ multilayer film with PMA after perpendicular field cooling from 160°C at 5kOe; (b)In-plane room temperature(300K) hysteresis loop of (Co,Ni)O_{16nm}/[$CoNi_{3.7nm}$/(Co,Ni)O_{16nm}]$_5$ multilayer film with PMA after longitudinal field cooling from 160°C.

It has been shown that the multilayers can be exchange coupled both at in-plane or out-of-plane directions. The in-plane exchange bias has a larger shift than the out-of-plane one. It seems that the uncompensated AFM spins are more easily to be magnetized in the film plane direction than the film normal direction. Such distinct difference is considered due to the demagnetization effect. Demagnetization effect

also effect on the uncompensated AFM spins, leading them to favor the film plane than the film normal plane.

We then study the effect of AFM layer thickness on the exchange bias field and coercivity(Figure 3.16). The H_e and H_C follow a peak like behavior. The H_e has a maximum value at the AFM layer thickness around 16nm. Such peak-like behavior is also observed at other exchange bias systems[41]. It can be attributed to the domain wall stability of the(Co,Ni)O layer. It is considered that 16nm is the critical thickness for the domain wall stability of the (Co,Ni)O layers. For $t_{(Co,Ni)O} <$ 16nm, H_e decreases as the AFM layer thickness reduces. When the AFM layer is thin, (Co,Ni)O domain wall is not sufficiently stable, so that it can not strongly pin the magnetization direction of the adjacent CoNi layer, which only leads to enhanced H_C with small H_e. On the other hand, for $t_{(Co,Ni)O} > 16nm$, the decline in the H_e for thicker AFM layer thickness is due to the reduction of domain wall density. Because further increase of AFM thickness will cause the formation of large magnetic domains which consequently decrease the density of domain walls. The decreased domain wall density results in a reduced H_e.

We have also check the training effect of the room temperature PEB(data not shown), exchange bias, coercivity and hysteresis loop shape stay the same for consecutive measures, no evident training effect is found for this multilayer film.

3.6 Summary

In summary, the CoNi/(Co,Ni)O multilayer structures with good periodicity and high interface quality are successfully fabricated. Microstructure and magnetic properties of CoNi/(Co,Ni)O multilayer structures have been investigated. It has been found that strong PMA can be established in as-deposited film. The mechanism under the PMA has been investigated by systematically varying two factors(CoNi layer thickness and CoNiO layer thickness) and comparing their microstructure and magnetic properties. The conclusions about the magnetic anisotropy are made as follows:

- The magnetic anisotropy of the multilayer structure is sensitive to the CoNi layer thickness. Strong PMA with maximum K_{eff} value of $2.55 \times 10^6 erg/cm^3$

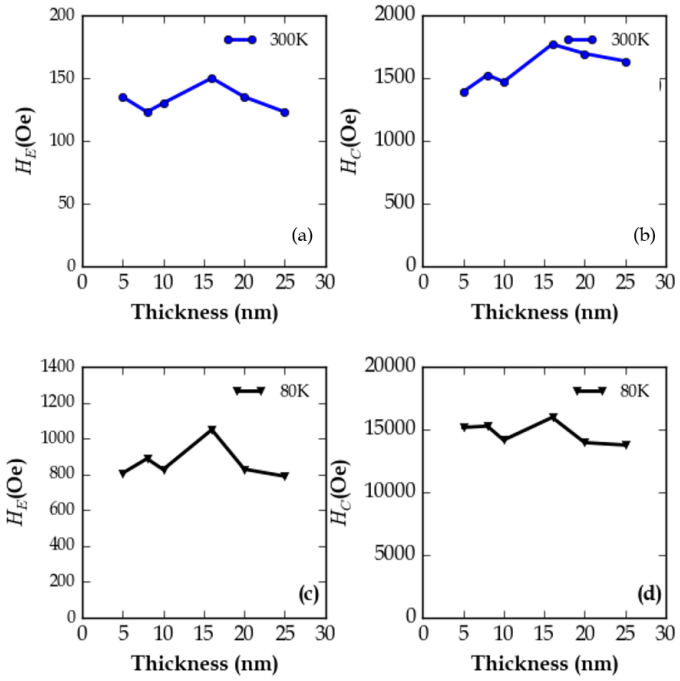

FIGURE 3.16: Variation of H_E (a,c) and H_c (b,d) with AFM thickness $t_{(Co,Ni)O}$ of the (Co,Ni)O$_{tnm}$/[CoNi$_{1.8nm}$/(Co,Ni)O$_{tnm}$]$_5$ multilayers after perpendicular field cooling to different temperatures: 80K(a,b) and 300K(c,d).

is obtained when the CoNi layer thickness is 1.8nm.

- The magnetic anisotropy of the multilayer structure is not sensitive to the (Co,Ni)O layer thickness. The (Co,Ni)O layer thickness to show PMA is between 2nm and 20nm.

- The PMA established in the CoNi/CoNiO layer is mainly from the interface anisotropy, due to the larger interfacial magnetic anisotropy energy and poor crystallinity of the CoNi layers.

Experimental results show that PEB is observed in the multilayer structure after perpendicular field cooling. Large PEB value and large coercivity are observed at low temperature. Significantly, PEB is also observed at the room temperature. This results are attributed to the success of role playing of Co and Ni in the (Co,Ni)O layer.

Chapter 4

Interface effect on the perpendicular magnetic anisotropy of the CoNi/(Co,Ni)O layered structures

4.1 Introduction

Perpendicular magnetic anisotropy(PMA) is an extensively-explored property of magnetic films. It plays a central role in various spintronic applications, particularly in magnetic random access memories(MRAM)[74, 75]. To date, PMA has been explored to display in rare-earth ferromagnet(RE-FM) alloys, $L1_0$-ordered (Co, Fe)-(Pt, Pd) alloys and transition ferromagnet(FM)/X layered structures(X refers to noble metals or metal oxides)[76]. Among these PMA frames, FM/metal oxide layered structure is considered as an ideal building block for the development of perpendicular spintronic devices since the PMA found in this frame presents high anisotropy strength together with a reduced damping parameter[27, 77]. Such PMA is known to originate from the electronic hybridization between the transition metal orbit and the adjacent oxygen across the interface[71]. This phenomenon can be commonly observed with various transition metals and metal oxides. Particularly, PMA at the FM/non-magnetic(NM) oxide (MgO, AlOx, TaOx, etc) interface has been intensively studied[71, 78].

Recently, antiferromagnetic(AFM) oxides are generating considerable interest

due to its ability to expand the functionality of the FM/AFM layered structure[40]. For instance, AFM layer can influence the adjacent FM layer by fixing the magnetization direction of the FM layer via interfacial exchange coupling[79]. It has now been demonstrated that AFM layer can also lead to the establishment or enhancement of the perpendicular magnetic anisotropy on the adjacent FM layer[80]. A recent study reports that the magnetic damping of the FM layer can be modified by the two magnon scattering at the FM/AFM oxide interface[81]. Furthermore, AFM insulator oxide can act as a tunneling barrier which provides an additional tunneling magnetoresistance[82]. Recent evidence shows that, for FM/AFM/NM layered structure, AFM oxide can influence the spin-current transmission between the FM and NM layer[83]. Spin-orbit torque strength can also be efficiently enhanced by attaching an AFM oxide layer to the FM layer[84].

Thus, it is of particular interest to explore FM/AFM oxide layer structures with interfacial PMA. Pt/Co/Cr_2O_3/Pt system has been found to exhibit interfacial PMA[85], but, due to the low Néel temperature nature of Cr_2O_3, this structure does not function at room temperature. In previous chapter, we have established a strong interfacial PMA in granular CoNi/(Co,Ni)O layered structures. The high blocking temperature allows the structure to exhibit perpendicular exchange bias at room temperature. We found that a sharp metal/oxide interface is responsible for the PMA. However, as shown in Figure 4.1, there exist two energy contribtions to PMA: the metal/oxide interfacial effect and the FM/AFM exchange coupling effect. How does the interface quality affect the interfacial PMA at the FM/AFM oxide interface remains unclear. Also, it is unclear whether FM/AFM exchange coupling plays a dominant role in the induced PMA.

In this work, we prepare (Co,Ni)O/CoNi/(Co,Ni)O layered structures on single crystal MgO(001) substrates to study the interface quality effect on the magnetic anisotropy. The (Co,Ni)O layer has a lattice parameter almost equal to the MgO[86]. It is easy to control the texture of the (Co,Ni)O by modifying the depostion condition. The CoNi layer is expected to show low magnetic damping which is suitable for energy-efficient spintronics[54]. We systematically investigated the deposition temperature effect and annealing effect on the magnetic anisotropy of the layered structure. We find that perpendicular magnetic anisotropy and smooth metal/oxide

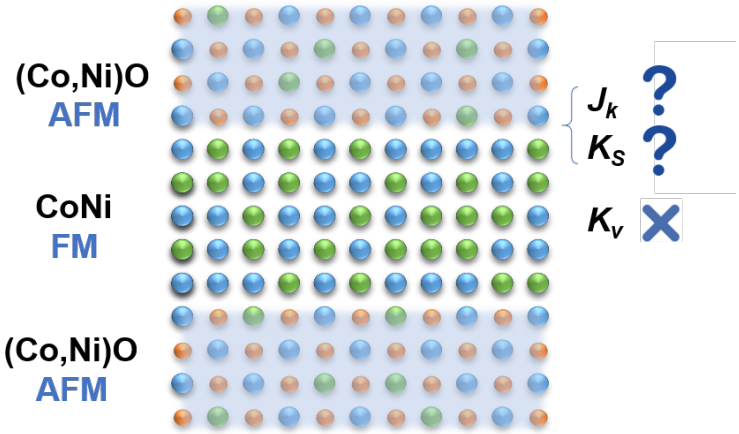

FIGURE 4.1: Schematical of energy contributions to the CoNi/(Co,Ni)O layered structure

interfaces are obtained simultaneously after annealing. We unveil the origin of the PMA by studying its temperature behavior and its relationship the structure change. We also discuss the mechanism of the metal/oxide smoothing phenomenon.

4.2 Experimental

All (Co,Ni)O/CoNi/(Co,Ni)O trilyer films were prepared on single-crystal MgO(001) by magnetron sputtering. The base pressure was better than 3.7×10^{-7} Torr and the working pressure was fixed at 1.5×10^{-3} Torr. The ferromagnet $Co_{0.47}Ni_{0.53}$ layer was DC sputter-deposited in pure argon atmosphere from two facing Co targets (A nickel chip on the bottom Co target) at a rate of 0.021 nm/s. The antiferromagnetic $Co_{0.33}Ni_{0.67}O$ layer was deposited from the same facing targets by reactive sputtering at a rate of 0.026nm/s. The bottom (Co,Ni)O layer was deposited at different substrate temperatures(T_{btm}) ranging from room temperature to 300°C. The middle CoNi and top (Co,Ni)O layers were deposited at room temperature, after the bottom (Co,Ni)O layer cooled down. Post thermal annealing at various temperatures(T_{ann} = 100 $\sim$ 400°C) for 15 minutes were carried out in a vacuum furnace under a pressure of 4×10^{-7} Torr with zero magnetic field. One mainly investigated series of samples with structure of $(Co,Ni)O_{16}/CoNi_{1.8}/(Co,Ni)O_{16}$ (nominal thickness with unit in nm) are listed in Tab. 4.1. Another series of samples with structure of $(Co,Ni)O_{16}/CoNi_x/(Co,Ni)O_{16}$ (x varies from 1.5 to 3, T_{btm} = 200°C) is prepared. Structural properties of the samples were characterized by x-ray diffrac-

TABLE 4.1: List of mainly investigated samples. All samples have the same structure: MgO(001)/(Co,Ni)O_{16}/$CoNi_{1.8}$/(Co,Ni)O_{16} with differnt treatments

label	treatment
Sample A	T_{btm} = 25°C, As-grown
Sample B	T_{btm} = 200°C, As-grown
Sample C	T_{btm} = 200°C, T_{ann} = 200°C
Sample D	T_{btm} = 200°C, T_{ann} = 350°C

tion (XRD), X-ray reflectometry (XRR) and transmission electron microscopy (TEM). The magnetic properties were measured using a vibrating sample magnetometer (VSM). Field cooling process(160 Oe and 5KOe) is also conducted on the VSM.

4.3 Results

4.3.1 Magnetic properties

Fig. 4.2(a) presents the magnetic hysteresis loop of sample A. It can be seen that this sample shows perpendicular magnetic anisotropy, which reproduce the results of previous chapter. In the case of sample B(See Fig. 4.2(b)), an in-plane easy magnetization is presented. It implies that the change of the deposition temperature of the bottom layer lead to a transition in the magnetic anisotropy of the trilayer film. Specially, the in-plane hysteresis loop of sample B shows a double branch shape. It is well known that deposite a AFM layer onto a FM layer leads to a exchange bias whose direction is determined by the orientation of the FM domains. Without a external magnetic field, the FM layer grows into domains with equally distributed orientations. These FM domains spontaneously couples with the AFM layers, results in the as-deposted sample with two branches of roughly equal size. To observe this transition in detail, we plot the out-of-plane hysteresis loop coercivity H_c and remanence ratio M_r/M_s, as a function of the bottom layer deposition temperature T_{btm} in Fig. 4.3(a). As can be seen, these two factors(M_r/M_s and H_c) follow the same decreasing trend as T_{btm} increases, and reaches a stable low value when $T_{btm} > 200°C$. We also calculated the effective magnetic anisotropy K_{eff} of the samples. K_{eff} was

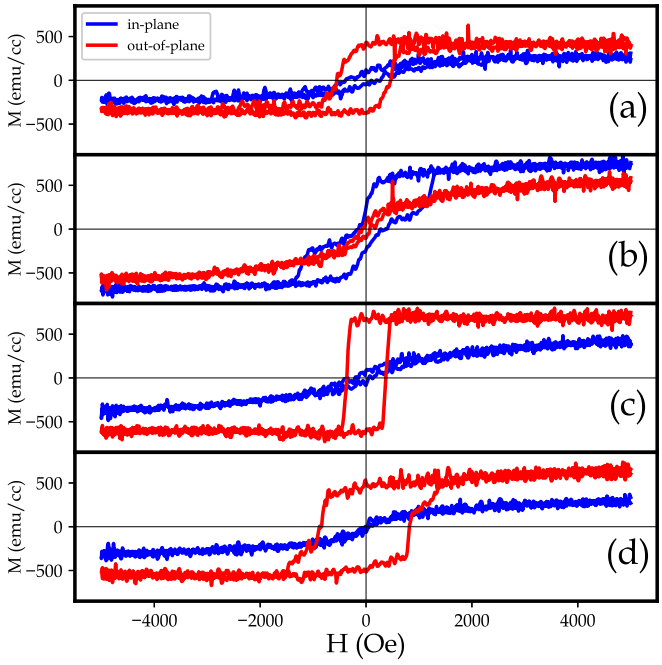

FIGURE 4.2: Room temperature hysteresis loops of mainly investigated $(Co,Ni)O_{16}/CoNi_{1.8}/(Co,Ni)O_{16}$ trilayer films:(a) Sample A; (b) Sample B; (c) Sample C; (d) Sample D.

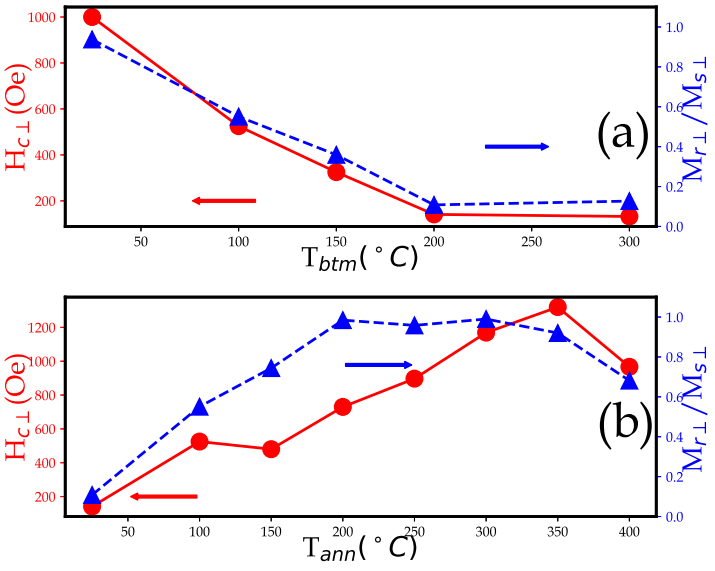

FIGURE 4.3: The out-of-plane remanence ratio $M_{r\perp}/M_{s\perp}$, out-of-plane coercivity $H_{C\perp}$ of various $(Co,Ni)O_{16}/CoNi_{1.8}/(Co,Ni)O_{16}$ trilayer film samples: (a) As-grown samples measured at room temperature in function of T_{btm}; (b)Sample B annealled at various temperatures(T_{ann}) measured at room temperature;.

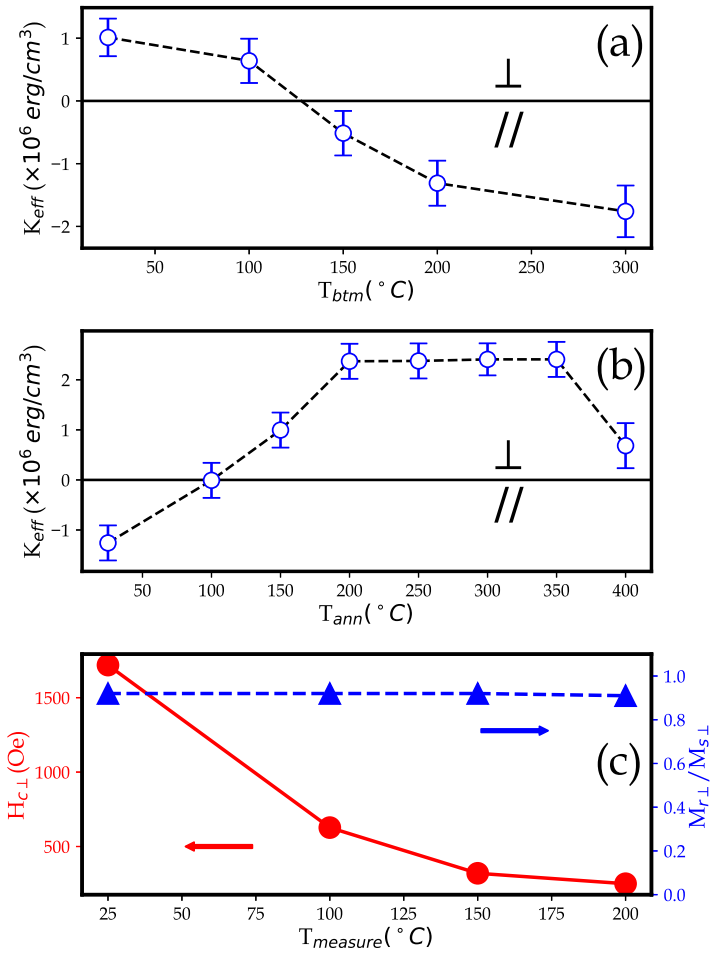

FIGURE 4.4: (a)The calculated effective anisotropy The out-of-plane remanence ratio $M_{r\perp}/M_{s\perp}$, out-of-plane coercivity $H_{C\perp}$ of various (Co,Ni)O_{16}/$CoNi_{1.8}$/(Co,Ni)O_{16} trilayer film samples: (a) As-grown samples measured at room temperature in function of T_{btm}; (b)Sample B annealled at various temperatures(T_{ann}) measured at room temperature; (c)Sample D measured at various temperatures($T_{measure}$).

determined by the following expression:

$$K_{eff} = H_k \times M_s/2. \tag{4.1}$$

where M_s is the saturation magnetization and H_k is the magnetic field needed to saturate the hard axis. Similar trend can also be observed in the calculated effective magnetic anisotropyK_{eff} in Figure 4.4(a). It indicates that a high value of T_{btm} significantly diminishes the PMA.

On the other hand, interestingly, the PMA is regained after annealing at 200 and 350 °C(see sample C and D in Figure 4.2(c-d)). The evolution of the magnetic

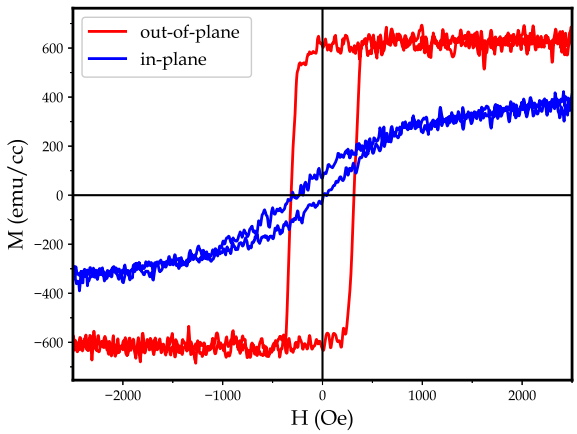

FIGURE 4.5: Room temperature hysteresis loop of Sample B after in-plane field cooling.

anisotropy with the annealing temperature T_{ann} is presented in Figure 4.3(b) and Figure 4.4(b). The magnetic anisotropy gradually transits from in-plane anisotropy to out-of-plane anisotropy as the annealing temperature increases. Strong PMA establishes as the anealing temperature exceeds 200°C, stablizes at a maximum strength until 350°C, whereas it degrades again at 400°C.

These results clearly demonstrate that the deposition temperature and bottom layer and post-deposition annealing treatment can significantly affect the magnetic anisotropy. Two possible origins are presumed of this reorienation behavior: the effect at the metal/oxide interface and the exchange coupling at the AFM/FM interface. To clarify which is the dominating factor, we check the temperature dependence of the PMA. Fig. 4.4(c) shows the out-of-plane magnetic property of Sample D measured at various temperatures. H_c $\perp$ decreases as temperature increases, whereas the remanence ratio remain the same value for the whole temperature range. We measure that the blocking temperatureT_b of the trilayer is around 100°C. The Néel temperatureT_N of the 16nm thick (Co,Ni)O layer is slightly above this temperature. The highest temperature 200° we measured is considered well above this T_N[86]. It reveals that the PMA exists both above and below the T_N. Previous reports by P. Kuświk show that exchange coupling at the AFM/FM could induce or enhance the PMA of the FM layer only below the Néel temperature of AFM layer[87]. Moreover, we perform an in-plane field cooling(5kOe, 160°C) on sample B and measure its hysteresis loop at room temperature. It can be seen in Figure 4.5,

although an in-plane exchange bias is shown, the sample exhibits a PMA, indicating that the induced PMA is purely from the thermal effect rather than exchange coupling. It indicates that the metal/oxide interface effect plays a more important role of the PMA, akin to the system of $Pt/Co/Cr_2O_3$[88]. The interfacical exchange coupling possibily contribute to enhancement of the coercivity, but cannot overide the determining role of the metal/oxide interface effect.

4.3.2 Structural Properties

From the results shown above, we know that the post-annealing considerably affect influence the magnetic anisotropy of the film. To understand this issue better, structural analyze are performed. We try to analyze the trilayer by XRD scan, however, unfortunately, the corresponding peaks of (Co,Ni)O layers overlap with the strong MgO(001) single crystal peaks. Thus, it is difficult to obtain information about the film structure.

Instead, we perform a TEM observation to directly view the trilayer structure, especially in Sample B and C. Figure 4.6(a) and (c) shows the cross section image of Sample B and C. Despite the low contrast, the topological difference of the metal/oxide interface can still be distinguished. Sample B shows a rough interface, represented by a discontinouity and tortuosity(pointed by arrows) of the CoNi layer (see Figure 4.6(a)). In contrast, sample C presents a continous CoNi layer with a sharp metal/oxide interface(see Figure 4.6(c)). For high rosultion image of Figure 4.6(b) and (d), in sample B, it can be seen that the metal/oxide interface boundary is partly rough and difficult to be distinuished. Also there exist discontinouity of the metal layer. However, in annealed sample C, a clear metal/oxide interface can be seen. We can also observe signatures of CoNi nanocrystallites, some of which are coherent with the orientation of the (Co,Ni)O layer. The lateral size of these nanocrystallites are around 4nm. The TEM observation confirms that the annealing treatment induce a topological smoothing of the metal/oxide interface. SAED patterns reveal the crystallinity of the samples before and after annealing. The central bright spot correspondings to the glue used for the sample preperation. Unfortunately, due to the thin nature of CoNi layer, it is difficult to find any pattern corresponding to the CoNi layer, all the pattern information originates the (Co,Ni)O layer. For Sample B

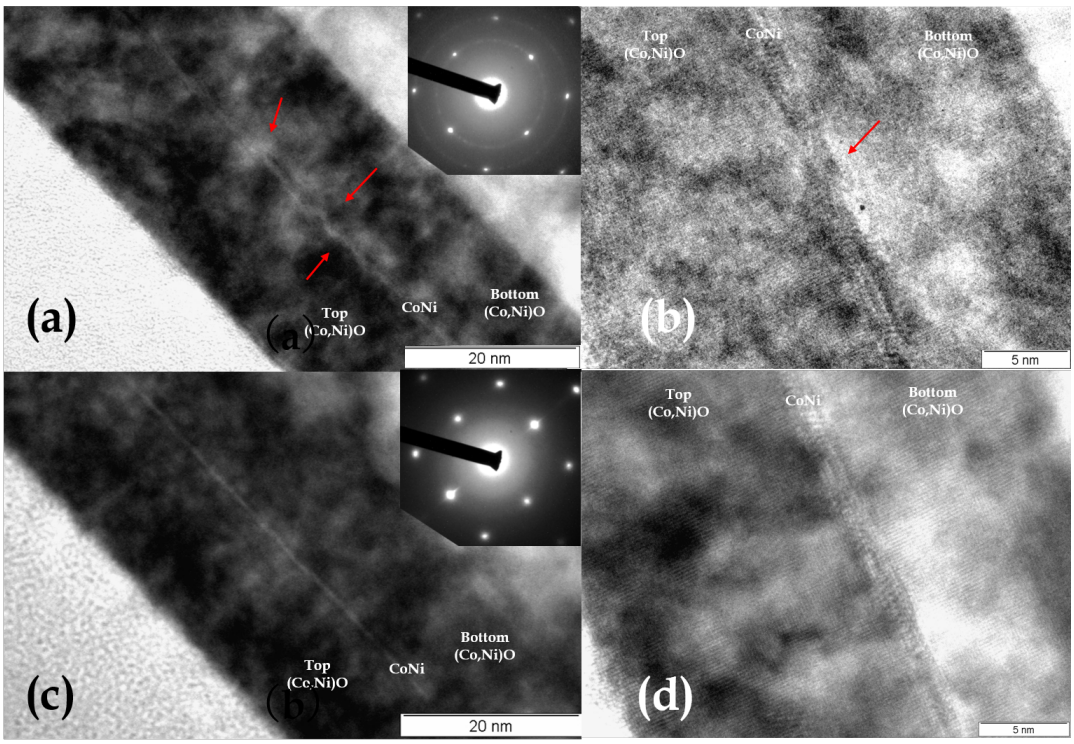

FIGURE 4.6: Cross Section TEM image for the trilayer films:(a)(c)Sample B; (b)(d)Sample C.

with top two layers prepared at room temperature, the SAED pattern shows bright spots together with rings consists of numerious small dots. The rings pattern is possibily from the top (Co,Ni)O, which was deposited at room temperature. Such ring pattern indicates that the top (Co,Ni)O layer grows into polycrystalline. However, the well ordered bright spots is considered from the bottom (Co,Ni)O layer, which was prepared at a high temperature, grows epitaxially on the MgO(001) structure. On the other hand, only bright spots are found for the annealed Sample C, revealing the epitaxial growth of all layers.

We then check the interfaces of sample A,B and C by XRR. As shown in Fig. 4.7 there is an evident difference in of the XRR spectra among the sample A,B and C. For sample A, ocillation of spectra can be observed at relatively high angle, suggesting a smooth interface. We consider that the growth of the bottom layer follows a layer-plus-island Stransky– Krastanov (SK) growth mode. We speculate that the bottom layer deposited at room temperature grows into homogeneous small grains. The

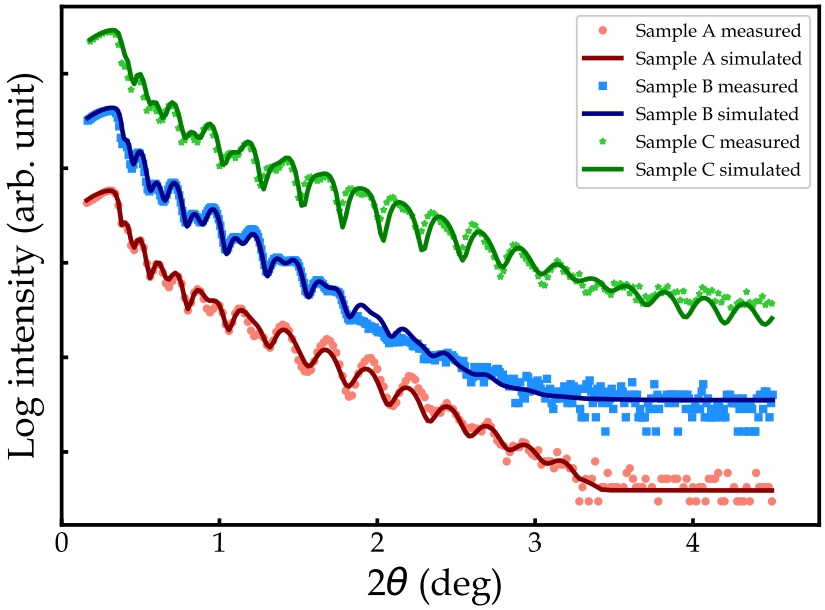

FIGURE 4.7: XRR spectrum of the trilayer film samples(A,B and C) with simulated spectra. Insert shows the average CoNi/(Co,Ni)O interface roughness of the Sample B annealled at various temperatures(T_{ann}).

ultrafine nature of the homogeneous grain islands leads to a smooth interface of the trilayer film. However, for sample B, the spectra clearly flattens out at high angle. It indicates that increasing the deposition temperature of the bottom layer lead to a rougher interface. Interestingly, as shown in the spectra of Sample C, after the post-annealing treatment, though the curve resembles the curve of sample B at low angle, the magnitude of fringes drastically increased at high angle. The curve of sample C shows a totally flatter slope when compared to sample A and B. Fitting data clearly shows that the roughness of the metal/oxide interfaces is reduced after annealing. The thickness of the CoNi layer also reduces from around 1.878 nm to 1.317nm, accomppanied by a slightly increased density. Since sample A and C both show PMA, we compare the roughness of metal/oxide interfaces and CoNi layer thickness of sample A and C and find them to be quite similar.

TABLE 4.2: Fitting parameters of the XRR measurements of sample B and C

layers	Sample B			Sample C		
	Thickness (nm)	Roughness (nm)	Density (g/cm^3)	Thickness (nm)	Roughness (nm)	Density (g/cm^3)
(Co,Ni)O_{Top}	15.295	0.507	6.723	16.595	0.329	6.688
CoNi	1.878	0.704	8.137	1.317	0.225	8.809
(Co,Ni)O_{Bottom}	15.399	0.516	6.723	15.469	0.244	6.503
MgO	∞	0.833	3.581	∞	0.656	3.590

4.3.3 Chemical properties

To study the oxygen distribution before and after annealing across the thin film, we conduct AES profiling on the Sample B and Sample C. The depth profile of the constituting elements of Sample B and C are shown in Figure 4.8. These two depth profiles are quite similar. However, although difficult to findm we can still find observe the slight difference of the oxygen distribution near the top (Co,Ni)O/CoNi interface(see the arrows in the figures). Sample C shows a slightly more abrupt oxygen contents transition at this interface area. It indicates that after annealing, a sharp oxygen/metal interface has been formed. For the other metal elements, Sample B and C show no obvious element distribution difference throughout the whole film thickness range. It is considered that compositional change of metal elements along the depth direction in this case is limited.

4.4 Discussion

Sample deposited at higher temperture leads to a degradation of PMA is mainly attribute to the interface roughnening. It is possibily that high temperature depostion increases the grain size, some grains grows larger than their adjacent ones, leaves large grain islands on the surface of (Co,Ni)O, consequently results in a higher roughness.

The sharpening of a reactive metal/oxide interface upon annealing seems counter-intuitive, however, is not a single case, such phenomenon has also been reported in CoFeB/AlO_x interface. In spite of this, in the case of CoFeB/AlO_x, the interface sharpening is a result of reduced interface width due to the compositional

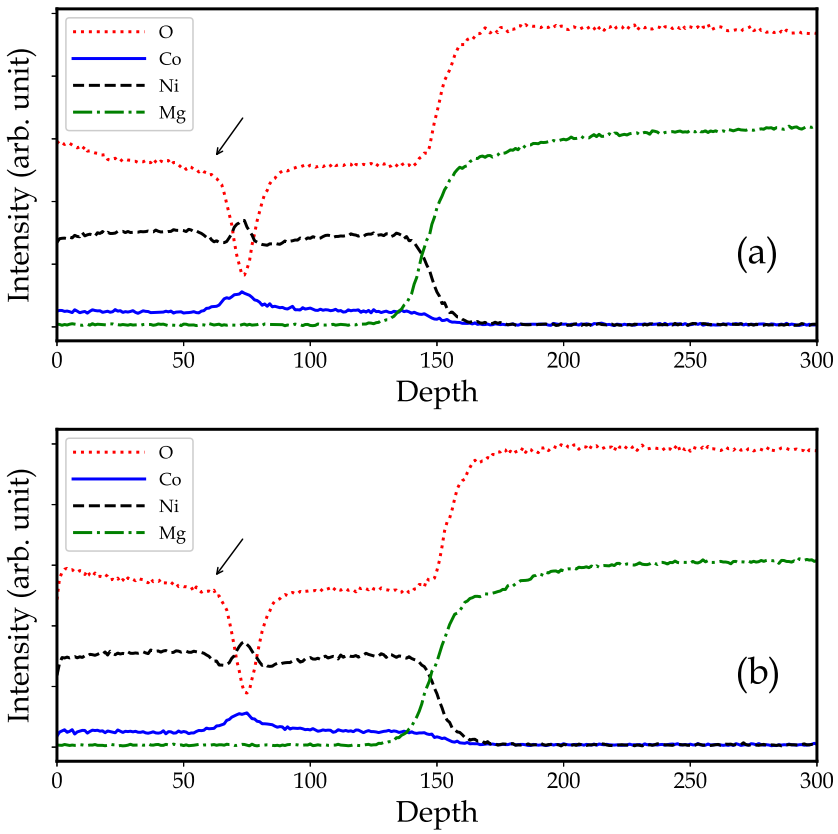

FIGURE 4.8: .
Auger electron spectroscopy (AES) depth profiles of the studied samples:(a)Sample B, (b)Sample C.

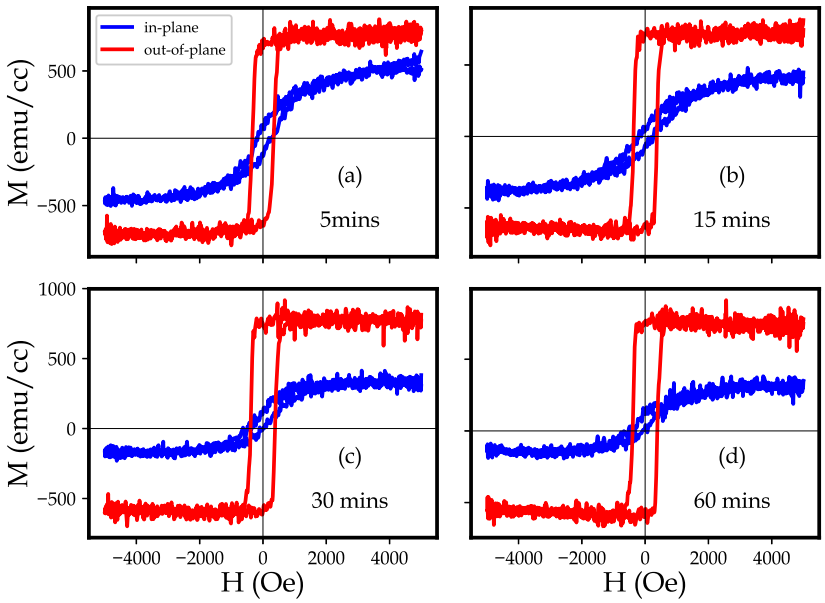

FIGURE 4.9: Annealing time effect on the PMA (Trilayer structure annealed at 200 °C).

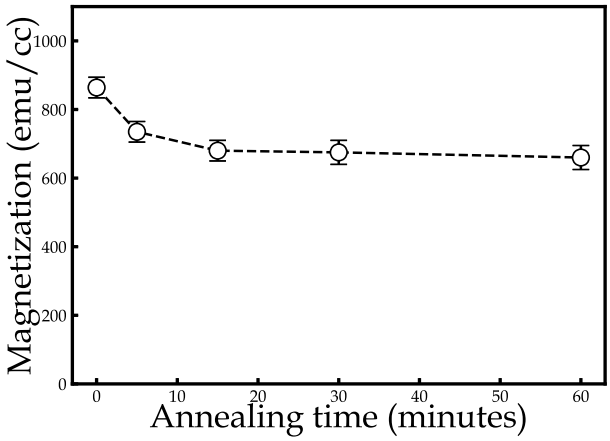

FIGURE 4.10: Annealing time effect on the magnetization.

change rather than topological smoothing, which slightly differs from the present case[89].

In the XRR analysis, we found a reduction of CoNi layer thickness, to confrim this point, we check the magnetization of the CoNi with regard to the annealing temperature and annealing temperature. M_s reduction can clearly seen after annealing(Figure 4.11). About 20% $\approx$ 30% reduction of magnetization upon annealing the sample from 100° to 250 °C. Figure 4.9 shows that the magnetic anisotropy transition to the PMA finishes mostly in a time as short as 5mins. Dependent of M_s on annealing time reveals that the transition reaches a equilibrium at a short time close to

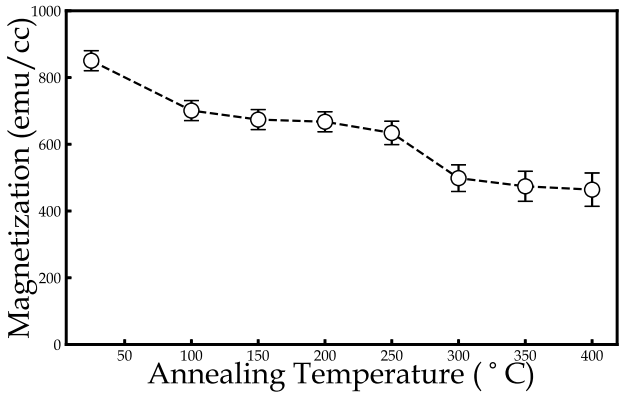

FIGURE 4.11: Annealing temperature effect on the magnetization.

15mins(Figure 4.10). It worths noting that, although the M_s of the sample annealed around 300°C shows a slight reduction, however, the improved PMA compensate the loss of M_s and lead to a K_{eff} comparable to the lower annealing temperature treatment.

To quantitatively study the magnetic anisotropy energy, we estimate the effective magnetic anisotropy K_{eff} from samples with various CoNi layer thickness. Phonomenologically, the effective magnetic anisotropy energy K_{eff} obeys a relation with t_{CoNi} as follows:

$$K_{eff} \times t_{CoNi} = K_v \times t_{CoNi} + 2K_s \tag{4.2}$$

Where, K_v is a volume contribution to the magnetic anisotropy and K_s is the interfacial contribution to the magnetic anisotropy. Results are summarized in Figure 4.12. It should be note that the t_{CoNi} used here is the nominal thickness. By fitting the points, it yields that before annealing, $K_v = -0.418 \times 10^6 erg/cc$ and $K_s = 0.2651 erg/cm^2$ for the as-deposited samples and $K_v = -0.6787 \times 10^6 erg/cc$ and $K_s = 0.8735 erg/cm^2$ for the annealed samples. If we consider the reduction of CoNi layer thickness due to the oxidation, the blue line should be corrected by a displacement to lower CoNi thickness. Neverthless, the corrected annealed K_s would still be higher than the as-deposited one. Thus, the enhanced K_s evidently contribute to the increased PMA.

Additionally, relatively small spontaneous exchange bias around 60Oe can be observed for most samples, which has an exchange coupling energy($J_K = H_{ex} M_s t_{FM}$) estimated around 0.01erg/cm^2. Such J_K is one order smaller than K_s, confirming

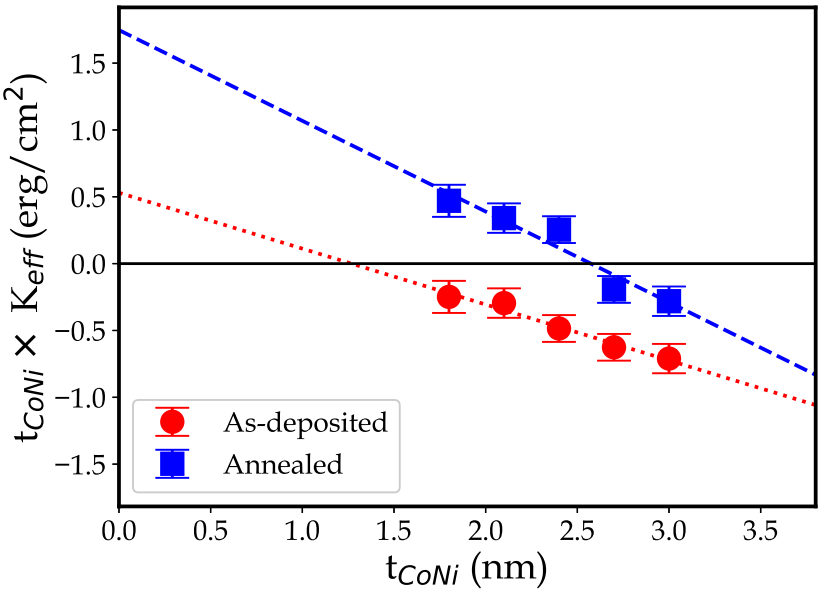

FIGURE 4.12: Plot of $K_{eff} \times t_{CoNi}$ in function of t_{CoNi} for samples with bottom depostion temperature at 200°C: as-deposited and annealed at 200°C.

that the exchange coupling is not the reason accounting for the induced PMA. We propose a possible menchanism to explain the interface sharpening phenomenon. (Co,Ni)O is a rocksaltlike structure from which three orientations can usually be obtained:(100), (110) and (111). The (001) plane has the lowest surface energy and is the most stable plane. The (110) plane has a higher surface energy than (100) plane. The most densely populated (111) plane have the largest surface energy(see Table 4.3). Oxidation on these surface will follow the sequence as (111), (110) and (100). Since there is no significant metal elements diffusion along the depth direction of the film(see Fig. 4.8), we only consider the diffusion of oxygen. Moreover, the oxygen diffusion is the limited at the inteface area where rich vacancy and defects exist. The density improvement of the CoNi layer indicates there exists a diffusion from the metal layer to the interface. Annealing triggers the oxygen diffusion from the metal layer to the interface area. Oxygen atoms gatther at the interface area, they oxidize the CoNi layer attached to the interface by flatten the defects and vacancies with large energy state planes, results in the formation of a sharp (001) inteface of the (Co,Ni)O lowest energy state(see Figure 4.13).

Previous studies on the thermal oxidation of CoNi alloys show that cobalt oxide tend to enrich at the surface du e to the preferential oxidation ability and higher

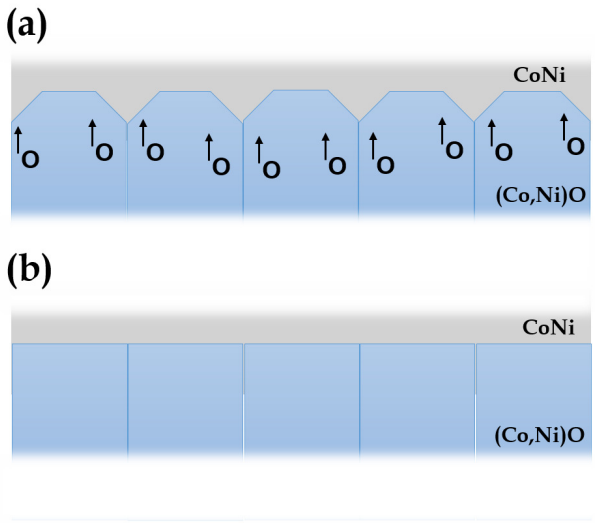

FIGURE 4.13: Schematic image of the CoNi/(Co,Ni)O interface upon annealing:(a)Sample B(during annealing);(b)Sample C(sample B after annealing).

TABLE 4.3: Surface energies of Co, Ni and their oxides[92–95].

surfaces	Ni (J/m^2)	NiO (J/m^2)	Co (J/m^2)	CoO (J/m^2)
fcc (100)	2.43	1.15	—	1.67
fcc (110)	2.38	2.77	—	2.56
fcc (111)	2.03	4.28	—	5.84
hcp (0001)	—	—	2.11	—

diffusion coefficient of Co than Ni. Past reports have also documented that a buffering thin CoO layer between Co and NiO can surve as a redox reaction barrier, lead to a sharp interface of metal/oxide layer[90]. In the present case, as evidenced in Fig. 4.8, Ni has a slight concentration reduction near the interface, whereas Co does not. It indicates that Co elements is richer at the interface than at the volumn of the (Co,Ni)O layer[91]. uch interface prevents the further intermixing and diffusion of Ni between the two sides of the interface. It links to the high thermal stability of the PMA at high temperature[90].

More importantly, the nature of PMA is the hybridization between the Co and oxide. oxygen migration leads to a rich Co-O bonding at the interface, resulting in a enhanced effective Co-O obital hybridization[26]. Additionally, interface sharpening lead to set the Co-O bonds normal to the film plane. Increasing the annealing temperature over 300°C results in the further oxidation of the CoNi layer, leading to the increased roughness and overoxidation of CoNi layer. Both of these factors

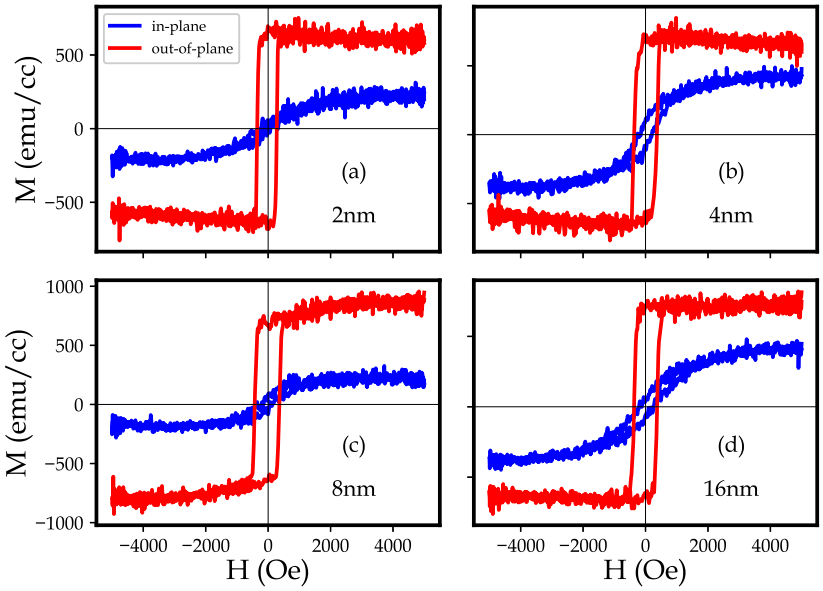

FIGURE 4.14: Hystereis loop of the trilayer structure of (Co,Ni)O (16nm)/CoNi (1.8nm)/(Co,Ni)O (xnm)/MgO trilayer structures with various bottom layer thickness:(a) 2nm, (b) 4nm, (c) 8nm, (d) 16nm.

will cause a degradation of PMA, which will finally overcome the improvement of the PMA induced by the CoNi layer thickness reduction. This accounts for the PMA degradation at the annealing temperature around 400°C.

4.5 Case of (Co,Ni)O/CoNi/MgO(001) layered structure

In this section, we firstly investigate the bottom layer thickness effect on the annealing induced PMA in this epitaxial system (see Figure 4.14). We fixed the thickness of top CoNi and (Co,Ni)O layer while changing the thickness of the bottom layer thickness. Before annealing, all the films show an in-plane anisotropy(data not shown). After annealing, they all show PMA. It reveals that the bottom layer thickness has little effect on the magnetic anisotropy.

Based on this result, we come out with a question: What if we get rid of the bottom (Co,Ni)O layer? To answer this question, we prepare samples with structure of (Co,Ni)O (16nm)/CoNi (1.8nm)/MgO(001) at room temperature to investigate the annealing temperature effect on the magnetic anisotropy. Annealing treatment is the same as mentioned in the beginning of this chapter.

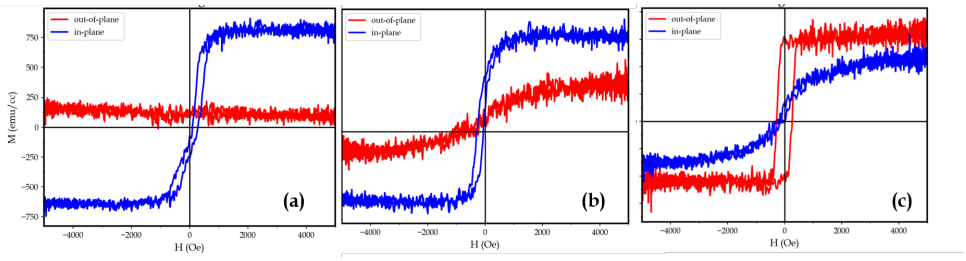

FIGURE 4.15: Hysteresis loops of epitaxial bilayer structure after annealing at various tempratures: (a) As-deposited; (b) After annealing at 200°C; (c) After annealing at 300°C.

.

Figure 4.15 presents the annealing effect on the magnetic anisotropy on the (Co,Ni)O/CoNi bilayer structure. It can be seen that, similar with the trilayer structure, at the as-deposited state, the bilayer is easy to be magnetized at film plane direction. Annealing at 200 °C, which is the temperature sufficient to cause a magnetic anisotropy transition in trilayer structure, do not trigger a similar transition here. The film is still easily to be magnetized at the film plane direction. After increasing the annealing temperature to 300°C, a transition of magnetic anisotropy to film normal direction occurs. Thus, despite the difference in transition temperatures, magnetic anisotropy transition to PMA can also be observed in bilayer structure. Further investigation show that such transition sustains to a high annealing temperature of 400∘C(data not shown).

We do an XRR scan to investigate the structural change of the bilayer film before and after annealing(See Figure 4.16). A distinct curve shape difference can be seen between the sample before and after annealing. Layer structure information is listed in Table 4.4 after fitting the curves. A similar CoNi layer thickness reduction can be seen, and the thickness where PMA is observed is comparable to the trilayer structure. However, contrast to the trilayer structure, bilayer film experiences an interface roughness increasement, especially at the CoNi/MgO interface. There may exists an intermixing of CoNi and MgO near the film/substrate interface. In spit of this, the surface of the bilayer film is improved after annealing, as the slope of the curve is flattened after annealing. We speculate that the roughness of the interface is mainly attributed to the interface roughness at the bottom CoNi/MgO interface. And the improvement of the surface quality is possibly due to the enhanced (Co,Ni)O/CoNi interface quality. As we have discussed above, such improvement would contribute

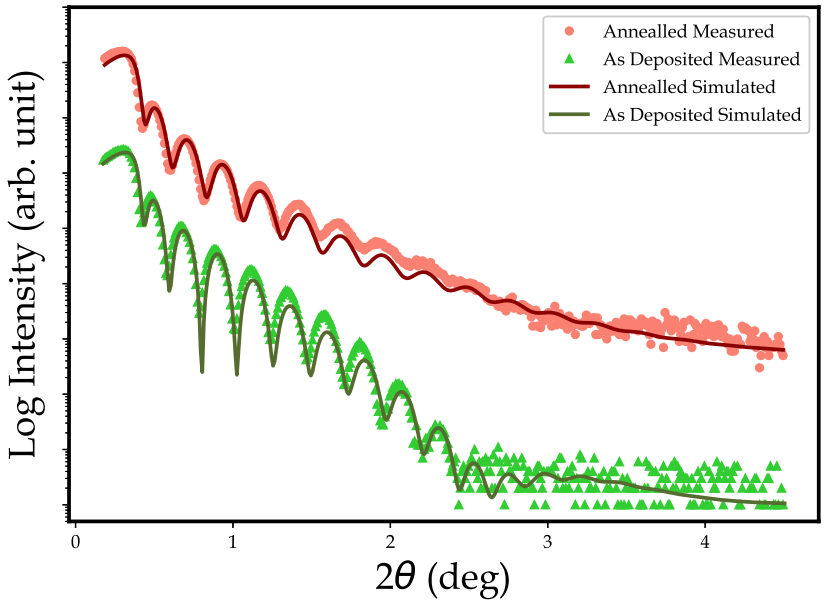

FIGURE 4.16: Xrr proile of epitaxial bilayer structure of (Co,Ni)O (16nm)/CoNi (1.8nm)/MgO(001) before and after annealing

.

TABLE 4.4: Fitting parameters of the XRR measurements of the bilayer structure of (Co,Ni)O (16nm)/CoNi (1.8nm)/MgO(001) before and after annealing at 300°C

layers	As-depo		Annealled		
	Thickness (nm)	Roughness (nm)	Thickness (nm)	Roughness (nm)	Density (g/cm^3)
(Co,Ni)O	16.859	0.677	16.154	0.226	6.587
CoNi	1.753	0.349	1.352	0.492	8.850
MgO	∞	0.410	∞	0.975	3.561

to the generation of PMA. However, due to the rough interface nature, the observed PMA is possibly different from the trilayer film case. The introduction of a MgO substrate surface may cause a Co-O-Mg bonding, which has been reported before, can also contribute to the development of PMA[96]. Thus, the generation of PMA in bilayer structure is may also due to the oxygen migration caused Co-O bonding increasement at the interface. Further study is required to clarify the determinant factor of the PMA in bilayer structure.

4.6 Summary

In summary, we investigate the interfacial effect on the perpendicular magnetic anisotropy(PMA) of (Co,Ni)O/CoNi/(Co,Ni)O trilayer film prepared on MgO(001) substrate. We find that when the bottom (Co,Ni)O layer is deposited at high temperature, it results in interface roughening, which degrades the PMA. On the other hand, post-deposition annealing causes interface smoothing, and promotes PMA. Such PMA sustains above the Néel temperature of the AFM, indicating that the main contribution to the PMA is not from the ferromagnetic/antiferromagnetic exchange coupling but the metal/oxide interface. The observed metal/oxide interface smoothing is considered to result from the interface energy minimization through oxygen diffusion and metal layer oxidation.

Chapter 5

Tuning magnetic anisotropy through exchange coupling in CoNi/(Co,Ni)O layered structures

5.1 Introduction

Due to its intriguing nature, the ferromagnetic(FM)/antiferromagnetic(AFM) layered structure has been receiving interests for decades[97]. The most fascinating phenomenon at the FM/AFM interface is exchange bias(EB)[98], which typically occurs after field cooling the FM/AFM structure through the Néel temperature of the AFM layer. It manifests itself as a shift along the field axis against the cooling direction and a coercivity enhancement. Such phenomenon is a result of the exchange coupling at the FM/AFM interface. Based on the magnetic anisotropy of the FM layer, this phenomenon can be observed at in-plane or out-of-plane configuration. In most applications, EB is only used as a tool to fix the magnetic anisotropy of the FM layer in a certain direction. Recently, however, it has been demonstrated that attaching an AFM layer with an FM layer can also switch the magnetic anisotropy of the FM layer from in-plane to out-of-plane anisotropy[99]. This FM/AFM structure induced PMA greatly extend the application of this system. It indicates a new method to design modern magnetic devices with desired magnetic anisotropy.

According to the previous studies, the magnetic anisotropy transition induced at the FM/AFM structure roots from the interfacial exchange coupling. For Mn/Fe epitaxial systems, the perpendicular uncompensated Mn moments couples with the

Fe moment in a collinear manner, forcing the Fe moment to align perpendicularly. Such PMA can be tuned by tetragonal distortion of the Mn layer[80, 99, 100]. In another Pd(001)/Ni/CoO(001) epitaxial system, with compensated AFM interface, the orthogonal interlayer exchange coupling is responsible for the perpendicular switching of the FM layer[87, 101]. In this system, the induced PMA is independent of the cooling field direction. For all these investigated epitaxial systems, the ordering of the AFM layer plays a central role in the inducing of PMA of the FM layer. It is demonstrated that these phenomena can only be observed below the Néel temperature of the AFM layer. For polycrystalline systems, PMA has been found enhanced after perpendicular field cooling[102, 103]. Many works conclude that the enhanced PMA is a result of enhanced interfacial anisotropy through the exchange coupling between the FM and the uncompensated AF spins[104]. However, switching the magnetic anisotropy along both the perpendicular and longitudinal directions is less reported. It also remains a question which kind of spins contribute mainly to the improved PMA.

Moreover, from technical point of view, exchange coupling induced magnetic anisotropy can be utilized to increase the thermal stability of perpendicularly magnetized MRAM or realize the zero-field switching of the SOT-MRAM. The thermal stability of the free layer with PMA in MRAM can be described as:

$$\Delta^{\perp} = \frac{K_{eff} V}{K_b T} \tag{5.1}$$

where K_{eff} is the effective magnetic anisotropy energy. Enhancement of K_{eff} by perpendicular exchange coupling could yield a free layer with much higher thermal stability. On the other hand, as shown in Figure 5.1(a), fast-switching of a perpendicularly magnetized SOT-MRAM requires an extra in-plane magnetic field H_x. It is because that the spin orbit torque is an in-plane torque, perpendicularly magnetized spins in free layer should break symmetry and produce an in-plane components to interact with the torque. However, integrating an additional field generator into the LSI is unpractical. Instead, it is more pratical to realize a zero-field switching. One of the promising method is generating an in-plane exchange coupling(exchange bias) to replace the external magnetic field, as shown in Figure 5.1(b). It is desired that

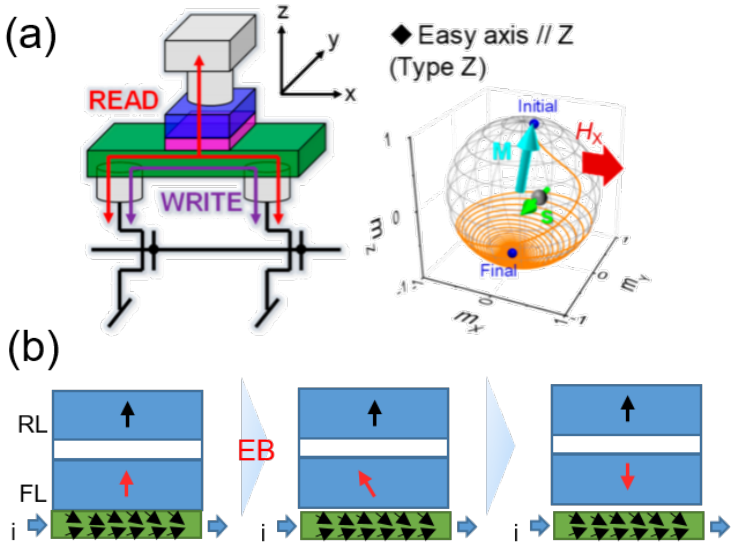

FIGURE 5.1: Zero-field switching of SOT-MRAM by applying an in-plane exchange bias field. Reproduced from[13]

the in-plane exchange coupling can tune the perpendicular magnetic anisotropy at room temperature.

Thus, the relationship between magnetic anisotropy and exchange coupling is of particular interest not only from a basic research point of view, but also from technical point of view. In previous chapters, we have investigated the origin of the PMA of CoNi/(Co,Ni)O layered structure and concluded that the PMA is mainly from the metal/oxide interfacial effect rather than the FM/AFM exchange coupling effect. It is not clear the relationship between the magnetic anisotropy and exchange coupling, in other words, how the exchange coupling influences on the magnetic anisotropy. In this work, we study the exchange coupling effect on the magnetic anisotropy of the FM/AFM layered structure by conducting field cooling at different directions and observing the modification. We also study the FM and AFM layer thickness effect on the induced magnetic anisotropy. It reveals that the modification of the magnetic anisotropy is mainly from the rotatable uncompensated AF spins at the FM/AFM.

The structure of this chapter goes as follows, we will first look deeper on some basic magnetic properties of the trilayer, which can not be easily investigated in a multilayer structure with several periods. Then we will discuss the interplay between the magnetic anisotropy and the exchange coupling.

5.2 Sample preparation

Samples with stacks of (Co,Ni)O /CoNi/(Co,Ni)O with various thickness of CoNi and (Co,Ni)O layers were prepared on fused quartz substrate at ambient temperature by magnetron sputtering. Another sample series with the structure of (Co,Ni)O/CoNi/(Co,Ni)O/CoNi/(Co,Ni)O was also prepared. The base pressure was better than 4.0×10^{-7} Torr. During the deposition, the working pressure was fixed at 1.5×10^{-3} Torr. The ferromagnet CoNi layer was DC sputter-deposited in a pure argon atmosphere from two facing Co targets (One nickel chip placed on top of the bottom Co target). The antiferromagnetic (Co,Ni)O layer was deposited from the same facing targets by reactive sputtering with an Ar and oxygen gas flow ratio of 9:1. The deposition rates were 0.021 nm/s and 0.026nm/s for CoNi and (Co,Ni)O layers, respectively. The compositions of CoNi and (Co,Ni)O layers, analyzed by ICP, are $Co_{0.47}Ni_{0.53}$ and $Co_{0.33}Ni_{0.67}O$, respectively. X-ray diffraction (XRD), X-ray reflectometry (XRR) and transmission electron microscopy (TEM) were used to characterize the structural properties. Room temperature hysteresis loop measurements and field cooling processes(160°C, 5kOe) were carried out by a vibrating sample magnetometer(VSM).

5.3 Structural characterization

The structural properties of the trilayers are firstly investigated. XRD profile of the trilayers is shown in Fig.5.4. The two peaks observed in the XRD profile corresponding to the (111) and (002) planes of the (Co,Ni)O layers. The (002) peaks are slightly stronger than the (111) peaks. It is well known that for (Co,Ni)O materials, the (111) is an uncompensated spin plane and (002) plane is a fully compensated plane. It is speculated that uncompensated spins clusters possibly exist at the FM/AFM interface. Similar to the multilayer structure with 5 periods, the trilayer structure here does not show peaks for CoNi layers. It may result from two reasons: the CoNi layer is too thin to show diffraction peak by the XRD or the poor crystallinity nature of this layer. We can barely see any changes from the XRD profiles of the samples

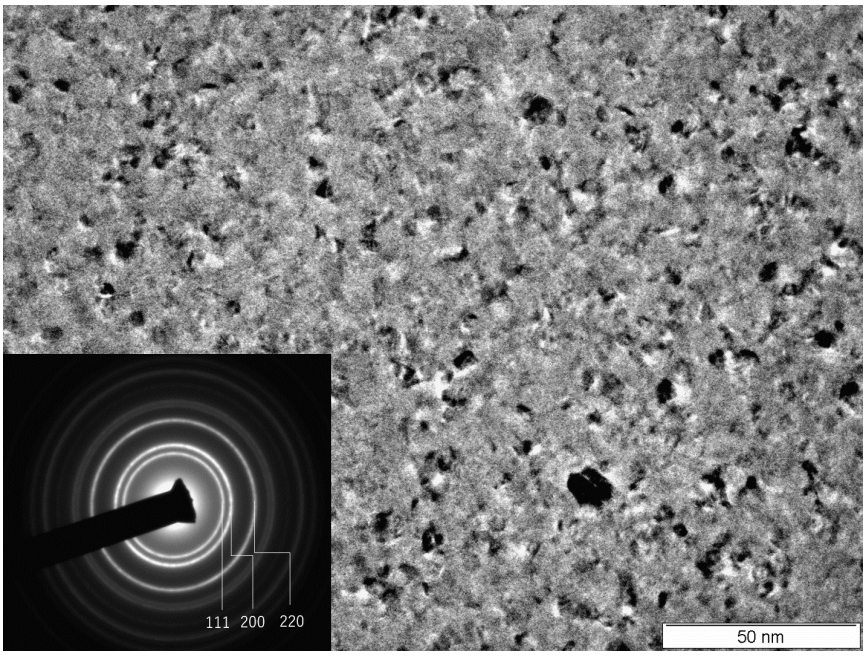

FIGURE 5.2: planar view transmission electron microscopy (TEM) images of a single (Co,Ni)O layer

before and after field cooling. It means that the field cooling process does not bring obvious change the textures of the trilayer films.

We take the planer view TEM images to observe the structure of the AFM (Co,Ni)O layer, one typical image is shown in Figure 5.2. The image depicts a polycrystalline structure of the AFM layer with an average grain size mostly around 4nm. The grain size distribution is presented in Figure 5.3. Results are averaged over 1000 grains from 20 images. It can be seen that the grain size are relatively small and the distribution is reasonably uniform. Moreover, the diffraction pattern shows a typical fcc rings pattern, indicating the polycrystalline feature of the AFM layers with fcc structure.

Interfaces play an important role in the functions of most of the heterostructures. Figure 5.5 shows the cross-sectional TEM image of the interfacial area of the trilayer structure. The (Co,Ni)O layers are well crystallized and the CoNi layers are continuously formed with poor crystallinity. Smooth metal/oxide interfaces can be observed.

Since the field cooling process is conducted by heating the sample to a temperature as high as 160°C. It is necessary to check the annealing effect on the interfaces. Figure 5.6 shows the XRR results of the samples before and after annealing at 160°C

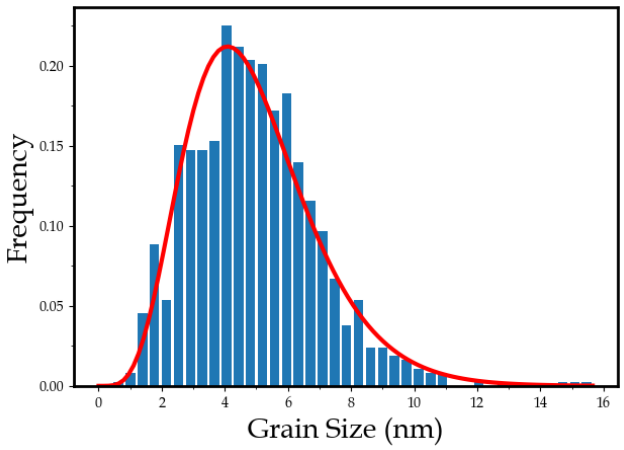

FIGURE 5.3: Grain size distribution of a single 16nm thick (Co,Ni)O layer

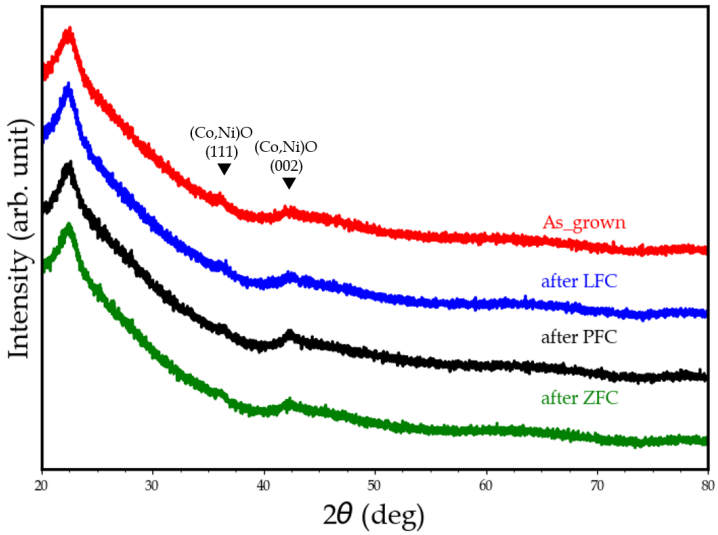

FIGURE 5.4: XRD profile of Glass/(Co,Ni)O $_{12nm}$(t)/CoNi$_{2.5nm}$(RT)/(Co,Ni)O$_{12nm}$) after various treatments

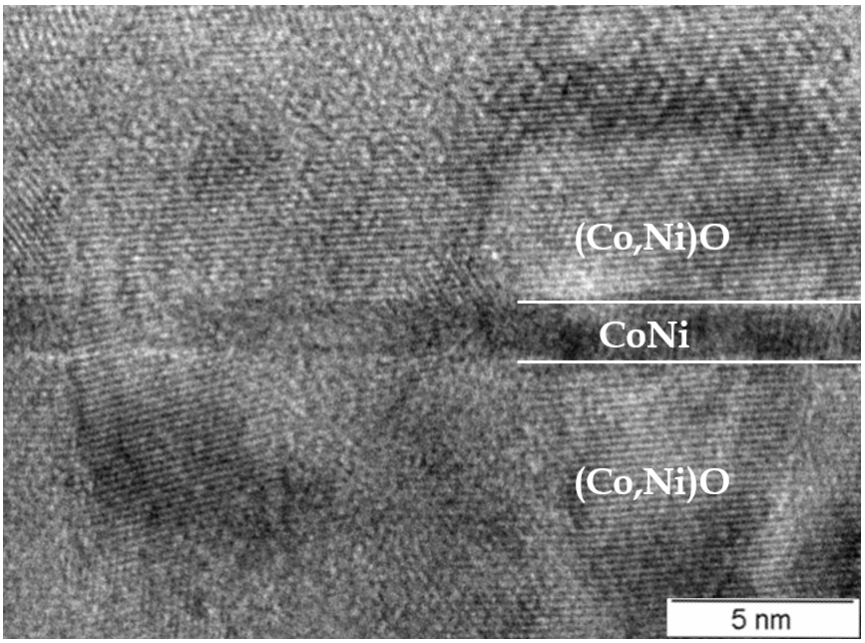

FIGURE 5.5: Cross section TEM image of the Glass/(Co,Ni)O $_{12nm}$(t)/CoNi$_{1.8nm}$(RT)/(Co,Ni)O$_{12nm}$) trilayer film

for 1h. Annealing causes slight changes to the films. The interfaces of the layer structure are slightly improved and the CoNi shows a slight thickness reduction. This result is consistent with the finding in Chapter 4. Based on the results in Chapter 4, we expect that the magnetic anisotropy of the trilayer structure at the out-of-plane direction could be improved by annealing.

5.4 Influence of the AFM layer thickness on the magnetic anisotropy

Thanks to the reduced structure, it allows us to study the effect of AFM layer thickness effect on the magnetic properties of the FM layers in a more simplified way.

Top/bottom layer thickness effect

We systematically investigate the top and bottom layer thickness effect on the magnetic anisotropy of the trilayer by fixing the CoNi layer thickness and varying the AFM layer thickness from 2nm to 8nm. A summary of the results is shown in Figure 5.7. PMA is shown for most of the layer thickness combinations. When the bottom layer is as thin as 2nm, it is difficult to obtain a PMA even with a top layer

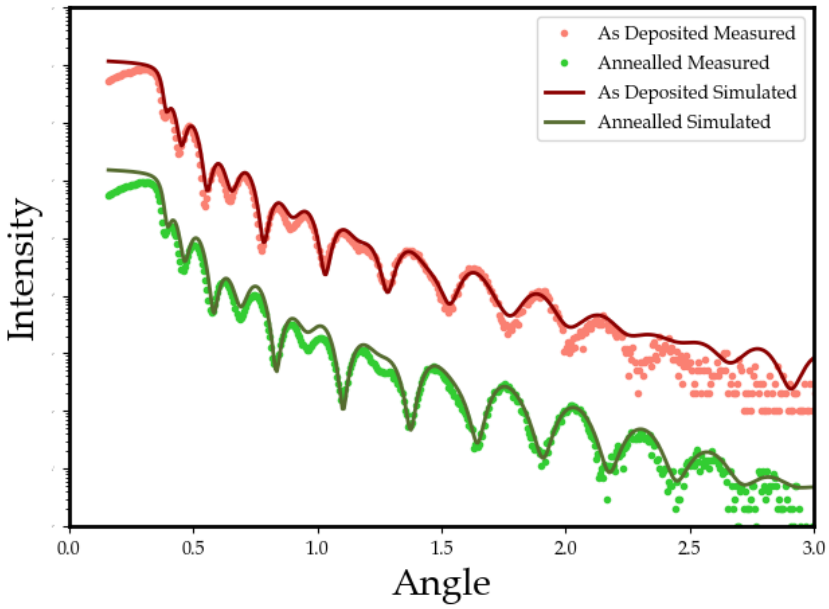

FIGURE 5.6: XRR profile of Glass/(Co,Ni)O $_{12nm}$(t)/CoNi$_{1.8nm}$(RT)/(Co,Ni)O$_{12nm}$) before and after annealing at 160 °C for 1h

as thick as 8nm. However, when the bottom layer is thick enough, PMA can be found even for a top layer as thin as 2nm. It reveals that the PMA is much more sensitive to the bottom layer than the top layer. To clarify the reason, we check the bottom layer/substrate interface in Figure 5.8. The interface between the bottom layer and the SiO/Si substrate is rather rough. It is understandable that, in order to form a smooth (Co,Ni)O layer, at the first stage of the (Co,Ni)O layer growth, around 3-4 nm thick (Co,Ni)O layer is sacrificed to wet the SiO/Si interface. We speculate that for (Co,Ni)O layer less than 3nm, the (Co,Ni)O layer will prefer island growth rather than film growth, yielding a rather rough surface of (Co,Ni)O layer. Such rough CoNi/(Co,Ni)O interface finally results in an in-plane anisotropy. On the other hand, as long as a smooth (Co,Ni)O layer is formed, it is easy to grow a continuous CoNi layer. As we have mentioned in Chapter 3, CoNi layer can serve a seed layer for the growth of the consequent (Co,Ni)O top layer. Thus, it is easier to obtain a smooth oxide/metal top interface. Consequently, PMA can be obtained even for a quite thin top layer.

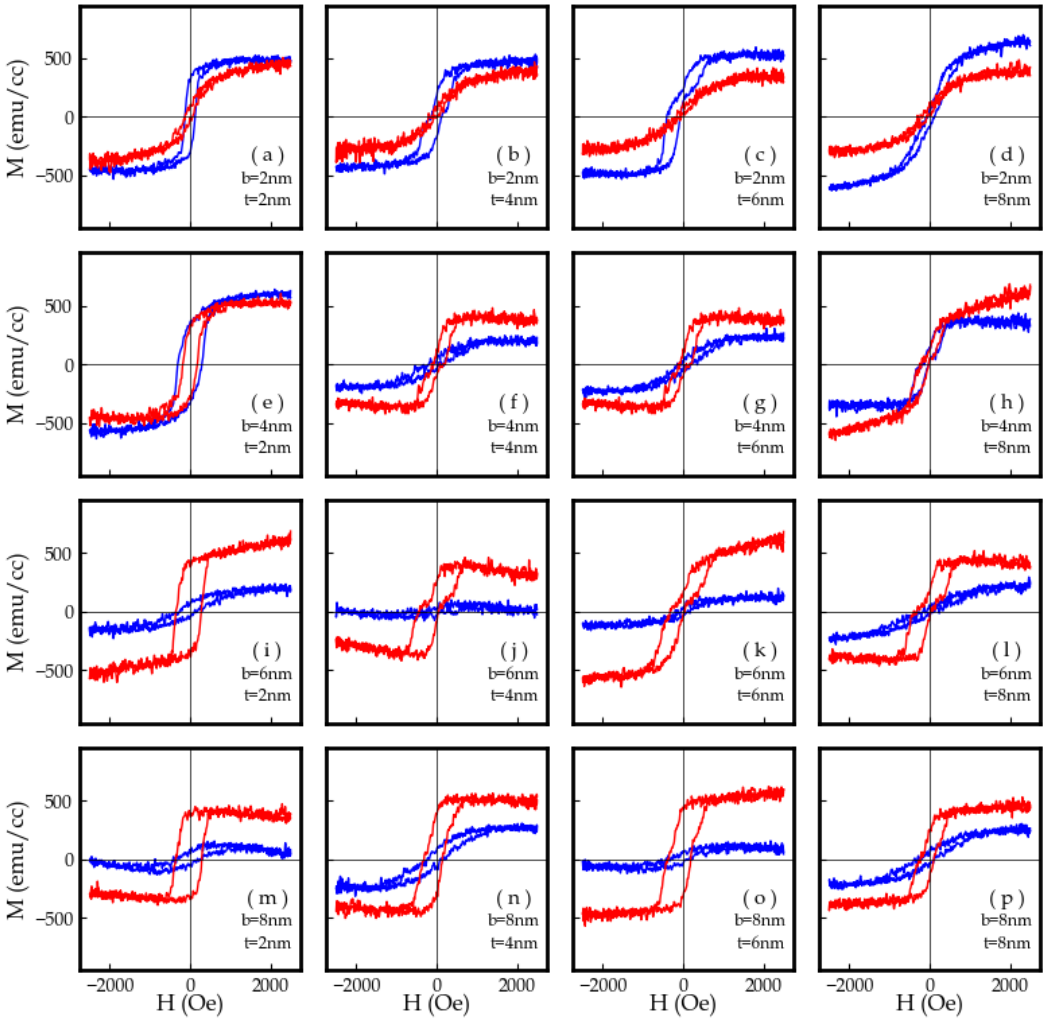

FIGURE 5.7: Hysteresis loop of Glass/(Co,Ni)O$_b$(t)/CoNi$_{1.8nm}$(RT)/(Co,Ni)O$_t$) with various top and bottom thickness.

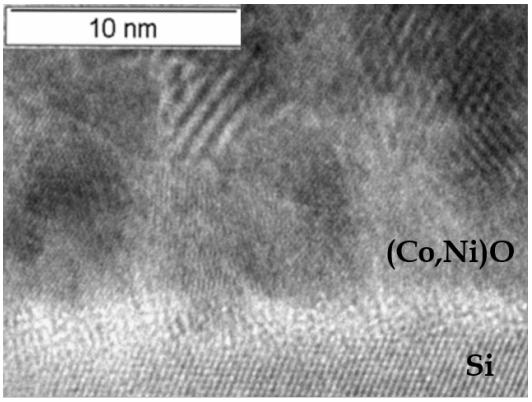

FIGURE 5.8: Cross section of the (Co,Ni)O layer/thermally oxidized Si substrate interface.

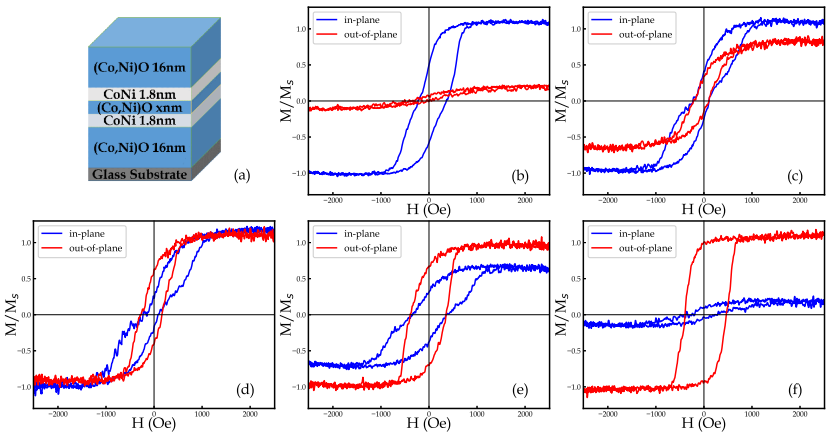

FIGURE 5.9: (a) Schematic illustration of the multilayer film. (b-f) Room temperature hysteresis loops of as deposited Glass/(Co,Ni)O $_{16nm}$)/CoNi$_{1.8nm}$/(Co,Ni)O$_{xnm}$/CoNi$_{1.8nm}$/(Co,Ni)O$_{16nm}$ multilayer films with different middle (Co,Ni)O layer thickness.(b)x =0 nm; (c)x = 0.4 nm; (d)x = 0.8 nm; (e)x = 1.2 nm; (f)x = 1.6 nm.

Middle layer thickness effect

Since the minimum AFM layer thickness for the layered structure to exhibit a PMA is at least 4nm for a bottom layer. There is still a possibility that the PMA may stem from the FM/AFM interface exchange coupling energy because a 4nm thick AFM layer may be thermally ordered at room temperature. Thus, it is necessary to clarify the minimum AFM thickness required to induce a PMA. As shown in Figure 5.9(a), we designed a 5 layered structure, where layer thicknesses are fixed for all the layers except the middle layer. We change the thickness of the middle layer in a small range from 0nm to 1.6nm. By increasing the thickness of the middle layer, the magnetic anisotropy of the structure gradually transforms from an in-plane configuration to an out-of-plane configuration. Strong PMA can be obtained for (Co,Ni)O layer as thin as 1.6nm. Such thin (Co,Ni)O layer can not hold a magnetocrystalline anisotropy large enough to force the FM layer to be of PMA at room temperature[105]. It confirms that, akin to the epitaxial layered structure, the FM/AFM exchange coupling is not the main contribution to the PMA obtained in polycrystalline trilayer structure.

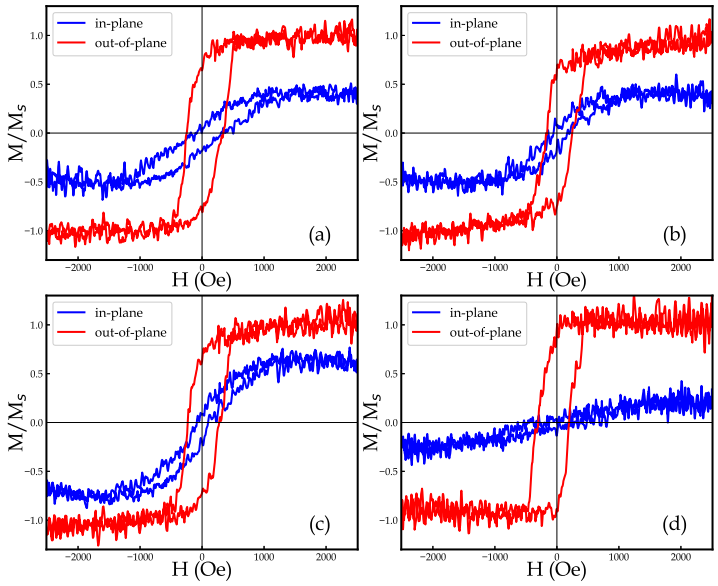

FIGURE 5.10: Room temperature hysteresis loops of as deposited Glass/(Co,Ni)O $_{16nm}$(t)/CoNi$_{1.8nm}$(RT)/(Co,Ni)O$_{16nm}$(RT) multilayer films with bottom CoNiO layer deposited at different temperatures: (a) Room temperature (RT); (b) t = 100°C ; (c) t = 150°C ; (d) t = 200°C.

Bottom layer deposition temperature effect

Additionally, the effect of the bottom layer deposition temperature T$_{btm}$ on the magnetic properties is studied. It is a parallel study compared with the work in Chapter 4. The bottom layer of the trilayer is deposited at various temperatures, whereas the top two layers are deposited at room temperature. Figure 5.10 shows that T$_{btm}$ does not have a significant effect on the magnetic anisotropy of the trilayer. Although a slight reduction of effective magnetic anisotropy is observed, PMA is established at the whole temperature range investigated.

To conclude this section, we have checked the influence of various (Co,Ni)O layer thickness and deposition temperature on the magnetic anisotropy of the trilayer structure. It is found that PMA can be obtained as long as a smooth CoNi/(Co,Ni)O layer is formed, confirming the metal/oxide interface induced nature of this PMA.

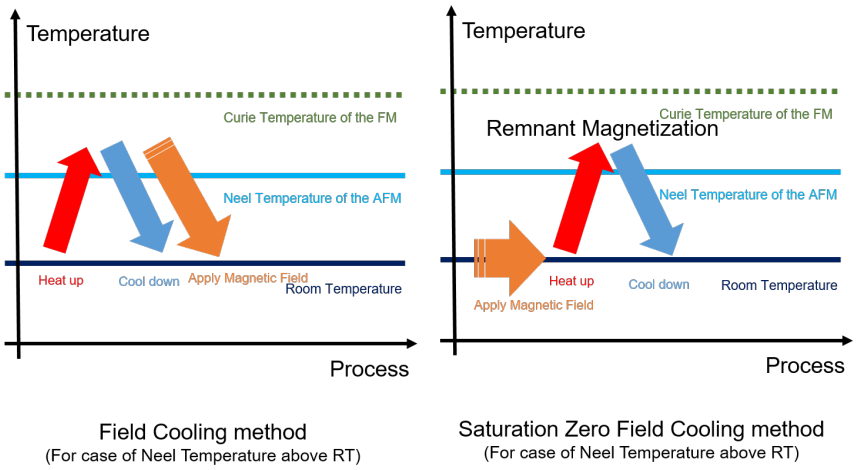

FIGURE 5.11: Schematic image of normal field cooling method and saturation zero field cooling method

5.5 Exchange bias induced by saturation zero-field cooling

In this section, we present an experiment on a series of samples with in-plane anisotropy. We apply a special field cooling process on the samples. The results and discussion in this section will help you to understand the results in the following sections.

Exchange bias can be induced by many methods. The orthodox method is normal field cooling(See Figure 5.11). The process is, heat the sample above the Néel temperature T_N of the AFM layer, hold on for several minutes, apply an external magnetic field to align the spins of the FM layer, then cool down the sample through the T_N, to the desired measuring temperature. As we can see, the magnetic field applied is only used to align the FM spins to a certain direction, rather than "order" the AFM spins. One could image that, if the FM layer of the sample maintains an ordered intrinsic magnetic field, then the cooling field is not a necessity, because the FM spins could keep most of their alignments towards one certain direction throughout the heating process. In this way, exchange bias can also be induced spontaneously after a zero-field cooling. As an instance, in a deposition process, when an AFM layer is deposited on an FM layer. The ordering of the AFM layer will be influenced by the existing FM layer, as shown in Figure 4.2(b) and Figure 5.12(a).

Here, based on the above discussion, we introduce a saturation zero-field cooling(SZFC) method, which can also induce an exchange bias in the samples in this

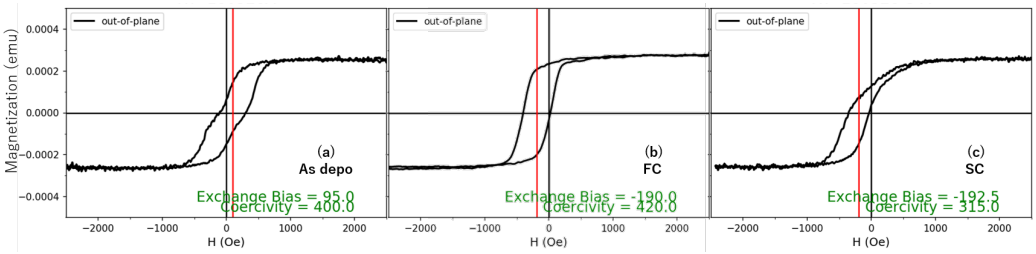

FIGURE 5.12: Room temperature hysteresis loop of (Co,Ni)$O_{12.5nm}$/$CoNi_{3.7nm}$/(Co,Ni)$O_{12.5nm}$ with different treatment:(a)As deposited state; (b)After in-plane field cooling at 80 °C; (c)Zero-field cooling at 80 °C with FM layer saturated.

work(See Figure 5.11). Instead of applying an external field during the cooling process, we saturate the sample at room temperature and then perform a zero-field cooling on the sample. Figure 5.12 shows the different results of the cooling treatments on a sample of (Co,Ni)$O_{12.5nm}$/$CoNi_{3.7nm}$/(Co,Ni)$O_{12.5nm}$ with in-plane anisotropy. For as-deposited sample(Figure 5.12(a)), the in-plane magnetic field in the chamber alongside the magnetron sputtering deposition randomly leaves remanent magnetization in the FM layer. The sample shows a spontaneous positive exchange bias of 95 Oe, possibly owing to the exchange coupling between the FM layer and the top AFM layer. However, due to its random nature, such exchange bias differs by samples significantly. Some samples show negative exchange bias, some do not show exchange bias at all. The slanted hysteresis loop shape with small M_s/M_r ≈0.45 indicates that the in-plane magnetic anisotropy of the FM layer is not strong at room temperature. Normal field cooling on the sample alter the direction of the exchange bias to be negative, yielding a typical exchange biased loop with $H_{eb} = -190Oe$ and a slightly increased coercivity(Figure 5.12(b)). Interestingly, after treating the sample with a saturation zero-field cooling, the sample also shows a negative exchange bias, however, with an asymmetric loop shape(Figure 5.12). The exchange bias value of $H_{eb} = -192.5Oe$ is comparable with the one obtained from the normal field cooling. However, the coercivity is smaller than the one after normal field cooling. The asymmetric shape is considered as a combination of superparamagnetic hysteresis loop and a shifted ferromagnetic hysteresis loop. The asymmetric shape is attributed to the partial exchange coupling between the FM and the AFM layer[106].

Figure 5.13 presents the zero-field cooling temperature T_{fc} effect on SZFC induced exchange bias. Both the H_{eb} and H_c do not follow a monotonous increasing

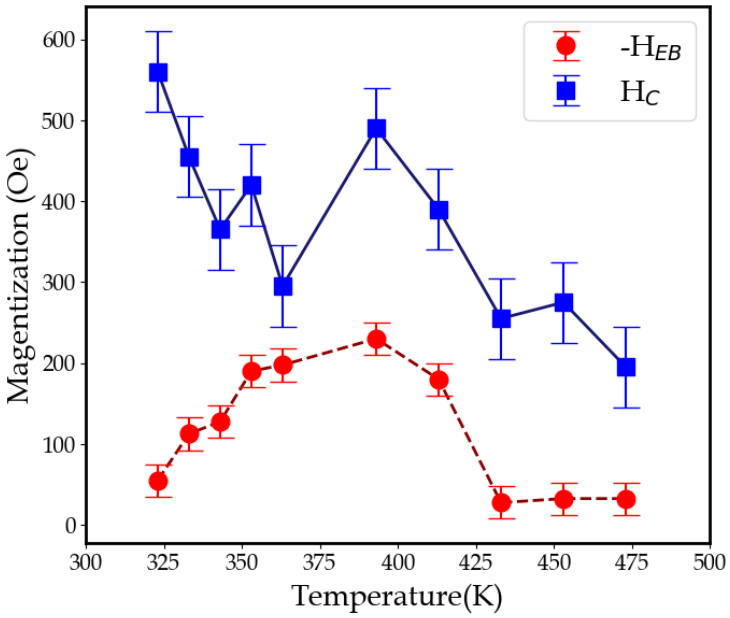

FIGURE 5.13: Exchange bias H_{eb} and coercivity H_c of $(Co,Ni)O_{12.5nm}/CoNi_{3.7nm}/(Co,Ni)O_{12.5nm}$ after saturation zero field cooling at various temperatures.

trend as the T_{fc} increases. The H_{eb} rises as T_{fc} increases until it reaches a maximum value when T_{fc} is around 400K, however, decreases for higher T_{fc}, finally, stabilized in a low value when $T_{fc} > 425K$. H_c behaves differently with H_{eb}, it shows a reversed decreasing trend as temperature increases for T_{fc} is less than 360K. In contrast, for temperature higher than 400K, it shows a similar decreasing trend with H_{eb} as T_{fc} increases.

Although the remanence magnetization of the CoNi layer is small, according to the curie-weiss's law, the remanent magnetization should maintain most of its value until it reaches Curie temperature. A sudden diminution of remanence magnetization is usually observable near the curie temperature. Thus, it is plausible to assume that the remanence magnetization of the FM layer only changes slightly until it reaches its curie temperature.

We utilize the exchange bias model which takes into account the polycrystalline structure of the AFM layer. It is considered that at the interface, the FM layer interacts with the uncompensated spins(UCSs) at the surface of AFM grains[107]. During the field cooling, the magnetization of the FM layer set the ordering of the AFM grains through interacting with the UCSs. At the measurement temperature, reversely, the AFM grains influence the magnetic behavior of the FM layer through

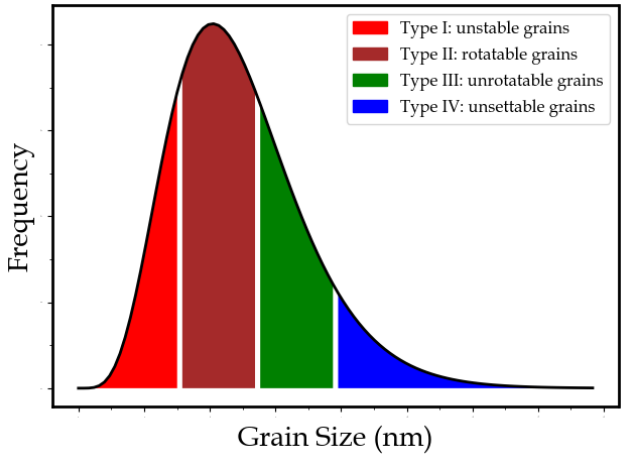

FIGURE 5.14: Schematical of the grain size distribution of diferent grain types in the AF layer at measuring temperature for a exchange bias system field cooled from a T_{set}.

the UCSs. The model assumes that the AFM grain size determines the thermal stability and the setting temperature of the UCSs. UCSs on AFM grains with large size behave thermally stable at the measuring temperature and require high temperature to be set to a certain direction during the field cooling. Thus, we can discuss the stability of the UCSs by considering the stability of the AFM grains. Based on the grain size, the AFM grains can be categorized into four types(see Figure 5.14). Grains with smallest grain sizes belong to type I, they are thermally unstable even at the measuring temperature, behaving like superparamagnet. Type II refers to small size grains which are unstable at the measuring temperature and can be set at a high temperature, however, their UCSs are rotatable during the measurements, contributing to the coercivity enhancement. Medium-sized grains in Type III, are settable during the field cooling, their UCSs are frozen and can not be rotated at the measurement temperature, contributing mainly to the unidirectional shift. Lastly, the Type IV grains with the largest size, hold the most stable UCSs, can not be set without a higher temperature. Note that, depends on the setting temperature and measurement temperature, the partition of each type of the UCSs might change. A higher setting temperature will lead to more stabilized grains with frozen UCSs. Contrarily, high measuring temperature will bring thermal instability to most of the grains.

Figure 5.15 shows the schematic image of the uncompensated spins at the

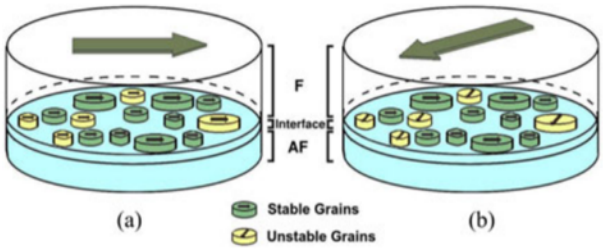

FIGURE 5.15: Uncompensated spins at the FM/AFM layered interface. (adapted from[108]):(a) alignments of UCSs at a setting temperature during the field cooling. (b) alignements of UCSs upon at measurement temperature upon a opposite external field.

FM/AFM layered interface. There are mainly two types of spins contributing to the magnetic anisotropy:rotatable UCSs(spins at the top of unstable grains) and unrotatable UCSs(spins at the top of stable spins). During the field cooling, both the two types of UCSs are set a certain direction at a setting temperture(See Figure 5.15(a)). However, as shown in the Figure 5.15(b), at the measurement temperature, the rotatable UCSs is unstable and can rotate with the external magnetic field, whereas the unrotatable UCSs is stable enough to resist change against the external magnetic field.

This polycrystalline exchange bias model is applicable to the current system. For T_{fc} less than 375K, as the temperature increases, the increase of exchange bias is much more significant than the decrease of coercivity. It might be mainly ascribed to the setting of TypeIII AFM grains, which results in most of the UCSs at the FM/AFM transit from rotatable to frozen. The increase of both the H_c and H_{eb} at T_{fc} near 390K is mainly caused by the fact that majority of the type II and Type III grains are set. UCSs on top of Type II and Type III grains mutually contributing to the enhanced coercivity and exchange bias. However, the setting force of the AFM grains is originally from the remanence magnetization of the CoNi layer. The sudden reduction of H_c and H_{eb} when T_{fc} passes 400K is mainly ascribed to the diminution of the remanence of CoNi layer. We can infer that the Curie temperature of the CoNi layer is around 430K. Additionally, we can see that, this trilayer system does not exhibit a single setting temperature, or in other words, a specific Néel temperature of the AFM layer. It is because AFM grains with different sizes may exhibit different Néel temperature. However, one can still define a nominal Néel temperature, above which

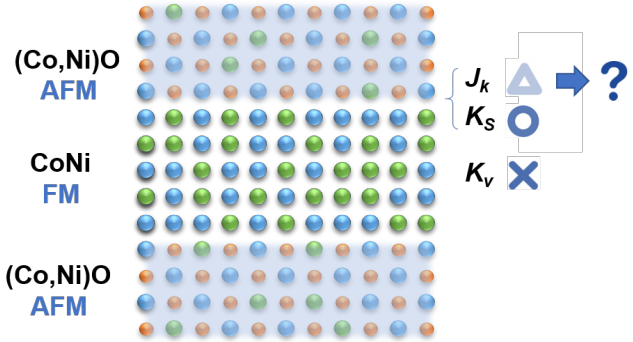

FIGURE 5.16: Schematic image of the (Co,Ni)O/CoNi/(Co,Ni)O interfaces.

all the AFM grains are thermally unstable.

To summarize this section, we have conducted a saturation zero-field cooling on the trilayer sample. FC temperature dependence of the exchange bias field and coercive field exhibits an intricate trend. This trend can be well explained by a polycrystalline exchange bias model.

5.6 Exchange coupling effect on the magnetic anisotropy

In this section, we investigate the effect of exchange coupling on the magnetic anisotropy in trilayer films. We know from the previous chapter that the PMA of the trilayer structure originates mainly from the metal/oxide (M/O) interfacial energy contribution(K_s), as shown in Figure5.16, In this trilayer structure, the M/O inteface is also an FM/AFM interface, which may induce exchange coupling anisotropy(K_x). These two interfacial effects seems similar but work differently. The M/O interfacial anisotropy(K_s) only force the easy magnetization axis of the FM layer to align in an out-of-plane direction. It changes the uniaxial and sometimes also the fourth fold anisotropy of the FM layer. However, the exchange coupling anisotropy(K_x), based on the setting direction, could force the FM layer orient to a certain direction. It mainly adds a unidirectional anisotropy layer as well as uniaxial or fourth fold anisotropy to the FM layer. This exchange coupling effect may significantly change the magnetic anisotropy of the trilayer films. Thus, it is necessary to investigate the relationship between the M/O interface induced magnetic anisotropy and the FM/AFM exchange coupling effect.

5.6.1 Results

The films studied in this section are (Co,Ni)O/CoNi/(Co,Ni)O trilayer sandwich structure prepared on glass substrate. Field cooling treatments are conducted with condition of 160°C and 5*KOe*.

Figure 5.17,5.18,5.19, shows the magnetic hysteresis loop of the trilayer structures with fixed FM and bottom AFM layer thickness. At as-deposited state, the in-plane and out-of-plane of all the films show roughly similar magnetic anisotropy. We name this state of magnetic anisotropy as "isotropic" magnetization. After zero-field cooling(ZFC), although samples may exhibit spontaneous exchange bias, for all the films, the out-of-plane anisotropy is enhanced. According to the previous chapter, the enhancement of the out-of-plane anisotropy is attributed to both the slight oxidation of the FM layer at the interface and an interface smoothing. Subsequently, we apply field cooling on these samples at both out-of-plane direction(PFC) and in-plane direction(LFC). For all samples, no matter the thickness of the top AFM layer, after PFC treatment, the out-of-plane anisotropy is enhanced, manifesting itself as an improved squareness. Accordingly, the corresponding in-plane anisotropy is suppressed. On the other hand, sample behaves differently after LFC treatment. Although the coercivity and exchange bias differs with samples, improvement of in-plane magnetic anisotropy is observed for all three samples. Obviously, after LFC, the suppression of the out-of-plane anisotropy differs for samples with different AFM top layer thicknesses. Degradation of PMA maximizes when the top AFM layer thickness is about 4.5nm. Further increasing the top layer thickness does not enlarge the degradation.

We also investigate the exchange coupling effect on samples with different FM layer thicknesses by fixing the AFM layer thickness. Figure 5.20 shows the hysteresis loop for samples with intrinsic PMA after field cooling in different directions. It is evident that although coercivity and remanence magnetization changes, PMA sustains for all the situations, regardless of the cooling field direction. A slight enhancement of the in-plane anisotropy is observed after LFC, however, the induced in-plane exchange coupling only slightly suppress the PMA(Figure 5.20(d)). Conversely, for the sample with intrinsic in-plane anisotropy, whose results can be seen

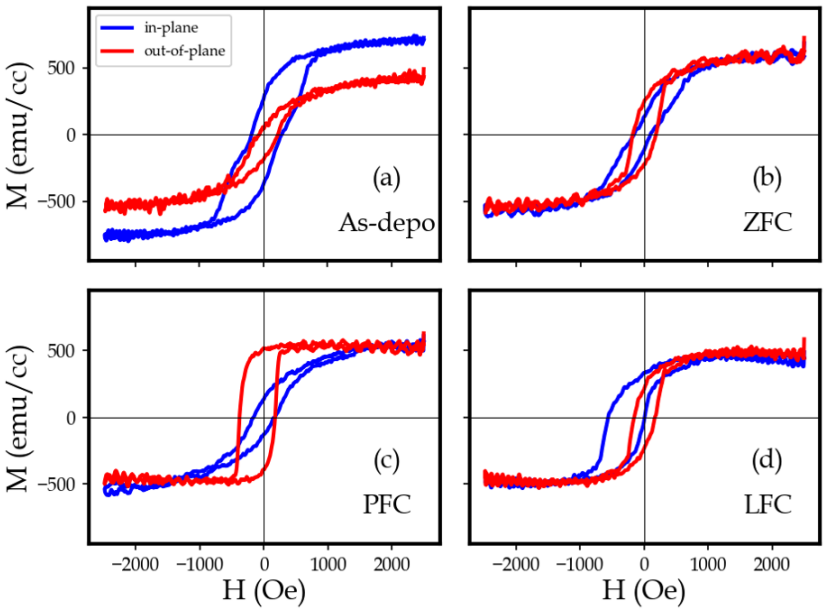

FIGURE 5.17: Field cooling effect on the magnetic anisotropy in (Co,Ni)O (12nm)/CoNi (2.1nm)/(Co,Ni)O (1.5nm) layered structure.

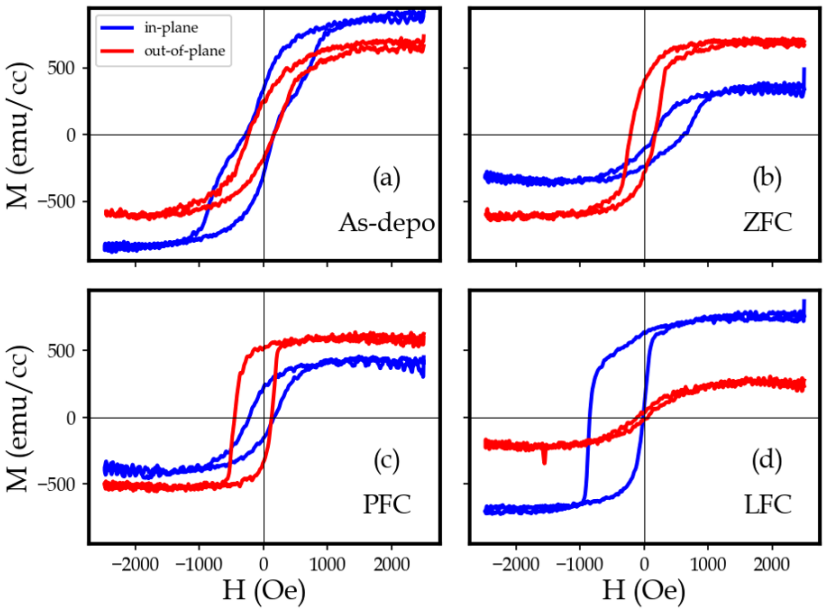

FIGURE 5.18: Field cooling effect on the magnetic anisotropy in (Co,Ni)O (12nm)/CoNi (2.1nm)/(Co,Ni)O (4.5nm) layered structure.

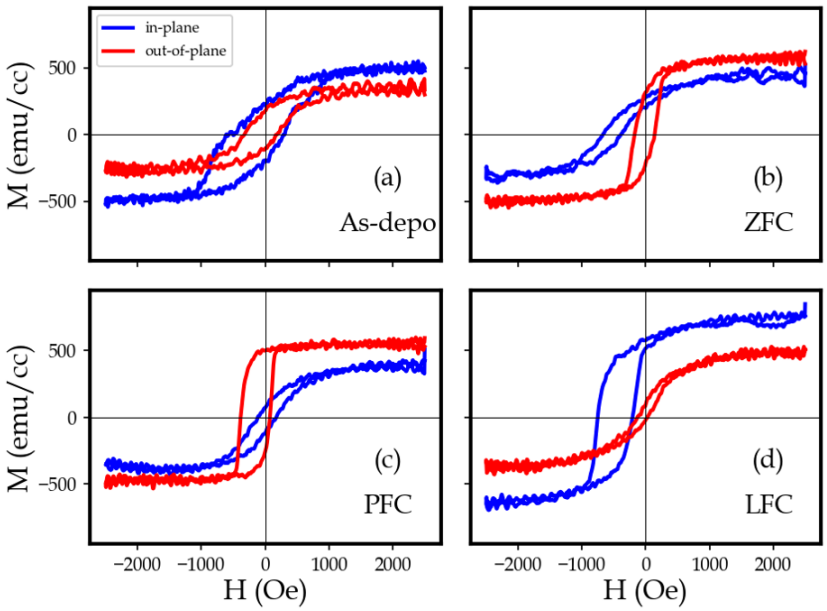

FIGURE 5.19: Field cooling effect on the magnetic anisotropy in (Co,Ni)O (12nm)/CoNi (2.1nm)/(Co,Ni)O (12nm) layered structure.

in Figure 5.21, manifest a reversed pattern. No matter the cooling field direction, in-plane anisotropy configuration is presented. No obvious improvement of out-of-plane anisotropy after PFC is shown.

5.6.2 Discussion

Based on the above results, we know that the magnetic anisotropy of the FM layer can be enhanced or suppressed by exchange coupling with the adjacent AFM layer in different configurations. Especially, when the FM layer shows an "isotropic" magnetization, its magnetic anisotropy can be tuned by exchange coupling.

Results from Figure 5.20 and Figure 5.21 reveal that the tuning of magnetic anisotropy is only significantly generated when there exist evident remanence magnetization on the field cooling direction. If the remanence magnetization of the FM layer in a certain direction is small, or in other words, such direction is a hard axis, it is difficult to develop a strong exchange coupling induced magnetic anisotropy. Field cooling process can not alter the hard axis to be an easy axis in this layered structure. From the energy point of view, as shown in the Figure 5.16, there are three magnetic anisotropic energies contributing to the CoNi/(Co,Ni)O layered structures. Especially, at the interface, there are two anisotropies; metal/oxide interface

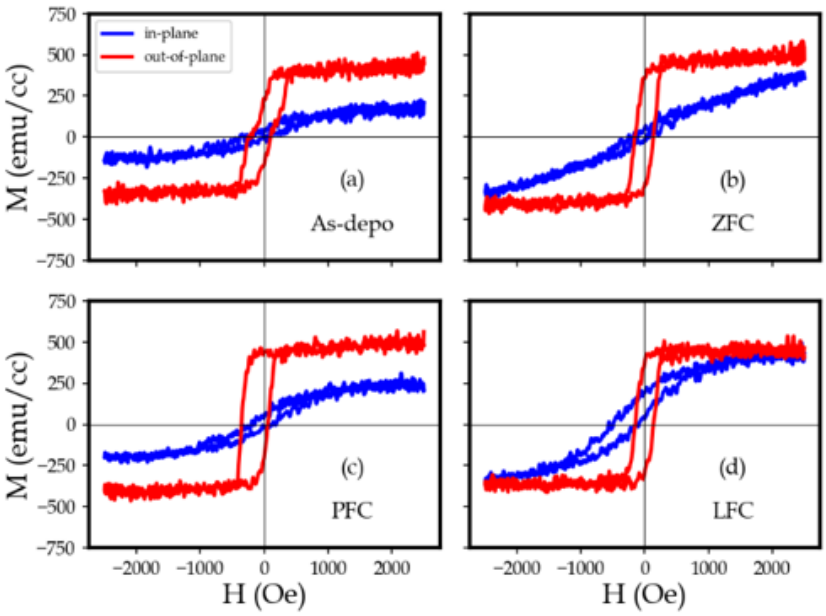

FIGURE 5.20: Field cooling effect on the magnetic anisotropy in (Co,Ni)O (12nm)/CoNi (1.8nm)/(Co,Ni)O (12nm) layered structure.

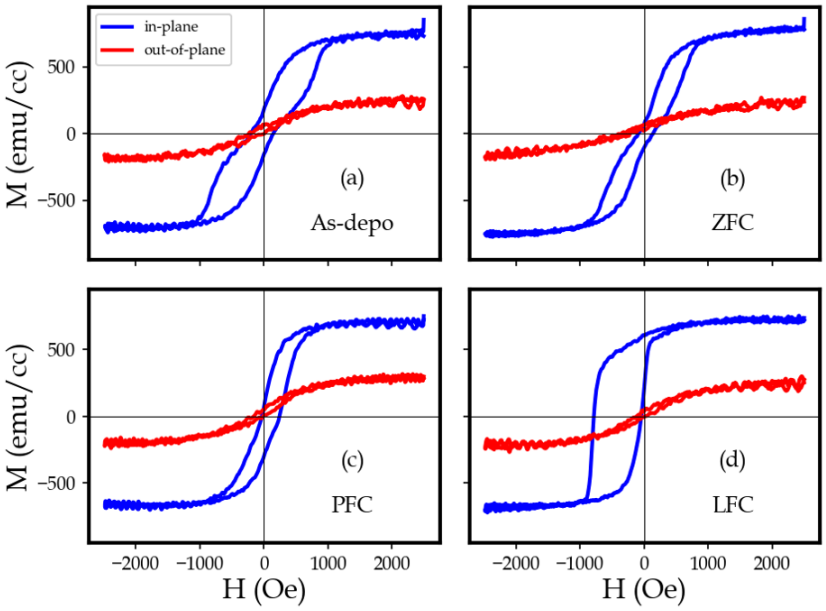

FIGURE 5.21: Field cooling effect on the magnetic anisotropy in (Co,Ni)O (12nm)/CoNi (2.5nm)/(Co,Ni)O (12nm) layered structure.

anisotropy energy(K_s) and FM/AFM exchange coupling energy(J_K). We have estimated the metal/oxide interface anisotropy(K_s) is about 0.9 erg/cm^2. The FM/AFM exchange coupling energy($J_k = H_{ex}M_s t_{FM}$) is around 0.05 erg/cm^2, which is one order smaller than the K_s. For polycrystalline FM/AFM system, exchange coupling roots in the interaction between the uncompensated spins(UCSs) and the FM spins. The UCSs couples collinearly to the FM spins, behave similar anisotropy concerning the FM spins. For films showing strong PMA at as-deposited state, large K_s force the FM spins to align normal to the interface. In this case, the UCSs are barely set along the in-plane direction. Thus, after in-plane field cooling, PMA is still shown. Films showing in-plane anisotropy at as-deposited state is a reversed case, volume anisotropyK_v combined with demagnetization energy force the FM spins to align in-plane. UCSs are barely set along the film normal direction, and thereby no evident out-of-plane anisotropy is shown after out-od-plane field cooling. Contrastly, for films showing "isotropic" magnetization at as-deposited state, where Metal/Oxide interface anisotropyK_s is balanced out by the volume anisotropy(K_v), the UCSs can be set by FM spins along the setting field. At the measurement temperature, UCSs and FM spins are exchange coupled along the setting field direction. Thus, in this case, the influence of the exchange coupling energy(J_K) to the magnetic anisotropy is significant.

One question needs to be clarified is, for polycrystalline exchange bias system, what kind of grains are responsible for the manipulation of the PMA. To better understand this question, we utilize the above-mentioned polycrystalline exchange bias model to explain the phenomenon in this FM/AFM layered system. It is well known that the exchange coupling roots in the interaction between the FM grains and UCSs located at the AF/AFM interface[107]. Based on the AFM grain sizes, after field cooling, these UCSs can be categorized to four types: unstable, rotatable, unrotatable and unsettable type. Since unstable and unsettable UCSs contribute neither to the unidirectional anisotropy nor to the uniaxial anisotropy of the adjacent FM layer, their contribution to the total energy of the system is negligible.[109] Rotatable UCSs cause the enhancement of the coercivity and unrotatable UCSs are responsible for the shift.

Figure 5.22 summaries the magnetic properties of the trilayer of various top

AFM layer thicknesses with "isotropic" magnetization. after field cooling(FC) at out-of-plane direction(PFC) or in-plane direction(LFC). It is clear that M_r/M_s with the collinear direction of the cooling field (Figure 5.22(a) and (e), (b) and (f)) follows the same trend with the H_c as top AFM layer thickness increases. They quickly reach a maximum value when the top AFM thickness is around 5nm, gradually decreases as the AFM layer thickness further increases. Similar trends are observable for the samples after different FC directions. In contrast, H_{eb} in both directions continue to develop larger values as the top AFM layer thickness increases(See Figure 5.22(c) and (d)). M_r/M_s and H_c are indicators for the uniaxial magnetic anisotropy, whereas H_{eb} is an indicator of unidirectional anisotropy[110, 111]. Based on the grain size distribution of the AFM layer as mentioned above (see Figure 5.14). UCSs at the top of medium size AFM grains behave rotatable, whereas UCSs at the top of large size AFM grains behave unrotatable. Since we only change the top AFM layer thickness, the FM/AFM interface is kept the same for all samples. It is speculated that if the AFM layer is thin, after FC, most of the UCSs at the interface are rotatable, they contribute to the enhancement of the uniaxial anisotropy[112]. As the AFM layer thickness increases, AFM grains grow to thermally stable large grains, UCSs on top of them behave unrotatable[113]. Thus, medium-thick AFM layer who offers abundant rotatable spins is favorable for the tuning of magnetic anisotropy for this trilayer structure.

Additionally, it worth noting that, after PFC, the in-plane M_r/M_s also follows the same top AFM thickness-dependent trend with the H_c ($\perp$) (Compare Figure 5.22 (a) and (f)). In contrast, after LFC, the out-of-plane M_r/M_s, does not show this trend with H_c ($//$). This difference implies that the rotatable UCSs favor in-plane direction. The UCSs can be easily magnetized at the film plane direction, as shown in Figure 5.23(a). In contrast, upon PFC, they can only be canted to the film normal direction, as described in Figure 5.23. This may be attributed to an extral contribution of the demagnetization term$\mu_0 \frac{1}{2} M_s^2$ with the volume anisotropy K_v. This explains why LFC drives larger in-plane anisotropy than the out-of-plane anisotropy driven by PFC.

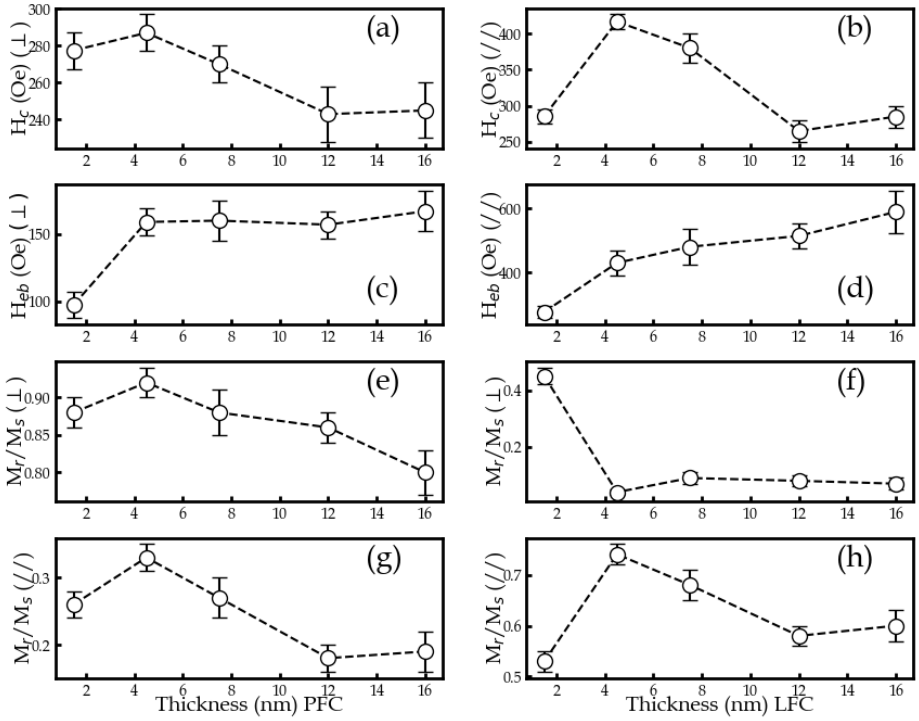

FIGURE 5.22: Top (Co,Ni)O thickness dependence of coercive field H_c, exchange bias field H_E, and remanence-to-saturation magnetization ratio (M_r/M_s) at room temperature in Glass/(Co,Ni)O (12nm)/CoNi (2.5nm)/(Co,Ni)O (x)nm trilayer structure after field cooling at different directions. Left column: PFC (out-of-plane field cooling); Right column: LFC (in-plane field cooling). (Note that // means in-plane, ⊥ means out-of-plane)

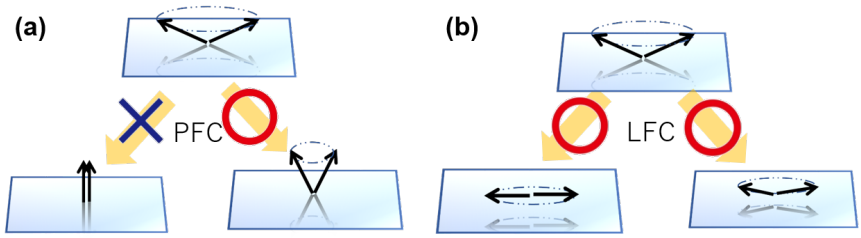

FIGURE 5.23: Schematic image of effect of field cooling direction on the magnetic anisotropy:(a) Perpendicular field cooling(PFC) can only cause a canting towards the film normal direction; (b) In-plane field cooling(LFC) can cause a canting or alignment towards the flim plane direction.

For SOT-MRAM, in-plane exchange coupling can be utilized to replace the external magnetic field during the switching. In this CoNi/(Co,Ni)O layered structure, as shown in Figure 5.20(d), after in-plane field cooling, an in-plane exchange bias is presented, albeit totally PMA is shown. It indicates that the switching symmetry is broken by an in-plane exchange coupling field. On the other hand, for STT-MRAM, there is a challenge to fabricate MTJ with size below 20nm[114]. In this CoNi/(Co,Ni)O layered structure, we have demonstrated that PMA can be enhanced through out-of-plane field cooling after deposition. However, the exchange coupling energy contribution(J_k) to the PMA is limited, which only extend the FM layer range showing PMA for only about 0.3nm. Our estimation shows that it is difficult to fabricate a sub-20 nm size MTJ based on the CoNi/(Co,Ni)O layered structure. There is a limitation to further narrow down the MTJ size simply by increasing the magnetic anisotropy through interface engineering. A promising method is to consider the volume anisotropy contribution[115]. In this work, the FM layer of CoNi is prepared by Co-sputtered, yielding a film with small volume anisotropy contribution(K_v). In a recent report, it has demonstrated that, the K_v can be increased by alternative monolayer deposition(AMLD), which deposits the Co and Ni monolayer alternatively[116]. It is expected that preparing the CoNi by AMLD method together with choosing a oxide buffer layer may significantly increase the PMA of CoNi, which is potentially suitable for the development of MTJ of sub-20nm size.

5.7 Summary

In summary, firstly, the AFM layer thickness effect on the magnetic anisotropy in a trilayer textured structure has been investigated. Results show that PMA can be induced as long as a smooth FM/AFM interface is formed. Secondly, it is found that the exchange bias can be set below the Néel temperature through zero-field cooling on a FM-saturated sample. The dependence of coercive field and exchange field on the field cooling temperature can be explained by a polycrystalline exchange model. Lastly, the relationship of the magnetic anisotropy and exchange coupling of the trilayer film is studied. If trilayer structure shows an "isotropic" magnetization,

after field cooling, the magnetic anisotropy of the film can be tuned to PMA or in-plane magnetic anisotropy. It is shown that such tuning is optimized at a medium AFM layer thickness, where the maximum coercive field is obtained. Based on the polycrystalline exchange bias model, the exchange coupling induced magnetic anisotropy enhancement is attributed to the uncompensated spins at the FM/AFM interface with rotatable anisotropy. It indicates that magnetic anisotropy could be modified even after the deposition.

Chapter 6

General Conclusions

The microstructure, magnetic anisotropy and exchange bias of CoNi/(Co,Ni)O layered structures has been systematically studied in this thesis. The CoNi/(Co,Ni)O layered structures were fabricated by magnetron sputtering. Three types of structures has been studied in this work: CoNi/(Co,Ni)O multilayer structures prepared on glass substrate, (Co,Ni)O/CoNi/(Co,Ni)O trilayer structures prepared on MgO (001) structure and (Co,Ni)O/CoNi/(Co,Ni)O trilayer structures prepared on glass substrate. To realize the perpendicular magnetic anisotropy and room temperature perpendicular exchange bias, microstructures and magnetic properties of the multilayer structures prepared on glass substrate have been investigated. The origin of perpendicular magnetic anisotropy is disclosed by studying the inteface effect on the magnetic anisotropy of trilayer structures prepared on MgO substrate. The relationship between the magnetic anisotropy and exchange bias has been studied in trilayer structures prepared on glass substrate. The main findings and detailed results are summarized and concluded as follows:

6.1 CoNi/(Co,Ni)O multilayer structure prepared on glass substrate

To realize the perpendicular magnetic anisotropy and room temperature perpendicular exchange bias, microstructures and magnetic properties of the multilayer structures prepared on glass substrate have been investigated. The CoNi/(Co,Ni)O multilayer structures are successfully fabricated on glass substrate at room temperature. Microstructure analysis shows that the (Co,Ni)O layer have fcc polycrystalline

structure of high quality (002) texture, whose texture is better for top layers than bottom layers. On the other hand, the CoNi layer is of poor crystallinity. Interface structure analysis shows that the as-deposited multilayered structure exhibits highly smooth metal/oxide interface.

Magnetic anisotropy of the as-deposited multilayer structure can be modified by changing the CoNi layer thickness while keeping the thickness of (Co,Ni)O layers. It is found that easy-axis magnetization direction changes dramatically from in-plane direction to out-of-plane direction as the CoNi layer thickness increases. The (Co,Ni)O(16nm)/[CoNi(1.8nm)/(Co,Ni)O(16nm)]$_5$ multilayer structure shows strong PMA with magnetic anisotropy energy as large as $2.55 \times 10^6 erg/cm^3$. However, the magnetic anisotropy is not sensitive to the (Co,Ni)O layer thickness. PMA emerges as the (Co,Ni)O layer thickness exceeds 2nm.

The bulk anisotropy energy and interface anisotropy energy are estimated. A large positive interface anisotropy energy is found. Since the CoNi layer is of a poor polycrystallinity, magnetoelastic anisotropy is considered to be very small. The total bulk anisotropy is not sufficiently large to overcome the demagnetization energy. Therefore, the origin of the PMA of the CoNi/(Co,Ni)O multilayer structure is mainly from the interface anisotropy.

Exchange bias is considered to be occurred in an interface of ferromagnetic material (FM) and antiferromagnetic material (AFM). PEB should exist in this FM/AFM multilayer structure with strong PMA. Experimental results show that room temperature PEB is observed in the multilayer structure after perpendicular field cooling. This results are attributed to the successful role playing of Co and Ni in the (Co,Ni)O layer. Of bulk CoO and NiO, CoO has the large crystalline anisotropy which contributes to the large PEB at low temperature and NiO has the high Neel temperature which contributes to the existence of PEB at room temperature.

6.2 (Co,Ni)O/CoNi/(Co,Ni)O trilayer structure prepared on MgO substrate

There are two possible contributions to the PMA: the metal/oxide interface anisotropy and the FM/AFM exchange coupling energy. To further study the origin of the PMA, we use MgO single substrate to control the texture of the AFM layer and the interface morphology. The (Co,Ni)O/CoNi/(Co,Ni)O trilayer structures deposited on the MgO single substrates exhibit different interface morphologies and magnetic anisotropies when deposited at different temperatures.

Film deposited at room temperature produces the results the previous chapter, However, increasing the bottom (Co,Ni)O layer deposition temperature to as high as 200 °C results in a film with in-plane anisotropy. Interestingly, after post-deposition annealing, the trilayer film presents perpendicular magnetic anisotropy. Temperature dependent study shows that such perpendicular magnetic anisotropy sustains at temperature as high as 260 °C, which is much higher than the Néel temperature of the antiferromagnetic (Co,Ni)O layer. It indicates that the FM/AFM exchange coupling energy is not the main contribution to the PMA.

The most striking structural feature in such trilayer film is after annealing at 200°C, a metal/oxide interface smoothing is observed. XRR results reveal a CoNi layer thickness reduction. However, the CoNi layer thickness reduction can not well explain the large enhancement of the perpendicular magnetic anisotropy. An obvious enhancement of the interface anisotropy is observed, which is closely related to the interface smoothing. Thus, the metal/oxide interface effect is considered as the main origin of the PMA. The mechanism of the interface smoothing is considered as follows: oxygen accumulates at the interface area, preferentially oxidize CoNi lattice plane of high energy, leading to a (001) plane with lowest energy. As a result, a smooth metal/oxide interface with low curvature is obtained.

6.3 (Co,Ni)O/CoNi/(Co,Ni)O trilayer structure prepared on glass substrate

To study the relationship between the FM/AFM exchange coupling and the magnetic anisotropy, we investigate the exchange coupling effect on the magnetic anisotropy of the CoNi/(Co,Ni)O trilayer structures prepared on glass substrate.

Firstly, we systematically investigated the AFM layer thickness effect on the magnetic anisotropy. Results confirm that perpendicular magnetic anisotropy can be induced as long as a smooth FM/AFM interface is formed. We then propose a saturation zero field cooling method to study the exchange bias in this trilayer structure. It is found that the exchange bias can be set without cooling through the temperature higher than the Néel temperature. The dependence of coercive field and exchange field on the cooling field temperature can be explained by a polycrystalline exchange model.

Lastly and most importantly, we investigate the field cooling direction effect on the magnetic anisotropy of the trilayer structure. For trilayer structure with slightly thicker CoNi layer(around 2.1nm), the film shows an "isotropic" magnetization. The magnetic anisotropy of such film can be tuned to perpendicular magnetic anisotropy after perpendicular field cooling or in-plane magnetic anisotropy after in-plane field cooling. The (Co,Ni)O thickness effect on the exchange coupling induced magnetic anisotropy transition is also investigated. It is shown that the maximum transition is achieved when the AFM layer is of a medium thickness, where the maximum coercive field is obtained. Based on the polycrystalline exchange bias model, the exchange coupling induced magnetic anisotropy enhancement is attributed to the uncompensated spins at the FM/AFM interface with rotatable anisotropy.

This perpendicularly magnetized CoNi/(Co,Ni)O layered structures can serve as a promising building block for future spintronic devices.

Publications

Publications

- H. Gao, T. Harumoto, W. Luo, R. Lan, H. Feng, Y. Du, Y. Nakamura, and J. Shi. Room temperature perpendicular exchange bias in CoNi/(Co,Ni)O multilayers with perpendicular magnetic anisotropy directly induced by FM/AFM interface, Journal of Magnetism and Magnetic Materials, Vol. 473, Page 490-494, Mar. (2019)

- H. Gao, Y. Gao, T. Harumoto, Y. Nakamura, and J. Shi. Interfacial magnetic anisotropy in (Co,Ni)O/CoNi/(Co,Ni)O/MgO (001) layered structures. Journal of Applied Physics. (Submitted)

- H. Gao, T. Harumoto, Y. Nakamura, and J. Shi. Annealing effect on the perpendicular magnetic anisotropy in (Co,Ni)O/CoNi/MgO (001) layered structures. (in preparation)

- T. Gong, H. Gao, Z. Wang and L. Shuai. Perceptual constraints on colours induce the universality of linguistic colour categorization. Scientific Reports. volume 9, Article number: 7719 (2019).

- Y. Gao, H. Sakimura, H. Gao, T. Harumoto, Y. Nakamura, and J. Shi. Perpendicular exchange bias independent of the NiO layer thickness in NiO/CoPt structures with orthogonal spin configuration. Physical Review B. (Submitted)

Presentations

- H. Gao, T.Harumoto, Y.Nakamura and J.Shi. Magnetic anisotropy and exchange bias in CoNi/(Co,Ni)O multilayers. The fifth ACEES Forum, San Diego, December,2016.

- H. Gao, T.Harumoto, Y.Nakamura and J. Shi. Perpendicular Magnetic anisotropy and Room Temperature Perpendicular exchange bias in CoNi/(Co,Ni)O multilayers. The 2017 MMM conference, Pittsburgh, USA, November,2017.

- H. Gao, T.Harumoto, Y. Nakamura and J. Shi. Room temperature perpendicular exchange bias in CoNi/(Co,Ni)O multilayer film. The sixth ACEES Forum, Teneriffe, Spain. December, 2017. Domestic Conferences

- H. Gao,T. Harumoto, Y. Nakamura, J. Shi. Magnetic Characterization of CoNi/(Co,Ni)O multilayer films. The 53th Autum Meeting of Japan Electronic Materials Society, Tokyo, November, 2016.

- H. Gao,T. Harumoto, Y. Nakamura, J. Shi. Magnetic anisotropy tuned by exchange coupling at CoNi/(Co,Ni) O layered structure, The 2018 Aunnual Fall Meeting of JIM, Sendai, September, 2018.

- H. Gao, T. Harumoto, Y.Nakamura and J. Shi. Perpendicular Magnetic anisotropy and Perpendicular exchange bias in CoNi/(Co,Ni)O multilayers. Joint Symposium of Tokyo Institute of Technology-Dalian University of Technology, Dalian, China, September,2018.

Bibliography

[1] Robert R Schaller. "Moore's law: past, present and future". In: *IEEE spectrum* 34.6 (1997), pp. 52–59.

[2] Antara Ganguly, Rajeev Muralidhar, and Virendra Singh. "Towards Energy Efficient non-von Neumann Architectures for Deep Learning". In: *20th International Symposium on Quality Electronic Design (ISQED)*. IEEE. 2019, pp. 335–342.

[3] PP Chougule, Bibhash Sen, and Tukaram D Dongale. "Realization of processing In-memory computing architecture using quantum dot cellular automata". In: *Microprocessors and Microsystems* 52 (2017), pp. 49–58.

[4] Evangelos Eleftheriou. ""In-memory Computing": Accelerating AI Applications". In: *2018 48th European Solid-State Device Research Conference (ESSDERC)*. IEEE. 2018, pp. 4–5.

[5] Abu Sebastian et al. "Temporal correlation detection using computational phase-change memory". In: *Nature Communications* 8.1 (2017), p. 1115.

[6] H-S Philip Wong and Sayeef Salahuddin. "Memory leads the way to better computing". In: *Nature nanotechnology* 10.3 (2015), p. 191.

[7] Weisheng Zhao and Guillaume Prenat. *Spintronics-based computing*. Springer, 2015.

[8] Jagan Singh Meena et al. "Overview of emerging nonvolatile memory technologies". In: *Nanoscale research letters* 9.1 (2014), p. 526.

[9] Syed Ghazi Sarwat. "Materials science and engineering of phase change random access memory". In: *Materials Science and Technology* 33.16 (2017), pp. 1890–1906.

[10] Varshita Gupta et al. "Resistive Random Access Memory: A Review of Device Challenges". In: *IETE Technical Review* (2019), pp. 1–14.

[11] Andrew D Kent and Daniel C Worledge. "A new spin on magnetic memories". In: *Nature nanotechnology* 10.3 (2015), p. 187.

[12] Yiming Huai et al. "Spin-transfer torque MRAM (STT-MRAM): Challenges and prospects". In: *AAPPS bulletin* 18.6 (2008), pp. 33–40.

[13] Tetsuo Endoh and Hiroaki Honjo. "A recent progress of spintronics devices for integrated circuit applications". In: *Journal of Low Power Electronics and Applications* 8.4 (2018), p. 44.

[14] AV Khvalkovskiy et al. "Basic principles of STT-MRAM cell operation in memory arrays". In: *Journal of Physics D: Applied Physics* 46.7 (2013), p. 074001.

[15] Saied Tehrani et al. "Magnetoresistive random access memory using magnetic tunnel junctions". In: *Proceedings of the IEEE* 91.5 (2003), pp. 703–714.

[16] XF Han et al. "Nanoelliptic ring-shaped magnetic tunnel junction and its application in MRAM design with spin-polarized current switching". In: *IEEE Transactions on Magnetics* 47.10 (2011), pp. 2957–2961.

[17] S Mangin et al. "Current-induced magnetization reversal in nanopillars with perpendicular anisotropy". In: *Nature materials* 5.3 (2006), p. 210.

[18] Liu Hou-Fang, Syed Shahbaz Ali, and Han Xiu-Feng. "Perpendicular magnetic tunnel junction and its application in magnetic random access memory". In: *Chinese Physics B* 23.7 (2014), p. 077501.

[19] David Jiles. *Introduction to magnetism and magnetic materials*. CRC press, 2015.

[20] Charles Kittel and JK Galt. "Ferromagnetic domain theory". In: *Solid state physics*. Vol. 3. Elsevier, 1956, pp. 437–564.

[21] PF Carcia, AD Meinhaldt, and A Suna. "Perpendicular magnetic anisotropy in Pd/Co thin film layered structures". In: *Applied Physics Letters* 47.2 (1985), pp. 178–180.

[22] C Chappert and P Bruno. "Magnetic anisotropy in metallic ultrathin films and related experiments on cobalt films". In: *Journal of Applied Physics* 64.10 (1988), pp. 5736–5741.

[23] PF Carcia. "Perpendicular magnetic anisotropy in Pd/Co and Pt/Co thin-film layered structures". In: *Journal of applied physics* 63.10 (1988), pp. 5066–5073.

[24] GHO Daalderop, PJ Kelly, and FJA Den Broeder. "Prediction and confirmation of perpendicular magnetic anisotropy in Co/Ni multilayers". In: *Physical review letters* 68.5 (1992), p. 682.

[25] M Sakurai, T Takahata, and I Moritani. "Magnetic and magneto-optical properties of co/ru multilayers". In: *IEEE translation journal on magnetics in Japan* 7.2 (1992), pp. 176–182.

[26] B. Dieny and M. Chshiev. "Perpendicular magnetic anisotropy at transition metal/oxide interfaces and applications". In: *Reviews of Modern Physics* 89.2 (June 2017).

[27] S. Ikeda et al. "A perpendicular-anisotropy CoFeB–MgO magnetic tunnel junction". In: *Nature Materials* 9.9 (July 2010), pp. 721–724.

[28] J Wang et al. "Perpendicular magnetic anisotropy and perpendicular exchange bias in sputter-deposited CoO/CoPt multilayer". In: *Journal of Applied Physics* 113.17 (2013), p. 17D714.

[29] Y Hodumi, J Shi, and Y Nakamura. "Controlling the magnetic anisotropy of Co Pt/ Al N multilayer films". In: *Applied physics letters* 90.21 (2007), p. 212506.

[30] Hongyu An et al. "Highly (001) oriented L10-CoPt/TiN multilayer films on glass substrates with perpendicular magnetic anisotropy". In: *Journal of Vacuum Science & Technology A: Vacuum, Surfaces, and Films* 33.2 (2015), p. 021512.

[31] J Wang et al. "Strong perpendicular exchange bias in sputter-deposited CoPt/CoO multilayers". In: *Applied Physics Letters* 103.4 (2013), p. 042401.

[32] Chun Feng et al. "Tuning perpendicular magnetic anisotropy and coercivity of L10-FePt nanocomposite film by interfacial manipulation". In: *Journal of Applied Physics* 109.6 (2011), p. 063918.

[33] W.Y. Zhang et al. "Origin of perpendicular magnetic anisotropy and evolution of magnetic domain structure of amorphous Pr–TM–B (TM=Fe, Co)

films". In: *Journal of Magnetism and Magnetic Materials* 322.8 (2010), pp. 900 –908.

[34] W. H. Meiklejohn and C. P. Bean. "New Magnetic Anisotropy". In: *Physical Review* 102.5 (June 1956), pp. 1413–1414.

[35] J. Nogués et al. "Exchange bias in nanostructures". In: *Physics Reports* 422.3 (Dec. 2005), pp. 65–117.

[36] F Garcia et al. "Exchange-biased spin valves with perpendicular magnetic anisotropy based on (Co/Pt) multilayers". In: *Journal of applied physics* 93.10 (2003), pp. 8397–8399.

[37] Stefan Maat et al. "Perpendicular exchange bias of Co/Pt multilayers". In: *Physical Review Letters* 87.8 (2001), p. 087202.

[38] B Kagerer, Ch Binek, and W Kleemann. "Freezing field dependence of the exchange bias in uniaxial FeF2/CoPt heterosystems with perpendicular anisotropy". In: *Journal of magnetism and magnetic materials* 217.1-3 (2000), pp. 139–146.

[39] Helio CN Tolentino et al. "Structure, morphology and magnetism of an ultrathin [NiO/CoO]/PtCo bilayer with perpendicular exchange bias". In: *Brazilian Journal of Physics* 39.1A (2009), pp. 150–155.

[40] V Baltz et al. "Antiferromagnetic spintronics". In: *Reviews of Modern Physics* 90.1 (2018), p. 015005.

[41] Philipp Zilske et al. "Giant perpendicular exchange bias with antiferromagnetic MnN". In: *Applied Physics Letters* 110.19 (2017), p. 192402.

[42] S Andrieu et al. "Co/Ni multilayers for spintronics: High spin polarization and tunable magnetic anisotropy". In: *Physical review materials* 2.6 (2018), p. 064410.

[43] William H Zachariasen. *Theory of X-ray Diffraction in Crystals*. Courier Corporation, 2004.

[44] Charles Kittel. *Introduction to solid state physics.* Tech. rep. 1966.

[45] Miho Yasaka. "X-ray thin-film measurement techniques". In: *The Rigaku Journal* 26.2 (2010), pp. 1–9.

[46] Brent Fultz and James M Howe. *Transmission electron microscopy and diffractometry of materials*. Springer Science & Business Media, 2012.

[47] Robert C Burghardt and Robert Droleskey. "Transmission electron microscopy". In: *Current protocols in microbiology* 3.1 (2006), 2B–1.

[48] HU-Berlin. *Characterization of magnetic materials by Lorentz microscopy and electron holography*. http://crysta.physik.hu-berlin.de/~woneu/MagnMaterials.pdf. 2019 (accessed February 3, 2019).

[49] Li-Cong Peng et al. "Lorentz transmission electron microscopy studies on topological magnetic domains". In: *Chinese Physics B* 27.6 (2018), p. 066802.

[50] Haifeng Du et al. "Edge-mediated skyrmion chain and its collective dynamics in a confined geometry". In: *Nature communications* 6 (2015), p. 8504.

[51] Paul K. Chu. *Auger Electron Spectroscopy(AES)*. http://www.cityu.edu.hk/phy/appkchu/AP5301/Lecture-10-AES.pdf. 2019 (accessed February 5, 2019).

[52] Simon Foner. "Review of magnetometry". In: *IEEE Transactions on Magnetics* 17.6 (1981), pp. 3358–3363.

[53] T Nishizawa and K Ishida. "Phase diagrams of binary nickel alloys". In: *Metals Park, OH: ASM* (1991), pp. 69–74.

[54] Takeshi Seki et al. "Magnetic Anisotropy and Damping for Monolayer-Controlled Co| Ni Epitaxial Multilayer". In: *Journal of the Physical Society of Japan* 86.7 (2017), p. 074710.

[55] Sanchai Kuboon and Yun Hang Hu. "Study of NiO- CoO and Co3O4- Ni3O4 solid solutions in multiphase Ni- Co- O systems". In: *Industrial & Engineering Chemistry Research* 50.4 (2011), pp. 2015–2020.

[56] AJ Devasahayam and MH Kryder. "The effect of sputtering conditions on the exchange fields of Co/sub x/Ni/sub 1-x/O and NiFe". In: *IEEE Transactions on Magnetics* 31.6 (1995), pp. 3820–3822.

[57] MJ Carey et al. "Strong interlayer coupling in CoO/NiO antiferromagnetic superlattices". In: *Physical Review B* 47.15 (1993), p. 9952.

[58] M. J. Carey and A. E. Berkowitz. "Exchange anisotropy in coupled films of Ni81Fe19 with NiO and CoxNi1xO". In: *Applied Physics Letters* 60.24 (1992), pp. 3060–3062.

[59] Josep Nogués and Ivan K Schuller. "Exchange bias". In: *Journal of Magnetism and Magnetic Materials* 192.2 (1999), pp. 203–232.

[60] William H Meiklejohn and Charles P Bean. "New magnetic anisotropy". In: *Physical review* 102.5 (1956), p. 1413.

[61] XF Han, ZC Wen, and HX Wei. "Nanoring magnetic tunnel junction and its application in magnetic random access memory demo devices with spin-polarized current switching". In: *Journal of Applied Physics* 103.7 (2008), 07E933.

[62] PP Freitas et al. "Magnetoresistive sensors". In: *Journal of Physics: Condensed Matter* 19.16 (2007), p. 165221.

[63] Andrew D Kent. "Spintronics: Perpendicular all the way". In: *Nature materials* 9.9 (2010), p. 699.

[64] Mitsuru Ohtake et al. "Epitaxial growth of fcc-Co x Ni 100- x thin films on MgO (110) single-crystal substrates". In: *Journal of Applied Physics* 106.12 (2009), p. 123921.

[65] AJ Devasahayam and MH Kryder. "The dependence of the antiferromagnet/ferromagnet blocking temperature on antiferromagnet thickness and deposition conditions". In: *Journal of applied physics* 85.8 (1999), pp. 5519–5521.

[66] K-W Lin et al. "Anomalous exchange bias behavior in ion-beam bombarded Ni Co/(Ni, Co) O bilayers". In: *Journal of Applied Physics* 103.7 (2008), p. 07C105.

[67] Florin Radu et al. "Soft X-ray resonant magnetic scattering studies on Fe/CoO exchange bias system". In: *Journal of magnetism and magnetic materials* 300.1 (2006), pp. 206–210.

[68] G Thomas. "Accommodation processes in nanostructured functional materials". In: *Progress in materials science* 49.3-4 (2004), pp. 607–626.

[69] P Kuświk et al. "Enhancement of perpendicular magnetic anisotropy of Co layer in exchange-biased Au/Co/NiO/Au polycrystalline system". In: *Journal of Applied Physics* 119.21 (2016), p. 215307.

[70] Piotr Kuświk et al. "Effect of CoO/Ni orthogonal exchange coupling on perpendicular anisotropy of Ni films on Pd (001)". In: *Physical Review B* 91.13 (2015), p. 134413.

[71] B Dieny and M Chshiev. "Perpendicular magnetic anisotropy at transition metal/oxide interfaces and applications". In: *Reviews of Modern Physics* 89.2 (2017), p. 025008.

[72] Atul Tiwari et al. "Interface sharpening in miscible and isotopic multilayers: Role of short-circuit diffusion". In: *Physical Review B* 99.20 (2019), p. 205413.

[73] Dinesh Martien et al. "Increasing the exchange-bias field of Ni 0.5 Co 0.5 O films by microstructural control". In: *Applied physics letters* 74.9 (1999), pp. 1314–1316.

[74] R. Sbiaa, H. Meng, and S. N. Piramanayagam. "Materials with perpendicular magnetic anisotropy for magnetic random access memory". In: *physica status solidi (RRL) - Rapid Research Letters* 5.12 (Oct. 2011), pp. 413–419.

[75] D. Bedau et al. "Ultrafast spin-transfer switching in spin valve nanopillars with perpendicular anisotropy". In: *Applied Physics Letters* 96.2 (Jan. 2010), p. 022514.

[76] Saeedeh Mokarian Zanjani and Mehmet C. Onbasli. "Thin film rare earth iron garnets with perpendicular magnetic anisotropy for spintronic applications". In: *AIP Advances* 9.3 (Mar. 2019), p. 035024.

[77] Can Onur Avci et al. "Magnetization switching of an MgO/Co/Pt layer by in-plane current injection". In: *Applied Physics Letters* 100.21 (May 2012), p. 212404.

[78] Jun Soo Bae et al. "Study of the effect of natural oxidation and thermal annealing on microstructures of AlOx in the magnetic tunnel junction by high-resolution transmission electron microscopy". In: *Applied Physics Letters* 80.7 (Feb. 2002), pp. 1168–1170.

[79] Josep Nogués et al. "Exchange bias in nanostructures". In: *Physics reports* 422.3 (2005), pp. 65–117.

[80] B. Y. Wang et al. "Driving magnetization perpendicular by antiferromagnetic-ferromagnetic exchange coupling". In: *Physical Review B* 83.10 (Mar. 2011).

[81] Hiroto Sakimura et al. "Enhancement of two-magnon scattering induced by a randomly distributed antiferromagnetic exchange field". In: *Physical Review B* 98.14 (2018), p. 144406.

[82] B. G. Park et al. "A spin-valve-like magnetoresistance of an antiferromagnet-based tunnel junction". In: *Nature Materials* 10.5 (Mar. 2011), pp. 347–351.

[83] T. Shang et al. "Effect of NiO inserted layer on spin-Hall magnetoresistance in Pt/NiO/YIG heterostructures". In: *Applied Physics Letters* 109.3 (July 2016), p. 032410.

[84] Shangkun Li et al. "Modulation of spin-orbit torque induced magnetization switching in Pt/CoFe through oxide interlayers". In: *Applied Physics Letters* 114.21 (2019), p. 212404.

[85] Kentaro Toyoki et al. "Magnetoelectric switching of perpendicular exchange bias in Pt/Co/-Cr2O3/Pt stacked films". In: *Applied Physics Letters* 106.16 (Apr. 2015), p. 162404.

[86] Q. Li et al. "Antiferromagnetic proximity effect in epitaxial CoO/NiO/MgO(001) systems". In: *Scientific Reports* 6.1 (Mar. 2016).

[87] P. Kuświk et al. "Effect of CoO/Ni orthogonal exchange coupling on perpendicular anisotropy of Ni films on Pd(001)". In: *Physical Review B* 91.13 (Apr. 2015).

[88] T. Nozaki et al. "Temperature-dependent perpendicular magnetic anisotropy of Co-Pt on Cr2O3antiferromagnetic oxide". In: *Applied Physics Letters* 103.24 (2013), pp. 1–5.

[89] A. T G Pym et al. "Interface sharpening in CoFeB magnetic tunnel junctions". In: *Applied Physics Letters* 88.16 (2006), pp. 1–4.

[90] F. Allegretti et al. "The formation of sharp NiO(1 0 0)-cobalt interfaces". In: *Surface Science* 601.14 (2007), pp. 73–76.

[91] Lili Han et al. "Interrogation of bimetallic particle oxidation in three dimensions at the nanoscale". In: *Nature Communications* 7.1 (Dec. 2016).

[92] Zhang Jian-Min, Ma Fei, and Xu Ke-Wei. "Calculation of the surface energy of FCC metals with modified embedded-atom method". In: *Chinese Physics* 13.7 (2004), p. 1082.

[93] PW Tasker and DM Duffy. "The structure and properties of the stepped surfaces of MgO and NiO". In: *Surface Science* 137.1 (1984), pp. 91–102.

[94] Marko PJ Punkkinen et al. "Surface properties of 3 d transition metals". In: *Philosophical Magazine* 91.27 (2011), pp. 3627–3640.

[95] Dingsheng Wang et al. "Shape control of CoO and LiCoO 2 nanocrystals". In: *Nano Research* 3.1 (2010), pp. 1–7.

[96] Zhenchao Wen et al. "Interdiffusion in epitaxial ultrathin Co2FeAl/MgO heterostructures with interface-induced perpendicular magnetic anisotropy". In: *Applied Physics Express* 10.1 (Dec. 2016), p. 013003.

[97] A.E. Berkowitz and Kentaro Takano. "Exchange anisotropy — a review". In: *Journal of Magnetism and Magnetic Materials* 200.1-3 (Oct. 1999), pp. 552–570.

[98] Ivan K Schuller. "Exchange bias ". In: 192 (1999).

[99] Bo-Yao Wang et al. "How Antiferromagnetism Drives the Magnetization of a Ferromagnetic Thin Film to Align Out of Plane". In: *Physical Review Letters* 110.11 (Mar. 2013).

[100] Bo Yao Wang et al. "Effects of the antiferromagnetic spin structure on antiferromagnetically induced perpendicular magnetic anisotropy". In: *Physical Review B* 96.9 (2017), pp. 1–8.

[101] Piotr Kuświk et al. "Impact of orthogonal exchange coupling on magnetic anisotropy in antiferromagnetic oxides/ferromagnetic systems". In: *Journal of Physics: Condensed Matter* 28.42 (Sept. 2016), p. 425001.

[102] N.H. Dung et al. "Out-of-plane exchange bias and magnetic anisotropy in MnPd/Co multilayers". In: *Journal of Magnetism and Magnetic Materials* 320.23 (Dec. 2008), pp. 3334–3340.

[103] S. M. Zhou et al. "Perpendicular exchange bias and magnetic anisotropy in CoO/permalloy multilayers". In: *Physical Review B - Condensed Matter and Materials Physics* 69.2 (2004), pp. 1–5.

[104] Hao Liang Liu et al. "Interplay between magnetocrystalline anisotropy and exchange bias in epitaxial CoO/Co films". In: *Journal of Physics Condensed Matter* 28.19 (2016).

[105] Jose Fermin. "Dependence of exchange bias in NiFe/NiO bilayers on film thickness". In: *Revista Mexicana de Fisica* 63 (Apr. 2017), pp. 145–150.

[106] Marcin Perzanowski et al. "Influence of Superparamagnetism on Exchange Anisotropy at CoO/[Co/Pd] Interfaces". In: *ACS Applied Materials and Interfaces* 8.41 (2016), pp. 28159–28165.

[107] K. O'Grady, L.E. Fernandez-Outon, and G. Vallejo-Fernandez. "A new paradigm for exchange bias in polycrystalline thin films". In: *Journal of Magnetism and Magnetic Materials* 322.8 (Apr. 2010), pp. 883–899.

[108] JN Rigue et al. "Exchange bias in bilayer and multilayer NiFe/IrMn". In: *IEEE Magnetics Letters* 6 (2015), pp. 1–4.

[109] J Geshev et al. "Role of the uncompensated interface spins in polycrystalline exchange-biased systems". In: *Journal of Physics D: Applied Physics* 44.9 (2011), p. 095002.

[110] Wei Zhang and Kannan M. Krishnan. "Epitaxial exchange-bias systems: From fundamentals to future spin-orbitronics". In: *Materials Science and Engineering: R: Reports* 105 (July 2016), pp. 1–20.

[111] T. Dias et al. "Rotatable anisotropy driven training effects in exchange biased Co/CoO films". In: *Journal of Applied Physics* 115.24 (June 2014), p. 243903.

[112] P. G. Barreto et al. "Ferromagnetic resonance study of the misalignment between anisotropy axes in exchange-biased NiFe/FeMn/Co trilayers". In: *Applied Physics Letters* 104.20 (2014), pp. 1–5.

[113] Cheng Hsun Tony Chang et al. "Enhanced exchange bias fields for CoO/Co bilayers: influence of antiferromagnetic grains and mechanisms". In: *Applied Surface Science* 405 (2017), pp. 316–320.

[114] Shouzhong Peng et al. "Interfacial perpendicular magnetic anisotropy in sub-20 nm tunnel junctions for large-capacity spin-transfer torque magnetic random-access memory". In: *IEEE Magnetics Letters* 8 (2017), pp. 1–5.

[115] K Watanabe et al. "Shape anisotropy revisited in single-digit nanometer magnetic tunnel junctions". In: *Nature communications* 9.1 (2018), p. 663.

[116] Shunsuke Fukami et al. "Coni films with perpendicular magnetic anisotropy prepared by alternate monoatomic layer deposition". In: *Applied Physics Express* 6.7 (2013), p. 073010.

Acknowledgements

The doctoral course was a great chance for learning, research and professional development. I am grateful for having so many wonderful people and professionals who led me through this period.

First of all, I am deeply grateful to my supervisor, Prof. Ji Shi. His general guidance in how to do research is the most valuable things I have learned so far. The door to his office is always open when I encountered obstacles or had questions about experiment, writing or presentation. Without his unmeasurable help this thesis would not have been possible. I also express my warmest gratitude for Prof. Yoshio Nakamura. From time to time, his honest suggestions and insightful opinions has helped me improve the quality of my research. Especially, his meticulous comments on crystal structure was an enormous help to me. I would like to express great thanks to Harumoto Sensei. He always helped me using, mentaining and better understanding the instruments. It was a pleasure to do experiment with him, dissuss with him and learn from him.

I would also like to thank Prof. Susa, Prof. Hayashi, Prof. Kimura and Prof. Nakagawa for being the examination commiittee. Their constructive comments and insightful questions have driven me to dig deeper for the fudementals, which greatly helped me get the final thesis of better quality.

Many sincere thanks also go to the labmates, past and present, in Nakamura-Shi group. I would like to thank Dr. Lei Guo, Dr. Hongyu An, Dr. Tenghua Gao and Dr. Yue Wang for their helps at the beginning of my research. Thanks to D3 member: Mr. Petrus Caesario for the stimulating discussion and for the funs we have together. Great thanks to D2 members: Mr. Fuxing Wan, Ms. Ying Gao for their help, encouragement and cooperation in the research as well as daily life. Special thanks to Mr. Hiroto Sakimura for providing assistance and helps in the research. Many thanks to the visiting members: Dr Rui Lan, Ms. Chunjiao Pan and Mr. Xiang Ji for their useful opinions and cooperations. Great thanks are also given to D1, Master and B4 members: Mr. Suiyu Qiu, Mr. Kaiwei Luo, Ms. Qianwen Wang, Mr Yunfeng You etc. for their help and cooperations. I also wish to give my thanks to all the other members, especially those have already graduated but have shared common

time with me in Nakamura-Shi group. They each have made my time in Tokyo Tech more positive and enjoyable.

Thanks to the staffs in Center for Advanced Materials Analysis in Tokyo Institute of Technology for their supports on structural characterizations.

With a special mention to Dr. Yi Du, Dr. Xun Xu, Dr.Jincheng Zhuang, Dr. Haifeng Feng, Dr.Zhi Li, Dr.Liang Wang and other members in STM lab in general. It was fantastic to have an intership research in your lab. Also special thanks to Mr. Denis Bristow for his hospitality during my short stay in Australia.

A very special gratitude goes out to all down to ACEEES for helping and providing special courses and financial support for my study in Tokyo Tech.

I also would like to thank Kawashima memorial scholarship fund and Secom cooperation for their financial supports during my study in Japan.

Lastly and the most importantly, I owe my deepest gratitude to my family: my parents and my sister, who have provided me through spiritual support throughout my life. Their love have helped me to overcome many obstacles during my study. I owe them a lot and I will repay my endless love to them in the rest of my life.